METimage Science Plan

A Report from the
METimage Science Advisory Group

Title:	METimage Science Plan
Issue:	v3R
Date:	20/07/2016

Executive Summary

Aim of the report

METimage is a cross-purpose medium resolution, multi-spectral optical imager serving operational and research meteorology, oceanography and climate applications. It stems from the long lasting heritage of the VIS-IR sensors onboard polar orbiting satellites such as the Advanced Very High Resolution Radiometer (AVHRR) and the MODerate resolution Imaging Spectroradiometer (MODIS). In this sense, it will ensure continuity of scientific and operational products for the atmosphere and the surface since the late 1970s. The instrument thus aims at ensuring the necessary level of continuity with its predecessors while at the same time adopting state-of-the-art technological advances.

It measures the optical spectrum of radiation emitted and reflected by the Earth from a low-altitude Sun synchronous orbit, over a swath with a minimum width of 2800 km. The primary objective is to provide high-quality imagery of clouds, water vapour, aerosols, atmospheric motion vectors, vegetation, snow, ice and sea surface temperature. In order that detailed information on the atmospheric and surface state can be retrieved, precise knowledge of all relevant radiative processes, and a consolidated capability to model them accurately in the framework of operational meteorology and climate monitoring, will be required.

The METimage Science Plan has been prepared by members of the METimage Science Advisory Group (SAG), a group established by DLR and EUMETSAT in 2009 with the objective of providing the scientific input needed for the preparation for the METimage mission, under the coordination of its chairmen. The Science Plan provides a framework for the scientific research and development that will be required to ensure that the METimage mission objectives are met, establishes the main areas where scientific research and development activities are needed in order to achieve these mission objectives, and reviews the currently available scientific expertise in these areas, in order to identify where current studies may best be directed. Many of these studies will provide the input required for the definition of the EPS-SG Ground Segment and for this reason, research and development activities will need to be closely coordinated with the development of these systems.

It is envisaged that this Science Plan will be updated in regular steps in order to keep current with the results of the most recent investigations from both within and outside the METimage SAG

Synopsis of the Science Plan

The Science Plan is divided into five main sections. Section 1 is an introduction to the EPS-SG mission in general and the METimage programme. Section 2 provides a summary of the main scientific objectives of the METimage mission and the operational rationale. The mission requirements derived from the operational needs and the specifications of the METimage instrument are described in Section 3. Following this, Section 4 summarises the current scientific knowledge, concepts and methods for METimage operational and research activities. Finally, in Section 5, areas requiring further work are described and the research and development priorities for METimage identified.

Contents

1 Introduction

1.1 The EPS-SG Programme

The current EUMETSAT Polar System (EPS) will end in the 2020 time frame, requiring a follow-on programme, the so-called EPS Second Generation (EPS-SG), to be in place by then to continue operational meteorological measurements from polar orbiting satellites in the mid-morning orbit.

It has been agreed between EUMETSAT and NOAA to establish the Joint Polar System in order to provide long-term continuity of observations from polar orbit supporting operational meteorology, oceanography, atmospheric chemistry, and climate monitoring including additional environmental services to support meteorology, hydrology, and land surface processes. The Metop Second Generation satellites for the EPS-SG will be developed in cooperation between EUMETSAT and the European Space Agency (ESA). The launch of the first Metop-SG satellites is foreseen in the 2020 time frame. EUMETSAT will be responsible for the development and operation of the related EPS-SG ground segment to control and monitor the satellite and its data and to process data up to level 1. The operational processing of level 1 data to higher levels, i.e. the generation of geophysical products will be done either at the EPS-SG ground segment or in the network of Satellite Application Facilities (SAF Network).

The Metop-SG satellites will carry a payload which is primarily dedicated to operational meteorology and climate monitoring. Secondary foci include operational oceanography and environmental services to the extent that they drive or are driven by operational meteorology. In addition to these operational applications, EPS-SG will contribute to a wide range of research activities, including global change, atmospheric chemistry and physics, hydrology, oceanic research, and the study of the cryosphere.

ESA will develop new instruments in support of the Radio Occultation (RO), Scatterometry (SCA), Microwave Sounding (MWS), Microwave Imaging (MWI), Multi-viewing, Multi-channel, Multi-polarisation (3MI) and Ice-Cloud Imaging (ICI) missions. The EU/ESA GMES Sentinel 5 will be embarked on the Metop-SG satellites in support of the nadir-looking UV/VIS/NIR/SWIR (UVNS) sounding mission. An infrared atmospheric sounding (IAS) mission will be developed in cooperation with the Centre National d'Études Spatiales (CNES). DLR will develop the METimage instrument implementing the Visible Infra-red Imaging (VII) mission. A further payload embarked on the Metop-SG satellites is the Argos-4 data collection and location system.

1.2 The METimage Project

DLR has proposed to implement the VII mission with the realisation of the METimage instrument. The cooperation between DLR and EUMETSAT foresees the provision of the first flight model as a German in-kind contribution to the EPS-SG programme; for the recurrent flight models DLR will act as the procurement agency. The co-operation between DLR and EUMETSAT is based on the established co-operation-model between EUMETSAT and ESA.

1.3 The Role of METimage SAG

For the scientific preparation of the METimage mission, DLR and EUMETSAT have established the METimage Science Advisory Group (METimage SAG), whose members are listed in Annex A3. The Terms of Reference for the SAG are listed in Annex A4. Some of the objectives of this advisory group are: to advice DLR/EUMETSAT on the scientific requirements of the METimage mission, system, instrument, and ground processing, and especially on requirements related to the EPS-SG ground segment; to review the progress of projects initiated in support of the METimage mission and to give recommendations to DLR/EUMETSAT on the direction of future work; to

participate in the coordination of the METimage SAG with external groups.

1.4 Purpose of the Science Plan

The Science Plan details the scientific work needed to meet the METimage mission objectives and provides a framework for required scientific research and development activities. By reviewing on-going activities in the areas of retrievals, software and databases, the level of compliance with the user needs can be established and the need for additional study and development identified.

2 METimage Rationale and Objectives

The METimage implements an optical imager for EPS-SG, according to the observation mission requirements for the Visible/Infrared imager (VII), as described in the Post-EPS Mission Requirements Document (MRD, EUMETSAT 2012) and the EPS-SG End User Requirements Document (EUMETSAT 2015). METimage will support a variety of user applications by measurements of the Earth atmosphere and surface in the optical spectrum.

2.1 Operational Rationale

METimage data will be very important in Nowcasting (NWC) applications, in particular in polar regions where space-borne imagery from geostationary satellites are not available. Numerical Weather Prediction (NWP) will benefit from a number of geophysical parameters to be derived from this instrument and which will be assimilated into the forecast models.

2.1.1 Numerical Weather Prediction (NWP)

With the evolution of NWP towards utilisation of rather high spatial resolution (< 10 km) an improved representation of atmospheric processes encompassing the whole Earth system (including land and ocean) will be required. Hence, the role of geophysical variables such as clouds and aerosols as well as surface parameters such as vegetation, and surface temperature will play an increasing role in a skilful weather forecast. Global models have almost reached the resolution of the current and planned spaceborne sounders. In the future, the relatively high resolution of the imagers will be necessary to get the additional high resolution information on a global scale which leads directly to the need for polar orbiting satellites and imagery missions. METimage is designed to provide high-quality imagery of many relevant parameters for NWP, with highest benefit in Polar regions.

2.1.2 Nowcasting (NWC)

Nowcasting heavily relies on the utilisation of cloud imagery, which is the most important satellite measurement in the related applications. Depending on his field of interest (or his duty), the forecaster, who has to predict the near future weather and to give out corresponding warnings, is mainly interested in topics like:

- Exact location and evolution of areas with fog
- Location of areas with the potential for heavy convection (stability indices) at high spatial resolution
- In areas with convection, the location and movement of the most active cells, together with an estimation of the amount of precipitation
- The wind field, including the location of jet stream axes

- For marine forecasting, the location of ice on the ocean

The design of METimage allows to attain this information through the provision of a range of geophysical observations such as cloud imagery (including some microphysical analysis and fog detection), aerosol and volcanic ash, atmospheric motion vectors and sea ice imagery. While in midlatitude regions one main focus is in increasing the spatial resolution of the geostationary satellites, in the high latitudes the polar orbiting satellites are the only source of information. Combination of these data (also from other orbiting platforms) allows for a satisfying temporal resolution. Although the impact of imagery data increases with latitude, this does not mean that LEO imagery data is not useful at lower latitudes. Many synergistic techniques using both high spatial resolution LEO imagery data and high temporal resolution GEO imagery data exist for improving cloud type assessments which are core to NWC.

2.2 Climate Monitoring

Climate observations are crucial for monitoring the Earth system under changing conditions. As raised by Goody et al. (2002), there is a societal need for a greater confidence in long-range climate projections that requires consistent and systematic high-quality observations as a basis for testing the predictive capabilities of climate models. This is particularly true for long-term studies of global change where exact variables in the climate model projections need to be clearly defined (Pielke 2008). With the intent of providing support to the work of the United Nations Framework Convention on Climate Change (UNFCCC) and the Intergovernmental Panel on Climate Change (IPCC) the Global Climate Observing System (GCOS) of the World Meteorological Organization (WMO) introduced the list of the Essential Climate Variables (ECV) deemed technically and economically feasible for systematic observation (see http://www.wmo.int/pages/prog/gcos/index.php?name=EssentialClimateVariables. Several of these variables (such as cloud properties, sea surface temperature and ice cover) will be observed by METimage and in this context METimage enters the key category of the polar orbiting imagers with an important list of predecessors such as the Advanced Very High Resolution Radiometer (AVHRR), the Moderate resolution Imaging Spectro-radiometer (MODIS), the Visible and Infrared Scanner (VIRS), the Along Track Scanning Radiometer (ATSR) and several others. METimage's radiometric performances and space-time resolution introduce novel observing capabilities that will enhance the observation potential.

2.3 Research Rationale

METimage will contribute to several research areas in both atmospheric and surface domains. Of paramount importance is the understanding of the role of clouds in modifying the Earth radiation budget, which represents a key uncertainty in predicting climate change. Key advances are still based on simultaneous observations of radiation budget and cloud properties and include cloud particle size and phase, improved detection of thin and multi-layered clouds, reduction of the ambiguities in partially cloud-filled satellite fields of view, improved calibration and stability of satellite-observed radiances, improved estimates of the radiative fluxes at the top of the atmosphere, at the surface and at levels in the atmosphere.

Other areas of importance concerning the contribution of METimage data to research are:

- Understanding the role of clouds in the water cycle
- Contributing observations for aerosol monitoring
- Improving the knowledge of atmospheric forcing from the lower boundary

- Contributing to studies of the cryosphere
- Providing additional observations for ocean studies

2.4 Mission Objectives

This section summarises the METimage mission objectives. METimage is a cross-purpose medium resolution, multi-spectral optical imager serving operational meteorology, oceanography and climate applications. It measures the optical spectrum of radiation emitted and reflected by the Earth from a low-altitude Sun synchronous orbit, over a swath with a minimum width of 2800 km. The primary objective is to provide high-quality imagery on:

- high horizontal resolution cloud products including microphysical analysis;
- aerosol products;
- atmospheric water-vapour gross profiles at high horizontal resolution;
- polar atmospheric motion vectors;
- vegetation;
- snow coverage;
- fire monitoring products;
- sea and ice surface temperature, sea ice coverage.

Other mission objectives include:

- land surface temperature (including inland waters and wetlands);
- atmospheric temperature gross profiles at high horizontal resolution for
    - supporting the EPS-SG sounders, particularly geolocation;
    - characterising cloud properties;
    - quantifying scene inhomogeneity for correction of the spectral response;
    - providing continuity of other key imager channels in support of long-term climate records.

Primary products to be derived from the VII mission are:

- cloud mask;
- cloud imagery;
- cloud cover profile;
- cloud optical thickness (COT);
- cloud top temperature (CTT);
- cloud top height (CTH);
- cloud type;
- cloud drop (liquid) or particle (solid) effective radius at the cloud top;
- polar atmospheric motion vectors (AMVs);
- water vapour imagery;
- aerosol optical depth (total columnar amount and gross profile);

- earth surface albedo;
- SW Earth's surface bi-directional reflection;
- SW cloud reflectance;
- vegetation:
    - leaf area index (LAI);
    - vegetation type;
    - fraction of vegetated land;
    - fraction absorbed photosynthetically active radiation (FAPAR);
    - photosynthetically active radiation (PAR);
    - normalised Differential Vegetation Index (NDVI);
- snow and land ice:
    - snow detection;
    - snow cover;
    - snow surface temperature;
    - snow albedo;
- fire:
    - fire detection;
    - fire fractional cover;
- sea surface temperature (SST);
- sea ice:
    - imagery;
    - sea ice coverage;
    - sea ice drift.

Further products to which the VII mission contributes include:

- land surface temperature (LST);
- aerosol type (total columnar amount and gross profile);
- aerosol effective radius (total columnar amount and gross profile);
- total aerosol single scattering albedo;
- downwelling SW radiation at the Earth's surface;
- glacier coverage;
- frozen soil and permafrost;
- fire smoke detection;
- fire temperature;
- fire radiative power;
- sea ice melt-pond fraction;
- lake surface water temperature.

Retrieval of these data will depend on the availability of:

- high vertical resolution temperature and water vapour sounding data;
- land type databases.

The user requirements for geophysical variables to be derived from METimage have been detailed in the Post-EPS position papers (Rizzi et al. 2006, Stoffelen et al. 2006, Stammer et al. 2006, Kerridge et al. 2006, Schulz et al. 2006). The accuracy and spatial resolution requirements of relevant parameters are summarised in the following tables (priority 1 = high, priority 4 = low).

Cloud		Accuracy (r.m.s.)				Bias	Stabil	Δx (km)			Δz (km)			Δt (h)			δ□(h)			Priority	
Parameter	**Application**	Unit	thresh	break	obj		decade	thresh	break	obj	thresh	break	obj	thresh	break	obj	thresh	break	obj	global	hi.lat
Cloud imagery	NWC, synoptic	MTF^{-1}	10	3.3	1.4			2	0.5	0.1	-	-	-	6	1	0.25	0.5	0.17	0.08	**1**	**1**
Water vapour imagery	NWC, synoptic	MTF^{-1}	10	3.3	1.4			10	3	1	2 layers	3 layers	5 layers	6	3	0.25	0.5	0.17	0.08	**2**	**1**
Cloud mask	NWP global	HR/ FAR	80/25	90/15	95/10			2	0.5	0.1	-	-	-	12	3	1	6	2	0.5	**2**	**2**
	NWC,NWP regional	HR/ FAR	85/20	95/10	98/5			2	0.5	0.1	-	-	-	6	1	0.5	0.5	0.35	0.25	**3**	**2**
Cloud cover profile	NWP global	%	20	10	5			50	15	5	1 layer	2 layers	3 lay	12	3	1	6	2	0.5	**1**	**1**
	NWP regional	%	20	10	5			20	5	2	1 layer	2 layers	3 lay	6	1	0.5	0.5	0.35	0.25	**1**	**1**
	climate	%	20	5	1	1	0.3	250	50	5	1 layer	3 layers	0.1	12	6	3	720	72	6	**1**	**1**
Cloud type	NWP regional	Classes	6	8	10			20	5	2	-	-	-	3	1	0.5	0.5	0.35	0.25	**4**	**4**
	NWC, synoptic meteorology	Classes	6	8	10			20	5	2	-	-	-	3	1	0.5	0.5	0.35	0.25	**2**	**1**
	climate	Classes	4	6	10			250	50	5	-	3 layers	0.1	12	6	3	720	72	6	**3**	**4**
Cloud optical depth	NWP global	%	50	20	10			50	15	5				12	3	1	6	2	0.5	**1**	**1**
	NWP regional	%	50	10	10			20	5	2				6	1	0.5	0.5	0.35	0.25	**2**	**1**
	climate	%	20	10	5	10	2	250	50	5	-	-	-	24	6	3	720	72	6	**2**	**2**

Table 1. User requirements for cloud observations.

Cloud		Accuracy (r.m.s.)				Bias	Stabil	Δx (km)			Δz (km)			Δt (h)			δ□(h)			Priority	
Parameter	**Application**	Unit	thresh	break	obj		decade	thresh	break	obj	thresh	break	obj	thresh	break	obj	thresh	break	obj	global	hi.lat
Cloud top height	NWP global	km	1	0.5	0.2			50	15	5	-	-	-	12	3	1	6	2	0.5	**2**	**2**
	NWP regional	km	1	0.5	0.2			20	5	2	-	-	-	6	1	0.5	0.5	0.35	0.25	**3**	**2**
	NWC, synoptic	km	1	0.5	0.2			10	3	1	-	-	-	6	1	0.25	0.5	0.35	0.25	**3**	**2**
	climate	km	1	0.5	0.2	0.15	0.03	250	50	5	-	-	-	12	6	3	720	72	6	**2**	**2**
Cloud top temperature	NWP global	K	5	2	1			50	15	5	-	-	-	12	3	1	6	2	0.5	**1**	**1**
	NWP reg., NWC	K	5	2	1			20	5	2	-	-	-	6	1	0.5	0.5	0.35	0.25	**2**	**1**
	climate	K	5	1	0.3	1	0.2	250	50	5	-	-	-	12	6	3	720	72	6	**2**	**2**
	NWP regional	μm	5	2	1			20	5	2	1 lay	2 lay	3 lay	6	3	0.5	2	1	0.5	**2**	**2**
	climate	μm	20	10	5			100	10	1	top	0.3	0.1	12	6	3	720	72	6	**2**	**2**
Cloud drop effective radius at cloud top	NWP global	μm	5	2	1			50	15	5	-	-	-	12	3	1	2	1	0.5	**2**	**2**
	NWP regional	μm	5	2	1			20	5	2	-	-	-	6	3	0.5	2	1	0.5	**3**	**2**
	climate	μm	20	10	5	1	0.2	100	10	1	-	-	-	12	6	3	720	72	6	**3**	**3**
	NWP regional	μm	25	10	5			20	5	2	1 lay	2 lay	3 lay	6	3	0.5	2	1	0.5	**2**	**2**
	climate	μm	10	10	5			100	10	1	top	0.3	0.1	12	6	3	720	72	6	**3**	**3**
Cloud ice effective radius at cloud top	NWP global	μm	25	10	5			50	15	5	-	-	-	12	3	1	2	1	0.5	**2**	**2**
	NWP regional	μm	25	10	5			20	5	2	-	-	-	6	3	0.5	2	1	0.5	**3**	**2**
	climate	μm	10	10	5	20	4	100	10	1	-	-	-	12	6	3	720	72	6	**3**	**3**

Table 2. cont.d

Aerosol		Accuracy (r.m.s.)				Bias	Stabil	Δx (km)			Δz (km)			Δt (h)			□δ□(h)			Priority	
Parameter	**Application**	Unit	thresh	break	obj			thresh	break	obj	thresh	break	obj	thresh	break	obj	thresh	break	obj	global	hi.lat
Aerosol optical depth profile	NWP global		0.06	0.03	0.01			50	10	5	3	1	0.5	12	3	1	6	2	0.5	**1**	**1**
	NWP regional		0.06	0.03	0.02			20	5	2	2	0.5	0.5	3	1	0.08	0.5	0.35	0.25	**1**	**1**
	Climate		0.06	0.03	0.01			50	10	5	3	1	0.5	12	6	3	720	72	6	**1**	**1**
Total aerosol optical depth	NWP global		0.06	0.03	0.01			50	10	5	-	-	-	12	3	1	6	2	0.5	**1**	**1**
	NWP regional		0.06	0.03	0.02			20	5	2	-	-	-	3	1	0.08	0.5	0.35	0.25	**2**	**1**
	NWC fog&low cloud		0.05	0.05	0.01			2	1	0.1	-	-	-	1	1	0.25	0.5	0.35	0.25	**4**	**4**
	NWC air quality		0.05	0.05	0.01			2	1	0.1	-	-	-	1	1	0.25	0.5	0.35	0.25	**4**	**4**
	NWC UV models		0.06	0.03	0.02			50	20	10	-	-	-	24	24	1	3	1.5	1	**4**	**4**
	Climate		0.06	0.03	0.01	0.01	0.005	50	10	5	-	-	-	12	6	3	720	72	6	**1**	**1**
Aerosol effective radius profile	NWP global	µm	0.6	0.4	0.2			50	10	5	1 layer	1	0.5	12	3	1	6	2	0.5	**2**	**2**
	NWP regional	µm	0.6	0.4	0.2			20	5	2	1 layer	1	0.5	3	1	0.08	0.5	0.35	0.25	**2**	**2**
	NWC air quality	µm	0.6	0.4	0.2			5	5	0.5	1 layer	1	0.5	1	1	0.25	0.5	0.35	0.25	**4**	**4**
	Climate	µm	0.6	0.4	0.2			50	10	5	1 layer	1	0.5	12	6	3	720	72	6	**2**	**2**

Table 3. User requirements for aerosol observations

Aerosol		Accuracy (r.m.s.)				Bias	Stabil	Δx (km)			Δz (km)			Δt (h)			□δ□(h)			Priority	
Parameter	**Application**	Unit	thresh	break	obj			thresh	break	obj	thresh	break	obj	thresh	break	obj	thresh	break	obj	global	hi.lat
Total aerosol effective radius	NWP global	μm	0.6	0.4	0.2			50	10	5	-	-	-	12	3	1	6	2	0.5	**2**	**2**
	NWP regional	μm	0.6	0.4	0.2			20	5	2	-	-	-	3	1	0.08	0.5	0.35	0.25	**3**	**2**
	NWC air quality	μm	0.6	0.4	0.2			5	5	0.5	-	-	-	1	1	0.25	0.5	0.35	0.25	**4**	**4**
	Climate	μm	0.6	0.4	0.2	0.1	0.05	50	10	5	-	-	-	12	6	3	720	72	6	**2**	**2**
Total aerosol type	NWP global	classes	2	4	8			10	3	1	-	-	-	12	3	1	6	2	0.5	**2**	**2**
	NWP regional	classes	2	4	8			10	3	1	-	-	-	12	3	1	6	2	0.5	**3**	**2**
	Climate	classes	2	4	8			10	3	1	-	-	-	12	6	3	720	72	6	**2**	**2**

Table 4. cont.d.

Radiation budget		Accuracy (r.m.s.)				Bias	Stabil	Δx (km)			Δz (km)			Δt (h)			δ□(h)			Priority	
Parameter	**Application**	Unit	thresh	break	obj			thresh	break	obj	thresh	break	obj	thresh	break	obj	thresh	break	obj	global	hi.lat
SW cloud reflectance	NWP global	%	10	3	1			20	10	2	-	-	-	168	24	3	3	1.5	1	**2**	**2**
	Climate	%	10	3	1			100	50	10	-	-	-	12	3	1	12	8	6	**2**	**2**
	Hydrology	%	10	3	1			100	50	10	-	-	-	12	3	1	3	1.5	1	**4**	**4**
SW Earth surface bi-directional reflectance	NWP global	%	5	2	1			20	10	2	-	-	-	720	168	24	72	36	24	**2**	**2**
	Climate	%	5	2	1			100	50	10	-	-	-	2160	720	168	720	360	168	**2**	**2**
	Hydrology	%	5	2	1			100	50	10	-	-	-	720	120	24	72	36	24	**3**	**3**
Earth surface albedo	NWP global	%	5	2	1			50	15	5	-	-	-	720	120	24	720	120	24	**2**	**2**
	NWP regional	%	5	2	1			20	10	2	-	-	-	720	6	0.5	24	3	0.5	**3**	**2**
	Climate	%	5	2	1			100	50	1	-	-	-	720	120	24	720	120	24	**1**	**1**
	Climate	W/m^2	20	10	1	1	0.2	100	50	10	-	-	-	720	6	3	4320	320	24	**2**	**2**
Surface emissivity in TIR window channels	NWP global	%	3	1	0.5			50	15	5	-	-	-	720	120	24	720	120	24	**4**	**4**
	hydrology	%	20	6	2			100	50	0.01	-	-	-	720	120	24	720	120	24	**3**	**3**

Table 5. User requirements for radiation budget observations.

Land surface		Accuracy (r.m.s.)				Bias	Stabil	Δx (km)			Δz (km)			Δt (h)			δ□(h)			Priority	
Parameter	**Application**	Unit	thresh	break	obj			thresh	break	obj	thresh	break	obj	thresh	break	obj	thresh	break	obj	global	hi.lat
Land surface temperature	NWP global	K	4	1	0.5			100	15	2	-	-	-	6	3	0.5	6	2	0.5	**2**	**1**
	NWP regional	K	4	1	0.5			20	5	2	-	-	-	6	3	0.5	1	0.7	0.5	**1**	**1**
	Climate	K	4	1	0.5	0.5	0.04	250	15	2	-	-	-	12	6	3	12	6	3	**2**	**2**
	Hydrology	K	4	1	0.5			100	15	2	-	-	-	6	3	0.1	6	2	0.5	**2**	**2**
Lake surface temperature	NWP global and regional	K	1	0.3	0.1			10	1	0.1	-	-	-	120	24	3	1	1	0.5	**3**	**3**

Table 6. User requirements for land surface observations.

Fire		Accuracy (r.m.s.)				Bias	Stabil	Δx (km)			Δz (km)			Δt (h)			δ□(h)			Priority	
Parameter	**Application**	Unit	thresh	break	obj			thresh	break	obj	thresh	break	obj	thresh	break	obj	thresh	break	obj	global	hi.lat
Smoke detection	NWC land surf.	HR/FAR	50/50	70/40	85/20			10	1	0.1	-	-	-	6	1	0.08	1	0.25	0.08	**3**	**4**
Fire detection	NWC air quality	HR/FAR	50/50	50/50	85/20			10	1	0.1	-	-	-	6	1	0.08	1	0.25	0.08	**3**	**4**
Fire fractional cover	Climate	%	20	10	5			5	1	0.025	-	-	-	720	24	3	720	360	168	**3**	**4**
	Hydrology	%	20	10	5			10	3	1	-	-	-	24	3	1	3	1	0.25	**3**	**4**
Fire temperature	NWC	K	100	500	25			10	1	0.1	-	-	-	6	1	0.25	2		1	**3**	**3**
	Agricultural met	K	200	100	50			10	0.5	0.01	-	-	-	24	12	6	2		1	**2**	**3**
	Climate	K	200	100	50			10	1	0.1	-	-	-	720	24	3	720	360	168	**3**	**3**
	Hydrology	K	500	300	200			10	3	1	-	-	-	24	3	1	3	1	0.25	**3**	**4**

Table 7. User requirements for fire observations.

Vegetation		Accuracy (r.m.s.)				Bias	Stabil	Δx (km)			Δz (km)			Δt (h)			δ□(h)			Priority	
Parameter	**Application**	Unit	thresh	break	obj			thresh	break	obj	thresh	break	obj	thresh	break	obj	thresh	break	obj	global	hi.lat
Leaf area index (LAI)	NWP global	%	20	10	5			50	10	2	-	-	-	240	120	120	120	36	6	**1**	**1**
	NWP regional	%	20	10	5			5	1	0.1	-	-	-	240	120	120	24	3	0.5	**3**	**1**
	NWC run-off	%	20	10	5			5	1	0.1	-	-	-	240	120	120	48	12	3	**4**	**4**
	Climate	%	20	10	5			5	0.2	0.1	-	-	-	240	120	120	720	400	240	**2**	**2**
	Hydrology	%	20	10	5			5	1	0.1	-	-	-	240	120	120	120	60	24	**2**	**2**
Normalised Difference Vegetation Index (NDVI)	NWP global	%	20	10	5			50	10	2	-	-	-	240	120	120	120	36	6	**2**	**2**
	NWP regional	%	20	10	5			5	1	0.1	-	-	-	240	120	120	24	3	0.5	**4**	**2**
	NWC run-off	%	20	10	5			5	1	0.1	-	-	-	240	120	120	48	12	3	**4**	**4**
	Climate	%	20	10	5			5	0.2	0.1	-	-	-	240	120	120	720	400	240	**2**	**2**
	Hydrology	%	20	10	5			5	1	0.1	-	-	-	240	120	120	120	60	24	**2**	**2**
Fraction of vegetated land	NWP regional	%	20	10	5			5	1	0.1	-	-	-	240	120	120	48	12	3	**4**	**4**
	Climate	%	20	10	5	3	1	5	0.2	0.1	-	-	-	240	120	120	120	60	24	**2**	**2**
	Hydrology	%	20	10	5			5	0.2	0.1	-	-	-	240	120	120	120	60	24	**3**	**3**

Table 8. User requirements for vegetation observations.

Vegetation		Accuracy (r.m.s.)				Bias	Stabil	Δx (km)			Δz (km)			Δt (h)			δ□(h)			Priority	
Parameter	**Application**	Unit	thresh	break	obj			thresh	break	obj	thresh	break	obj	thresh	break	obj	thresh	break	obj	global	hi.lat
Vegetation type	NWP S & IA	classes	9	12	18			2	0.5	0.1	-	-	-	87600	43800	8760	720	120	24	**4**	**4**
	NWC run-off	classes	4	10	10			2	0.5	0.1	-	-	-	87600	43800	8760	720	240	72	**4**	**4**
	Climate	classes	10	20	50			2	0.5	0.1	-	-	-	87600	43800	8760	8760	2500	720	**3**	**3**
	Hydrology	classes	5	20	50			100	15	0.1				8760	720	24	720	120	24	**4**	**4**
Photo-synthetically Active Radiation (PAR)	NWP S & IA	W/m^2	20	10	1			20	10	1	-	-	-	24	3	1	3	1.5	1	**1**	**1**
	Climate	%	5	3	2			50	10	1	-	-	-	24	3	1	168	120	72	**2**	**2**
Fractional Absorbed Photo-synthetically Active Radiation (FAPAR)	NWP S & IA	%	20	10	5			5	1	0.1	-	-	-	240	120	120	120	60	24	**2**	**2**
	Climate	%	20	10	5			5	1	0.1	-	-	-	240	120	120	120	60	24	**2**	**2**
	Hydrology	%	20	10	5			5	1	0.1	-	-	-	24	3	1	3	1.5	1	**3**	**3**

Table 6. cont.d.

Snow and ice		Accuracy (r.m.s.)				Bias	Stabil	Δx (km)			Δz (km)			Δt (h)			δ□(h)			Priority	
Parameter	**Application**	Unit	thresh	break	obj			thresh	break	obj	thresh	break	obj	thresh	break	obj	thresh	break	obj	global	hi.lat
Snow detection	Hydrology	HR/FAR	80/25	90/15	95/10			5	2	0.5	-	-	-	24	6	1	24	6	2	**2**	**2**
Snow cover	NWP global	%	50	20	10			100	15	5	-	-	-	120	24	6	120	24	3	**1**	**1**
	NWP regional	%	50	20	10			50	10	3	-	-	-	60	24	6	1	0.7	0.5	**2**	**1**
	NWC run-off	%	25	20	10			50	5	1	-	-	-	60	24	6	3	1	0.25	**2**	**2**
	NWC transport	%	50	30	10			50	10	1	-	-	-	60	24	3	1	0.5	0.25	**2**	**2**
	Climate	%	20	5	1	5	4	100	10	1	-	-	-	168	60	24	168	24	3	**2**	**2**
	Hydrology	%	20	10	5			10	3	1	-	-	-	24	6	1	24	6	2	**1**	**1**
Snow surface temperature	NWP & NWC	K	3	1	0.2			50	20	0.1	-	-	-	12	12	1	24	6	1	**3**	**2**
	Climate	K	5	2	0.1			50	10	1	-	-	-	12	12	3	24	6	1	**3**	**3**
	Hydrology	K	5	2	0.1			50	10	1	-	-	-	12	12	3	24	6	1	**2**	**2**
Snow albedo	Climate	%	20	5	1			250	50	1	-	-	-	320	120	24	24	6	1	**3**	**3**
Glacier cover	Climate	%	20	15	10			0.1	0.02	0.01	-	-	-	438000	260000	87600	1500	1000	720	**4**	**4**

Table 9. User requirements for snow and ice observations.

Observation	Application	Units	Bias	Stability	Accuracy			Δx (km)			Δt (hr)			δ (hr)			Priority
SST					thresh	break	obj	thresh	break	obj	thresh	break	obj	thresh	break	obj	1=high 4=low
Sea surface temperature at depth (specified)	Climate	K	0.25/0.1/0.025	0.04	2	0.5	0.3	500	200	100	72	48	24	12		3	1
Sea surface temperature	NWP global	K			1.5	0.5	0.3	250	15	5	120	24	3	120	24	3	2
	NWP regional	K			1.5	1.0	0.5	50	10	1	24	6	1	3	1	0.1	2
	NWP S & IA	K			0.5	0.2	0.1	50	20	1	48	12	1	120		3	2
	Oceanography global	K			0.5	0.4	0.1	50	10	1	120	48	3	48		1	1
	Oceanography coastal	K			1	0.3	0.1	10	1	0.1	120	24	3	1		0.5	1
Sea-ice surface temperature	Climate	K	?/?/?	?	2	1	0.5	500	100	25	24	12	6	48		24	1
Sea-ice surface temperature	NWP global	K			4	1	0.5	250	15	5	12	3	1	4		1	2
	NWP regional	K			2	?	0.5	100	?	5	2	?	0.5	4	?	1	3

Table 10. User requirements for SST observations.

Observation	Application	Units	Bias	Stability	Accuracy			Δx (km)			Δt(hr)			δ (hr)			Priority
ICE					thresh	break	obj	thresh	break	obj	thresh	break	obj	thresh	break	obj	1=high 4=low
Sea ice cover	Climate	%	12.5/5/1	4	5	3	2	50	30	15	72	48	24	168		24	1
Sea ice cover	NWP global	%			20	10	5	100	15	5	120	24	24	120		3	2
	NWP regional	%			20	5	2	50	10	1	24	6	3	1		0.5	2
	Oceanography global	%			10	5	2	20	10	5	120	24	24	120		3	1
	Oceanography coastal	%			10	3	2	10	5	1	120	12	6	120		3	1
Sea ice type	NWP global	%			20	10	5	100	25	10	120	24	24	120		3	2
	NWP regional	%			20	10	2	50	25	5	120	24	24	120		3	2
	Oceanography global	%			20	10	5	50	10	5	120	24	24	120		3	1
	Oceanography coastal	%			20	10	5	10	5	2	120	12	6	120		3	1
Sea ice drift	Climate	cm/s	?/?/?	?	20	10	5	20	10	5	120	24	24	120		6	1
Sea ice drift	NWP regional	cm/s			10	5	2	10	5	1	120	24	6	60		3	3
	Oceanography global	cm/s			20	10	5	20	10	5	120	24	24	120		6	1
	Oceanography regional	cm/s			10	5	2	10	5	1	120	24	6	60		3	1
Iceberg drift	Oceanography coastal	km/h			0.2		0.1	1	0.2	0.1	24		6				3

Table 11. User requirements for sea ice observations.

3 The METimage Instrument

This section describes the measurement principles implemented in the METimage design and the expected performances.

3.1 Basic Principles

METimage is a cross-track scanning imaging spectro-radiometer measuring reflected solar and emitted terrestrial radiation in the visible to infrared spectral domain between 0.445 and 13 µm with a moderate sampling resolution of 0.5 km. Derived from a whisk-broom scanner principle, the instrument records 24 image lines simultaneously during each scan across-track. By proper selection of rotation frequency, the scanner produces a gap-free scan pattern on ground. Output is an image sampled at discrete locations. The sampling within each line is performed at constant scan angle increments.

The instrument consists of a rotating scan mirror, followed by a telescope and de-rotator assembly in order to compensate for the rotation of the image in the focal plane. In-field separation of spectral channels is used to image different spectral channels on to rows of detector elements which are located side-by-side in the image plane. Due to the scan motion, the image moves sequentially over the detector channels and filters mounted in front of the detectors define the spectral bands.

The METimage optical system is divided into six functional units:

- **Telescope** (3 mirror off-axis optical design) with rotating **scan mirror** which realizes the scanning of the Earth scene. The axis of rotation of the mirror is aligned with the optical axis of the telescope. The normal of the scanning mirror is tilted 45° with respect to the optical axis so that the incidental beam forms an angle of 90° with the optical axis.
- **De-rotator** to compensate the rotation of the image introduced by the scan mirror. It uses 5 mirrors in two perpendicular planes. The incident angles on the mirrors are arranged in such a way that the polarisation sensitivity is minimized for the chosen coating over the spectral range of the instrument.
- A **Beamsplitter** assembly for spectral band separation into 3 bands:
    - Visible/near infrared (VIS/NIR) 443 to 914 nm;
    - Shortwave infrared/midwave infrared (SWIR/MWIR) 1.20 to 4.15 µm;
    - Longwave infrared/very long-wave infrared (LWIR/VLWIR) 6.28 to 13.78 µm.
- **Filters and field mask** assembly in the intermediate image of the telescope combining the filters for the channels of the instrument with a field mask for co-registration. For the SWIR/MWIR band different thicknesses of the filters help compensating chromatic aberrations of the following optics.
- **Relay optics** for the SWIR/MWIR and LWIR bands. These optics reduce the intermediate image by a factor of 0.135 to match the detector element size.

Following the optics, the image is focused onto three **focal plane arrays (FPAs)**, one for band as described above. From these, the SWIR/MWIR and LWIR/VLWIR focal planes are cooled to around 60 K. Figure 1 illustrates the main functional elements of the instrument.

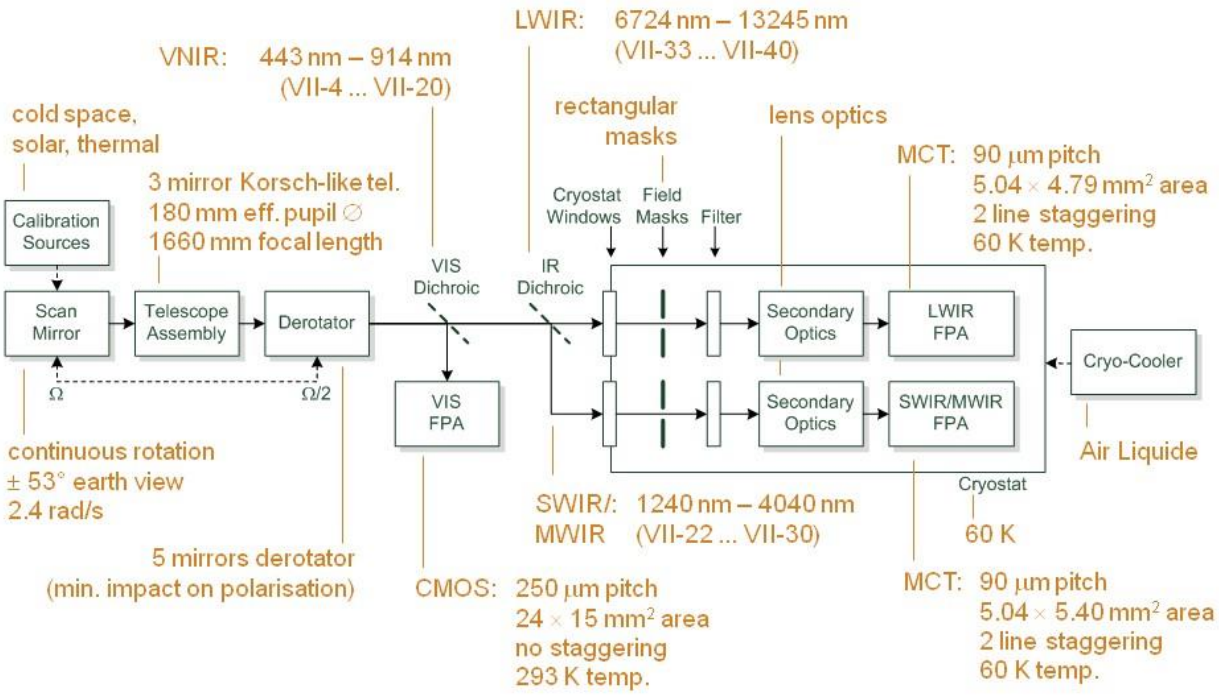

Figure 1. METimage instrument functional elements.

The METimage scanner performs a continuous rotating motion which allows viewing of calibration sources that are located outside the operational field-of-view (FOV) and are scanned with every rotation of the scan mirror. Thus calibration can be performed frequently and without any interruption of operational image acquisition. In order to improve the radiometric noise, the scanner accelerates over the back of the scan where no measurements are made, allowing for a longer integration period for Earth view and calibration target measurements.

Figure 2 illustrates the scan geometry including the positions of calibration targets with respect to the Earth views and nadir direction.

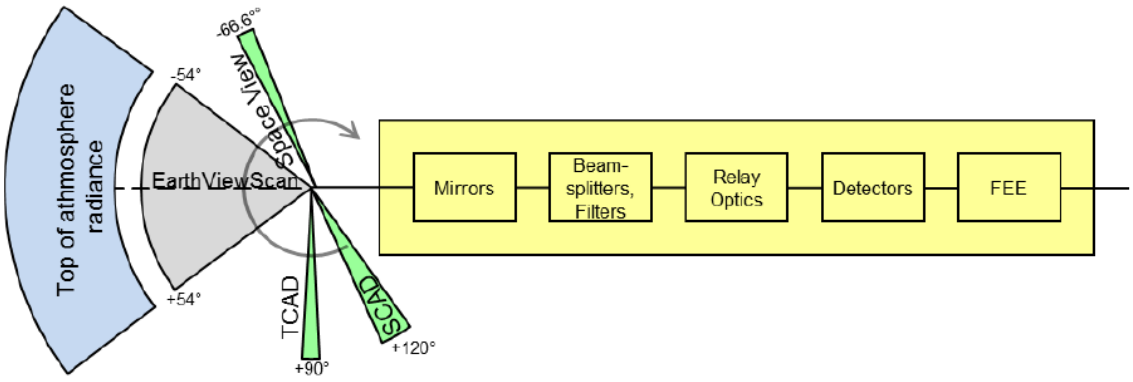

Figure 2. Position of EV scan and calibration targets.

A full rotation of the scanner takes 1.729 seconds including periods of acceleration around the back of the scan where no measurements are made and deceleration allowing for a longer integration

period for Earth view and calibration target measurements (maximizing integration time) and minimising the need for having to compensate for the satellite motion. The scan rate is constant during Earth view as well as solar and thermal calibrations. In this scan period on-board calibration for all channels is also done – though full calibration of the solar channels can only be done in the region of the South Pole.

3.2 Performances

The user requirements have been translated into observation mission requirements, as detailed in the EPS-SG End User requirements Document (EUMETSAT 2010). The mission requirements contain ranges of radiometric, spectral, and geometric requirements, specified in terms of threshold, breakthrough, and objective values. Thresholds provide a minimum level of expected performances, below which the respective measurements become useless. Breakthrough levels identify a performance at which a delta-improvement can be realised in the targeted user application. Objective levels give the utmost performance level for a requirement above which any further improvement would not provide added value. For the METimage design the breakthrough performance values have been adopted as part of the instrument specification.

3.2.1 Spectral Specifications

The VII shall simultaneously provide images in a number of spectral channels as listed in Table 12. These channels have been chosen from a sample of a total of 45 possible channels that have been investigated for best combination. Spectral channels and their bandwidths are defined in terms of the full width at half maximum (FWHM). Acquisition in the shortwave channels shall be limited to the daytime part of the orbit defined as solar zenith angle < 88° at sub-satellite point. The channels at wavelengths ≥ 3.74 µm shall be operated both in day and night-time conditions.

3.2.1.1 Spectral response function

The total out-of-band response of the VII channels 1 to 25 shall be < 1% of the total integrated response within two times the full width half maximum bandpass region when viewing a source that simulates the solar spectral energy distribution (e.g., 1985 Wehrli standard extraterrestrial solar irradiance spectrum, Wehrli 1986).

The total out-of-band response of the VII channels 33 to 45 shall be < 1% of the total integrated response within two times the full width half maximum bandpass region when viewing a blackbody source at $T_{typical)}$(Table 13) .

The total out-of-band response of VII channels 26 to 32 shall meet both previous requirements.

The VII spectral response functions shall be characterised over the spectral range Λ where they exceed a value of 0.1% of the peak response. The relative magnitude accuracy shall be better than 2% of the peak response at a sampling interval of 1 nm (Threshold), 0.5 nm (Objective) for channels below 3 µm and 2 cm^{-1} (threshold), 1 cm^{-1} (Objective) for channels above 3 µm. It shall be known to this accuracy for the lifetime of the mission over the wavelength range corresponding to 80% of the channel FWHM and centred on the channel centre wavelength.

The spectral sampling intervals for characterising the VII spectral response functions shall be known with an accuracy < 0.1 nm for channels below 3 µm and 0.25 cm^{-1} for channels above 3 µm (TBC).

The knowledge of the spectral response function central wavelength and FWHM over the lifetime of the mission shall be:

- 0.5 nm for all bands below 1µm except for channels VII-15 and VII-16;
- 0.5 nm (threshold) / 0.1 nm (goal) for channels VII-15 and VII-16;
- Better than 0.1% of the centre wavelength for all bands above 1 µm centre wavelength.

Channel	Central Wavelength (µm)	FWHM (µm)	Primary Use
VII-4	0.443	0.03	Aerosol, 'true colour imagery' (blue channel), vegetation
VII-8	0.555	0.02	Clouds, vegetation, 'true colour imagery' (green channel)
VII-12	0.668	0.02	Clouds, vegetation, 'true colour imagery' (red channel)
VII-15	0.752	0.01	Atmospheric corrections (aerosol), optical cloud top height assignment, vegetation
VII-16	0.763	0.01	
VII-17	0.865	0.02	Vegetation, aerosol, clouds, surface features
VII-20	0.914	0.02	Water vapour imagery, water vapour total column
VII-22	1.24	0.02	Vegetation, aerosol
VII-23	1.375	0.04	High level aerosol, cirrus clouds, water vapour imagery
VII-24	1.63	0.02	Cloud phase, snow, vegetation, aerosol, fire
VII-25	2.25	0.05	Cloud microphysics at cloud top, vegetation, aerosol over land, fire (effects)
VII-26	3.74	0.18	Cloud variables, cloud microphysics at cloud top, absorbing aerosol, SST, LST, fire, sea and land ice
VII-28	3.959	0.06	SST, LST, fire
VII-30	4.05	0.06	SST, LST fire
VII-33	6.725	0.37	Water vapour imagery (including wind in polar regions), water vapour profile (coarse vertical resolution)
VII-34	7.325	0.29	
VII-35	8.54	0.29	Cirrus clouds, cloud emissivity
VII-37	10.69	0.5	Cloud variables including cirrus detection, surface temperatures and other radiative variables, surface imagery (snow, ice etc)
VII-39	12.02	0.5	
VII-40	13.345	0.31	CO_2 slicing for accurate cloud top height. Temperature profile (coarse vertical resolution)

Table 12. METimage channels.

3.2.2 Radiometric Specifications

Unless otherwise stated the requirements in this section apply:

to all spectral channels;

to all spatial samples.

3.2.2.1 Radiometric noise

a) The VII radiometric sensitivity shall meet the requirement as given in Table 13. The quoted figures are understood as one standard deviation.

b) The VII dynamic range shall meet the requirements given in Table 11

Channel	Central Wavelength (μm)	$L_{typical}$ (W m^{-2} sr^{-1} μm^{-1})	L_{high} (W m^{-2} sr^{-1} μm^{-1})	L_{low} (W m^{-2} sr^{-1} μm^{-1})	SNR at $L_{typical}$
VII-4	0.443	42	704	7.8	221
VII-8	0.555	22	678	5.7	215
VII-12	0.668	9.5	673	2.9	66
VII-16	0.752	28	434	1.7	400
VII-15	0.763	20	370	0.36	400
VII-17	0.865	6.04	379	0.8	60
VII-20	0.914	15	294	6.1	250
VII-22	1.24	5.4	150	5.4	75
VII-23	1.375	6	81	2	300
VII-24	1.63	7.3	72	0.4	300
VII-25	2.25	1	32	0.12	110
Channel	**Central Wavelength (μm)**	**$T_{typical}$ (K)**	**T_{high} (K)**	**T_{low} (K)**	**NEΔT at Tt_{ypical} (K)**
VII-26	3.74	300	350	186	0.050
VII-28	3.959	300	345	185	0.074
VII-30	4.05	300	344	185	0.074
VII-33	6.725	238	271	186	0.215
VII-34	7.325	250	282	186	0.200
VII-35	8.54	300	330	185	0.050
VII-37	10.69	300	345	185	0.050
VII-39	12.02	300	345	185	0.050
VII-40	13.345	260	290	185	0.20

Table 13. METimage radiometric and scene dynamic range requirements.

The VII radiometric requirements for channels at wavelengths greater than 3 μm shall be met in the target brightness-temperature range. At brightness temperatures different from the typical

brightness temperature $T_{typical}$, the specified radiometric sensitivity shall be multiplied by the radiometric scaling function, taking the typical brightness temperature as reference temperature. This implies a constant requirement in terms of radiance. The upper limits given in Table 14 shall apply.

Requirement	Requirement Objective	Upper Temperature Limit for Scaling
VII-03080	NE∆T	320 K
VII-03100	Bias	320 K
VII-03110	Orbit stability	257 K for VII-33 270 K for VII-34 290 K for VII-40 300 K for all other channels
VII-03120	Lifetime stability	257 K for VII-33 270 K for VII-34 290 K for VII-40 300 K for all other channels
VII-03130	Inter-channel homogeneity	280 K
VII-03140	Inter-spatial homogeneity	280 K

Table 14: VII upper limit to radiometric scaling.

3.2.2.2 Bias accuracy

a) The bias error of the shortwave (≤ 2.25 µm) VII channels shall be < 5% (Threshold), < 4% (Breakthrough), < 3% (Objective) over the dynamic range 0.05 L_{high} to L_{high} (L_{high} defined in Table 11 for a uniform, unpolarised scene.
b) The bias error of the longwave VII channels (≥ 3.74 µm) shall be < 0.5 K for a typical target Table 11. For all other temperatures, the bias error shall be multiplied with the radiometric scaling function.

3.2.2.3 Orbit stability

a) Maximum differences of radiometric biases in the shortwave (≤ 2.25 µm) VII channels during any single orbit (limited to the daytime part) shall be < 1% over the dynamic range 0.05 L_{high} to L_{high} (L_{high} defined in Table 11.
b) Maximum differences of radiometric biases in the longwave (≥ 3.74 µm) VII channels during any single orbit shall be < 0.15 K for typical target brightness temperatures given in Table 11 for

reference scene, $T_{typical}$. For other brightness temperatures the required value shall be multiplied by the radiometric scaling function.

3.2.2.4 Lifetime stability

a) Maximum differences of running averages over one orbit (limited to the daytime part) of the radiometric biases in the shortwave (≤ 2.25 μm) VII channels are < 1% in reflectance over the dynamic range 0.05 L_{high} to L_{high} (L_{high} defined in Table 11.
b) Maximum differences of running averages over one orbit of the radiometric biases in the longwave (≥ 3.74 μm) VII channels are < 0.15 K for typical target brightness temperatures given in Table 11. For other brightness temperatures the required value shall be multiplied by the radiometric scaling function.

3.2.2.5 Radiometric homogeneity

a) Inter-channel radiometric bias differences between different shortwave (≤ 2.25 μm) VII channels of the same spatial sample shall be as listed for the channel groups below in terms of reflectance, when viewing the same spectrally and spatially un-polarised homogeneous target over the dynamic range 0.05 L_{high} to L_{high} (L_{high} defined in Table 1) .

   VNIR-VNIR < 1.00 %
   SWIR-SWIR < 1.05 %
   VNIR-SWIR < 1.25 %
   where VNIR corresponds to channels VII-4 to VII-20 and SWIR to channels VII-22 to VII-30.
b) Inter-channel brightness temperature bias differences between different longwave (≥ 3.74 μm) VII channel pairs of the same spatial sample shall be as listed in Table 15 for a spatially and spectrally un-polarised homogeneous target of 280 K.

(K)	**VII-28**	**VII-30**	**VII-33**	**VII-34**	**VII-35**	**VII-37**	**VII-39**	**VII-40**
VII-26	0.12	0.12	0.11	0.11	0.12	0.12	0.125	0.12
VII-28		0.11	0.10	0.10	0.11	0.11	011	0.11
VII-30			0.10	0.10	0.11	0.11	0.11	0.10
VII-33				0.10	0.10	0.10	0.10	0.10
VII-34					0.10	0.10	0.10	0.10
VII-35						0.11	0.115	0.11
VII-37							0.115	0.11
VII-39								0.11

Table 15: VII inter-channel homogeneity for longwave channel pairs.

a) Inter-spatial radiometric bias differences between different VII spatial samples of the same shortwave channel shall be < 1%, in terms of reflectance, when viewing the same spectrally and spatially un-polarised homogeneous target over the dynamic range 0.05 L_{high} to L_{high} (L_{high} as in Table 11).
b) Inter-spatial brightness temperature bias differences between different VII spatial samples of the same longwave channel shall be < 0.1 K for a spatially and spectrally un-polarised homogeneous target of 280 K. For other brightness temperatures the required value shall be multiplied by the radiometric scaling function.

3.2.2.6 Stray light and crosstalk

The error due to stray light and detector crosstalk shall be included in the VII radiometric error budgets.

Solar channels:

a) For a VII image consisting of 21 × 21 dark pixels at radiance $L_{typical}$ in the centre of 101 × 101 bright pixels at radiance L_{high}, the dark signal contamination from the bright neighbours in the centre of the 21 × 21 dark pixels shall be less than 1%.

Thermal channels:

b) For a VII image consisting of 11 × 11 dark pixels at brightness temperature $T_{typical}$ in the centre of 101 × 101 bright pixels at brightness temperature T_{high} < 350 K the dark signal contamination from bright neighbours in the centre of the 11 × 11 dark pixels shall be less than 0.1 K.

3.2.2.7 Polarisation

a) The VII channels (VII-3 to VII-25) shall be insensitive to polarisation. The polarisation sensitivity shall be < 5% (threshold), < 2% (objective).
b) For the VII channels (VII-26 to VII-40)), the polarisation sensitivity shall be < 11% (threshold, < 5% (breakthrough) and 0% (objective).
c)The polarisation sensitivity shall be characterised to within 0.5%.
d) The polarisation sensitivity shall not vary by more than 2% (threshold), 1 % (objective) across the swath.

3.2.3 Geometrical and temporal Specifications

3.2.3.1 Swath

The VII shall provide measurements over a total scan angle of 106° (T), 110° (O), perpendicular to the satellite velocity, symmetrically about the geocentric nadir direction.

3.2.3.2 Spatial sampling

3.2.3.3 The VII spatial sampling distance at geocentric nadir shall be < 0.5 km for all channels. Angular sampling

The VII shall have a constant angular sampling for the entire swath derived from the spatial sampling distance at geocentric nadir. For off-nadir measurements, the spatial sampling distance will be determined by the orbit and Earth projection.

3.2.3.4 MTF

The VII modulation transfer function (MTF) shall be as described in Table 16.

Note: The MTF specification does not include the sampling MTF component.

f/f_{Nyq}	**MTF** **Normalised to local maximum**
0.00	1.0
0.25	> 0.9
0.50	> 0.7
0.75	> 0.5
1.00	> 0.3
1.50	< 0.55 * MTF@f_{Nyq}
> 2.00	< 0.35 * MTF@f_{Nyq}
> 4.00	< 0.20 * MTF@f_{Nyq}

Table 16. VII MTF specification.

Note 1: f is the spatial frequency, f_{Nyq} is the Nyquist frequency, defined as $1/(2 \cdot SSD_{nadir})$.

The VII Modulation Transfer Function (MTF) shall be isotropic within 35%/20%/10% (T/B/O).

Note: Isotropy is defined as $100\% \times (MTF_{ALT} - MTF_{ACT})/MTF_{ALT}$, where indices ALT and ACT refer to along-track and across-track, respectively.

In order to achieve homogeneity along scan, the VII MTF (normalised to its local maximum as in Table 16) must not vary by more than 0.05 @ $f/f_{Nyq} = 0.50$.

The VII MTF must not vary by more than 0.05 @ $f/f_{Nyq} = 0.50$ over the mission lifetime.

3.2.3.5 Geolocation

The VII geolocation shall be known with accuracy < 100 m (Objective), < 250 m (Breakthrough), < 500 m (Threshold).

3.2.3.6 Pointing knowledge

The VII pointing knowledge shall be better than 0.25° (Threshold), 0. 1° (Breakthrough).

3.2.3.7 Co-registration

Measurements from different spectral channels shall be spatially co-registered such that

$$(1-\Delta_{scan})(1-\Delta_{track}) > 0.8$$

where Δ_{scan} and Δ_{track} are the channel spatial sample mis-registrations in the scan and along-track directions respectively, normalised to the SSD.

Note: all inter-channel co-registrations are absolute within an arbitrary frame of reference, i.e. the observations must physically overlap. However, only knowledge of the location of the arbitrary reference frame with respect to the Earth's surface is required, as specified by the geolocation requirement.

Measurements at different VII spectral channels shall be temporally co-registered within < 1 s (objective), < 2 s (breakthrough), 3 s (threshold).

4 METimage Science

4.1 Overview

METimage data will have potential for use in a range of operational and research applications. To exploit this potential, substantial research and development is required to prepare for successful interpretation and application of METimage data and products. Many areas of scientific activity are involved, and these can be divided into the following main areas:

Earth/atmosphere radiative transfer

METimage measures the VIS to IR radiation emitted from the top of the atmosphere (TOA) or scattered by clouds, aerosols and the surface. This measured spectrum is then used to retrieve information about the state of the atmosphere and of the surface of the Earth. Before we can solve this "retrieval" problem, we must first understand and be able to model accurately the associated "forward" or "radiative transfer" (RT) problem. In other words, we must be able to simulate, given a description of the state of the atmosphere, the radiance spectrum emitted from the TOA as measured by the instrument for a wide range of atmospheric conditions. Such calculations must be performed not only accurately but also very efficiently if they are to be used as part of operational retrievals.

Retrieval of geophysical parameters

The procedures for extracting from the measured TOA radiances the information on geophysical parameters to which they are sensitive are not straightforward. They require the capability not only to model the "forward problem" (as explained above) but also to solve the associated inverse problem. In other words, given the measured TOA radiances, how do we estimate the most probable geophysical parameters to which they correspond, given the fact that the problem might often be underconstrained and be highly reliant on accurate a priori information. In this section, the status of the operational retrievals of the various METimage products is described and areas requiring further development identified.

METimage data ingest process

No instrument is perfect and will inevitably introduce some artefacts in to the measurement data that need to be corrected for. In order to be able to do this, it is important to understand the

processes that affect the passage of photons through the instrument and conversion to counts at the detector stages.

Level 1 processing

Level 1 processing concerns the conversion of instrument raw data counts to calibrated and geolocated radiances. This section describes the level 1 processing itself, beginning with generic requirements before moving on to describe the main tasks for generation of level 1b data (calibration and geolocation) and the various types of calibration required. It then moves on to describe the scientific needs in terms of the calibration and role of auxiliary data, traceability, transparency and re-analyses.

Level 2 processing

Level 2 processing involves the retrieval of geophysical products beginning with calibrated level 1b radiances. For METimage, level 2 retrievals must be based on proven operational techniques. This section describes the scientific needs for the operational level 2 processors themselves and their validation. The role of prototype processors, test data and the need for instrument characterisation parameters are discussed.

Monitoring and validation of METimage data and products

When the METimage data become available, they must be monitored, at various stages of the processing, to ensure that their characteristics conform to those expected by the data processing and to quantify aspects of their quality and quantity. It is expected that a small proportion of the data will not meet normal standards of quality. These data must be detected, through quality control procedures, otherwise they will seriously degrade subsequent products. Some characteristics of the data will be uncertain prior to launch and may change with time after launch. These characteristics must be monitored carefully, and relevant aspects of the data processing must include ongoing tuning to take account of these changes. Appropriate methods and tools must be generated for:

- monitoring the performance of the METimage instrument and each stage of the data processing;
- performing necessary quality control steps;
- tuning relevant stages of the data processing;
- validation of METimage data and products.

Data re-processing for climate

Since several METimage variables correspond to the Global Climate Observing System (GCOS) ECVs, the needs for data reprocessing must be taken on board in order that artefacts arising from changes in the behavior of the instrument and algorithm updates are not erroneously interpreted as a climate change signal.

Applications of METimage data and products

METimage is designed to provide high quality image including many relevant parameters for NWP NWC, climate monitoring, research and process studies with highest benefit in Polar regions where space-borne imagery data from geostationary satellites are not available. This section describes the benefits of METimage observations for these application areas.

Needs of direct read-out users

The availability of a direct data broadcast facility is considered mandatory for remote locations

which must be able to perform level 0 to level 1b processing in an end-to-end fashion within 5 minutes from acquisition. The creation of simple, modular and transportable processors for use in such locations is essential.

4.2 Earth-atmosphere Radiative Transfer

4.2.1 Atmospheric and Surface variables

4.2.1.1 Clear Atmosphere

Clear-sky radiative transfer at solar (< 3 µm) and thermal IR wavelengths (> 3 µm) is determined by the vertical concentration distribution of radiatively active gases and their vertical pressure and temperature profiles. In the solar spectral region, the emission of the Earth and atmosphere is negligible and radiative transfer in the clear aerosol-free sky is solely determined by molecular (Rayleigh) scattering and gaseous absorption. For solar wavelengths larger than 0.4 µm the main atmospheric absorbers which play a role in the shortwave energy budget are H_2O, O_3, O_2, CO_2, and NO_2, CO, CH_4 and N_2O. Since O_2 is a uniformly mixed gas in the homosphere absorption in the O_2 A-band can be used to infer information on cloud top heights and cloud geometrical thickness. Regarding water vapour continuum effects for solar wavelengths it has been found recently that continuum effects in the NIR window channels may have some impact on the retrieval of cloud properties (Ptashnik et al. 2011).

Apparently comprehensive data bases of all such gases detailing line shape parameters for relevant pressures and temperatures exist, notably the HITRAN data base (Rothman et al. 2004, 2008). The continuum absorption of water vapour is critical for many wavelengths, and must be represented consistently with the formulation of the lines in the spectroscopic database used. Line-by-line (lbl) integration of monochromatic radiative transfer to channel-integrated results appears to be adequate if the spectral resolution is ~0.01 cm^{-1}. These lbl models constitute the benchmark basis from which faster radiative transfer treatments and paramaterisations can be derived. The required vertical resolution of temperature and the poorly mixed gases is dependent on the channel wavelength and typically varies considerably with pressure, so this must be assessed carefully. Radiatively active gases need only be included that cause variability in brightness temperature that is significant relative to the channel NEΔT. For example, the gases that affect brightness temperatures in any of the IR window channels by > 0.005 K are H_2O, CO_2, O_3, N_2O, CH_4, HNO_3, C_2H_6, F11, and F12 (Embury et al. 2011).

4.2.1.2 Clouds

Atmospheric radiation is strongly influenced by clouds. This holds for the solar as well as for the thermal spectral range. The net radiative effect of a cloud in observation depends on the wavelength, the observation geometry, the particle phase, particle size, and particle shape. All cloud properties are subject to strong temporal and spatial variations. These physical parameters translate to the following three parameters, required for radiative transfer and remote sensing:

1. Single scattering albedo as a measure of macroscopic absorption/emission;
2. Volume extinction coefficient as a measure of the probability of interaction (absorption + scattering);
3. Scattering phase-function (see Figure 3) as a measure of the energy distribution in case of a scatter-event.

The preparation for the METimage requires the whole bandwidth of variations to be taken into

account. A realistic dataset of clouds is essential to determine unique features or thresholds for the later discrimination of properties. The integration of complex, multi-layered clouds will give valuable hints on possible problems and limits of the detectability.

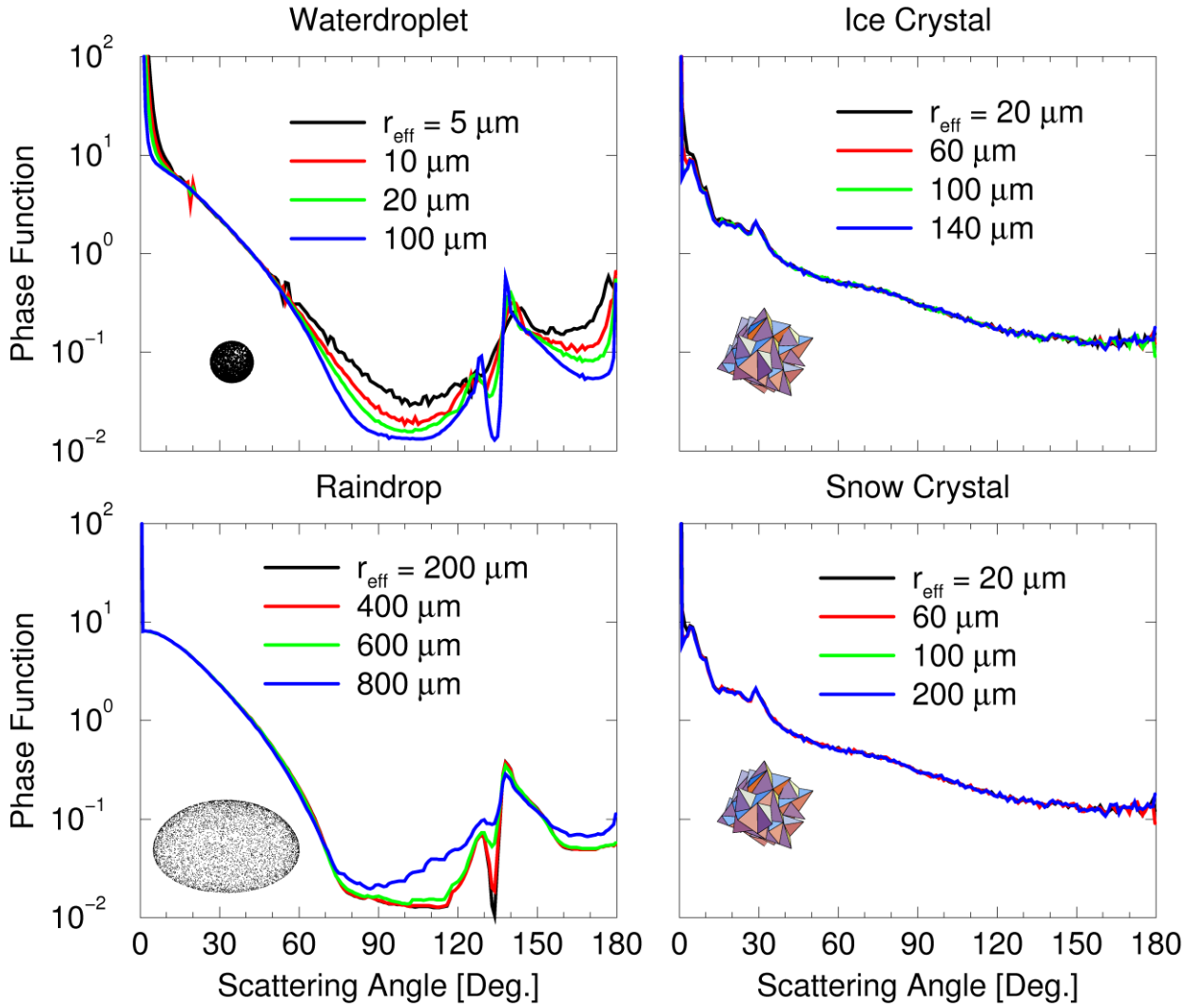

Figure 3: Scattering phase-functions for the wavelength of 550 nm for cloud hydrometeors and their characteristic effective radii, following Macke et al. (1996) and Macke and Grossklaus (1998).

With decreasing cloud optical thickness (COT), the cloud becomes transparent and the underlying surface properties become more important. For satellite pixels containing cloudy and cloud free parts, surface contributions have to be taken into account as well. In both cases, it is not possible to process the cloud properties without separating the signals of the cloudy and cloudless parts.

Generally cloudy pixels are brighter (i.e., have a higher reflectivity) in the visible spectral range compared to their cloud-free counterparts and provide a lower brightness-temperature in the infrared. Certain atmospheric or surface conditions can destroy this relationship:

- Snow covered surfaces can be colder than clouds and may display an even higher reflectivity;

- Desert sand provides a high reflectivity too and due to a reduced emissivity (in the near infrared) it may appear very cold;
- Strong inversions may increase the temperature of the clouds compared to the ground.

Additional information on 'clear-sky' atmosphere and surface properties and condition are essential to tackle such situations.

In retrievals, based on a domain-size considerably smaller than 1 km × 1 km, individual pixels can not be considered independent (Varnai and Marshak 2001), but contaminated by information from surrounding pixels. This so called radiative smoothing (e.g., Davis et al. 1997) is most pronounced under high sensor zenith angles in combination with inhomogeneous clouds. A realistic simulation of observations requires therefore cloud parameters provided at high resolution and 3D.

4.2.1.3 Aerosols

Aerosols are a ubiquitous constituent of the atmosphere. They are essential for the radiation balance of the cloud free atmosphere in the VIS and SWIR, and they affect the formation and life cycle of clouds and their radiative properties through direct and indirect aerosol effects. Their chemical composition, the particle shapes, the size distributions and consequently their optical properties are highly variable, as are their natural and anthropogenic sources. In addition, the aerosol life cycle in the atmosphere is also highly variable, influenced by humidity, wind fields, surface properties, volcanic eruptions and abundance of hydrometeors.

In satellite based passive remote sensing aerosols are commonly characterised by their optical properties, the latter four being wavelength dependent:

- optical thickness (typically at 550, 675 nm, or similar) τ, e.g. for MODIS separated into fine and coarse mode;
- spectral slope of the extinction coefficient or optical thickness, expressed by the Ångstrøm parameter α;
- single scattering albedo ω, aerosol absorption index (in the UV);
- scattering asymmetry parameter g;
- scattering phase function.

Some aerosol types are known for changing their radiative properties with time. Black carbon for instance becomes generally denser with time. This is accompanied by a change in fractal dimension which on the other hand alters the single scattering albedo and scattering phase function (see Kahnert and Devasthale 2011). Also processes like coating or bridging (sintering) are pronounced to affect optical properties. Aerosol coagulation proceeds different compared to cloud-dynamics. Secondary aerosol, for example, is known for absorption of nano-aerosol particles without a noteworthy growing of larger particles.

In addition to the optical and temporal properties of aerosols, vertical distribution of the aerosol is also important. Column integrated aerosol optical thickness (AOT) alone does not provide enough information for accurate TOA radiance calculations and is insufficient for many applications including air quality forecasts and volcanic ash tracking where height resolved aerosol information is needed.

Several studies have shown that volcanic aerosols may have a direct influence on cloud formation and cloud microphysics (Martucci et al. 2012, Yuan et al. 2011). For example, sulfate aerosol can act as an additional source for cloud condensation nuclei (CCN) as was found by the degassing Mount Michael volcano on Saunders Island in the South Atlantic Ocean. Based on satellite observations from the MODIS instrument on board NASA's Aqua satellite Gassó (2008) found

large reductions in the cloud effective radius for low-level marine clouds. More recently the eruption of the Icelandic Eyjafjallajökull volcano in 2010 had a severe impact on aviation over Europe. It could be demonstrated (O'Dowd et al. 2012) that for the majority of the ash plumes, all condensation nuclei (CN) were activated into CCN. Also it was found that, compared to background levels, aerosol absorption increased by about a factor of two in the plume.

The remote sensing of aerosols above land and ocean differs due the fact that the optical properties of the surface and the type of aerosols present are usually quite different. For example, at red wavelengths, aerosol appears bright over a dark ocean whereas blue wavelengths can be used to sense aerosol (which appears dark) over brighter land surfaces.

Due to their omnipresence aerosols must be always considered when doing remote sensing between the UV and the SWIR (even the TIR for high aerosol loadings) as if ignored, artefacts can be introduced in to the retrieval of other products. Situations where this is important include:

- atmospheric correction of clear sky imagery (vegetation, albedo);
- correction of multiple scattering influence for trace gases (water vapour, surface pressure) retrievals;
- absorbing aerosols above low level clouds (otherwise the wrong cloud microphysics / liquid water is retrieved);
- modulation of cloud properties due to volcanic emissions;
- SST, in particular after desert dust outbreaks;
- vertically resolved heating rates;
- fire monitoring;
- aerosol loads over megacities (black carbon and brown clouds);
- volcanic ash tracking: eruptions (e.g., Pinatubo) can impact the generation of time series related to land surface products. If ignored, increased AOD can result in a bias / offset in trend calculation particularly for "dark" surfaces (vegetation, chlorophyll-sea).

Either the correction of aerosol effects is inherently included in the aforementioned retrievals or they need to be based on the retrieved properties. In the latter case it is essential to use exactly the same aerosol models in the correction algorithms as in the retrieval algorithms.

4.2.1.4 Land Surface

Land surface plays an important role in the TOA radiance for channels with weighting functions that sense the surface as it forms the lower boundary for atmospheric radiative transfer. Compared to ocean surfaces, the high heterogeneity means that single observations can be influenced by several surface types in some areas. In general, almost every pixel (independent of the spatial resolution) is influenced by surface types at subpixel scale. Hence, the final reflectance/emission distribution is composed by different surface types, which has to be taken into account for product generation using appropriate methods. The behaviour of the surface response is a function of surface type, illumination/heating conditions and directionality in terms of the illumination/observation geometry at all wavelengths (VIS-NIR-TIR).

For the thermal channels, the heterogeneity of the land surface within a satellite pixel is, of course, important, and consists of two aspects. First, within the pixel, different surfaces (e.g., leaves, woody matter, soil, rock, tarmac, etc) have different, wavelength-dependent thermal emissivity. Second, within the pixel, different objects may have markedly differing temperature; this is particularly significant during the day, as a function of differential heating of objects by absorption of sunlight, shadowing, height (e.g., within a vegetation canopy), etc. but also during night due to the different

storage capacity of heat and emission of radiation in the thermal spectrum. Thus, temperature-radiance relationships for heterogeneous land surfaces are significantly more complex than for water bodies, for example. Indeed, the whole concept of "land surface temperature" over a satellite pixel scale is subject to an intrinsic definitional uncertainty, and emissivity modelling on this scale is impractical except in a statistical sense (e.g., parameterised in terms of some definition of land surface cover). The issues will be relevant for channels with weighting functions that significantly intersect the surface (e.g., for channels with spectral positions in the range of 3-4 μm, and 10-12 μm). At thermal infra-red wavelengths (TIR, central wavelength > 4.1 μm), the upwelling radiance from the land surface is dominated by thermal emission, with a smaller (but highly variable) contribution from reflected sky radiation, and a yet smaller (often negligible) contribution from the reflected direct solar radiance (during the day) but thermal sensing of mountains (e.g., valleys) is influenced from the emission of neighbouring slopes (cavity effect) which cannot be neglected. For the IR channels in the range 3.5 to 4.1 μm (VII-26 – VII-30), the comments for the TIR channels apply, and in addition, for day time images, there is the complexity of the reflected solar component no longer necessarily being small (depending on the surface emissivities present).

For solar radiation, the upwelling radiance form the land surface is determined by the land surface reflectance as a function of illumination and observation conditions. The bi-directional reflectance distribution function (BRDF) describes how the reflectance depends on the view and solar angles and provides land surface reflectance explicitly in terms of its spectral, directional, spatial and temporal characteristics. The resulting reflectance function is composed of a surface contribution and a volume scattering. Appropriate kernels based on the listed parameters below weigh the contribution from each layer. Key causes for land surface reflectance anisotropy and the resulting nonlinear relationship between albedo and the reflectance are:

- specular reflection (e.g., forward scattering from snow, leaf or soil);
- surface roughness;
- volume scattering (e.g., vegetation, snow);
- shadow effects (e.g., forests where trees cast shadows, mountains).

Detailed maps of land type, surface elevation (aspect and slope) and illumination conditions are thus needed in order to represent the land-atmosphere boundary in retrievals.

4.2.1.5 Cryosphere

In a broader sense, the cryosphere comprises all material with a significant amount of frozen water (e.g., snow, glacier ice, river ice, permafrost, sea ice, shelf ice, ice sheet, etc.). The following sections will give a brief description of the different parameters (more can be found at http://www.wmo.int/pages/prog/gcos/index.php?name=EssentialClimateVariables).

Sea ice

The inter-annual variability of sea ice in the Northern and Southern hemisphere is an important parameter for our climate. Sea ice can be classified into the following table:

Type	***Properties***
frazil ice	*liquid mixture between ice particles and water*
pancake ice	*beginning of solidification*
first year ice	*solid, thickness up to 2 m*
multiyear ice incl. ridges	*solid, thickness up to 4 m*

polynyas	*open water, short time event, high energy loss from ocean due to temperature contrast between ocean (-1.7°C) and atmosphere.*

Table 17. Sea ice types

Sensor channels in the visible are used to monitor the following parameters but only during day light:

- sea ice distribution (pure sea ice or sea ice with snow show high spectral reflectance in VIS);
- sea ice concentration (%); sea ice coverage/open sea; open water: low reflectance in VIS;
- melt ponds on sea ice (needed spectra: see table based on Tschudi et al. 2008).

Thermal spectra can be used as an additional information to distinguish between sea ice and water if there is a high temperature difference (e.g., polynyas during polar night). With increased solar radiation during spring sea ice starts melting on the surface, too. Melt ponds form and cover part of the sea ice. The temperature difference between ocean and sea ice covered with melt ponds is too small for a successful classification. But the day-night variability of the temperature between both surface types can be used as additional information to improve sea ice detection. Hence, a high temporal resolution of satellite data is needed. Furthermore, the mixed pixel problem (melt ponds are smaller than the spatial resolution of the sensor) require a spectral unmixing procedure to gain an information on the percentage of melt pond coverage per pixel.

Channels needed: (based on figure of Tschudi et al. 2008)

Sea ice type	albedo (500 nm)	albedo (600 nm)	albedo (1000 nm)	albedo (1600 nm)
dry snow	0.95	0.95	0.78	0.12
melting snow	0.75	0.75	0.4	0.05
bare white ice	0.73	0.73	0.32	0.05
dirty bare ice	0.4	0.45	0.28	0.02
deep blue pond	0.3	0.25	0.07	0.05
blue – green pond	0.25	0.25	0.09	0.02
dark pond	0.15	0.12	0.07	0.02

Table 18. Albedo of sea ice types and snow as a function of wavelength.

Snow

The high spectral albedo of snow in the short wave (0.4 – 0.7 µm) makes this coverage an important factor for weather forecast models and climate related investigations. Almost 80% of the short wave irradiance is reflected, which is an essential contribution in the energy balance.

Snow detection

Snow detection relies on the contrast between ground and snow in the visible spectra. Pure snow covered pixels can be detected by threshold methods or

normalized indices, like the normalized difference snow index (NDSI) combining short wave and near or mid infrared channels. In general, during night or polar winter sensors working in the optical and thermal spectra have not the capability to detect on a reliable basis snow cover but improved sensitivity for low radiances (e.g., VIIRS) provide reliable snow cover information considering only moon light as illumination source. Critical for the quality to monitor snow extent is a reliable cloud detection and masking approach.

Snow cover

Similar methods as those mentioned for snow detection are valid for mapping the extent of snow. Monitoring of snow cover has a spatial and temporal component. Daily monitoring capabilities are a requirement to monitor the high temporal and spatial changes of the snow cover (i.e., during the accumulation phase at the beginning of winter). A spatial resolution of 250-500 m is recommended for global applications to make the sensor usable for small snow fields in the mountains.

Snow grain size

Typical snow grain sizes range from 0.1 (fresh snow) to 2.0 mm (old snow). The snow grain size is a rough measure of the age and density of the snow layer. Due to the absorption characteristic of ice the snow layer shows an absorption maximum at 960 – 1090 nm. This spectral range is sensitive to the grain size (see Figure 4 and Figure 5).

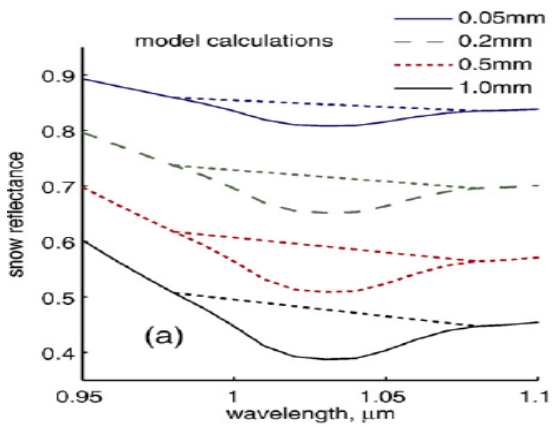

Figure 4. Model calculations of the scaled area for snow grains from 0.05 – 1.0 mm (Dozier et al. 2009).

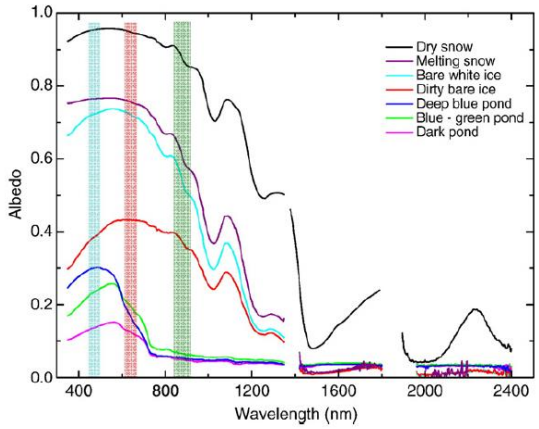

Fig. 2. Spectral reflectance of surface feature types measured near Barrow, Alaska, June 2004. MODIS spectral coverage for, from left to right, bands 3,1,2.

Figure 5. Spectral reflectances (Tschudi et al. 2008).

Snow albedo

The broad band albedo of snow (350 – 3000 nm) is dominated by the low absorption of ice in the shortwave spectra, which cause high reflectance values in the wavelengths 400 – 700 nm. The albedo of fresh fallen snow can exceed 80% whereas old snow with some impurities has values lower than 40%. The contribution in the NIR and SWIR spectral range for the high reflectance values is limited by the increased absorption coefficient of ice. Snow albedo is influenced by impurities (soot, dust, algae) on the surface, BRDF, shadow effects in mountains and depth, density and grain size of the snow cover.

Snow surface temperature

The maximum temperature of snow is 0°C resulting in a longwave heat flux of 214 W m^{-2}. The snow surface temperature can be as low as -60°C in the Northern Hemisphere during polar winter and even colder in Greenland or Antarctica. Hence, the temperature range between 0 and -70°C should be detectable by thermal sensors. In the spectral band 10 – 12 µm the emissivity of snow ranges between 0.998 and 0.97 depending on snow conditions (wet, dry, grain size) and wavelength (Figure 6). A precise measurement of the snow surface temperature (→ split window approach) requires a detailed knowledge on the spectral emissivity and a reliable cloud masking to eliminate clouds and sub pixel clouds as well.

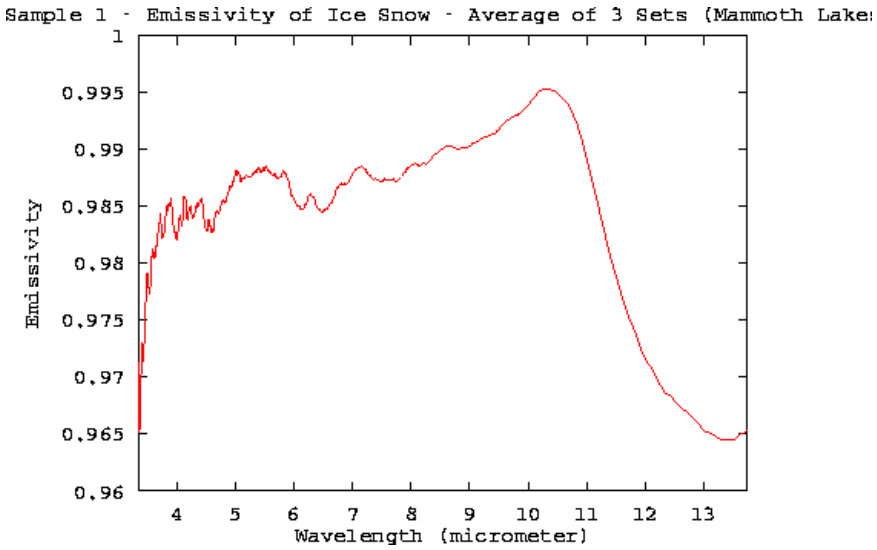

Figure 6. Emissivity of ice snow at 3.5 – 13.5 µm (http://g.icess.ucsb.edu/modis/EMIS/images/snowmam01.gif).

Land ice

Definition of land ice (glaciers, ice caps)

Land ice has a density of ca. 980 kg m^{-3} and is composed of compacted frozen snow. Due to the compression the amount of interfaces air-ice-air are no longer existent. Hence, the reflectance of pure glacier ice is reduced of about 30 – 40%. Only some gaseous bubbles and impurities (ash layer, dust, etc.) may further modify the reflectance. However, the shape of the reflectance curve remains the same like snow. Glacier ice exposed for a longer time is covered by dust and rocks resulting in a further decrease of albedo.

Land ice cover

Monitoring and mapping of small mountain glaciers require a high spatial resolution of 50 m or better as recommended by the Integrated Global Observing Strategy (IGOS) and the World Glacier Monitoring Service (WGMS). Subsequently, small glaciers will be not the core feature to be sensed by post-EPS mission sensors. But ice caps and ice fields, like the Southern Patagonia ice field with about 13.000 km^2 can be mapped with sufficient accuracy by sensors with a spatial resolution of 500 m. Operational satellites overpassing glaciated areas on a daily cycle are an advantage for an compositing that minimizes cloud coverage. In general, the same spectra as for snow (see table) are useful for land ice monitoring, derivation of albedo and ice surface temperature.

Permafrost

The term “permafrost” describes frozen soil not melted during summer with depths of 4 – 300 m. The permafrost affected area (Siberia, Canada, Alaska, etc.) cannot be detected by data available from METimage. There is no possibility to distinguish between frozen soil and permafrost. It is not recommended to monitor permafrost based on visible and thermal channels without any auxiliary data (climate data, land cover) and models.

4.2.1.6 Water Surfaces

Water surfaces are dynamic in that the statistical distribution of the slope of the air-sea interface changes in response to the wind. Because reflection and emission from a plane water surface varies in a textbook manner with the viewing angle (and incidence angle, in the case of reflection), this clearly causes both the interface bidirectional reflectance distribution and the effective emissivity of a water surface to vary with wind speed. Strictly, wind speed alone is insufficient, since fetch and the maturity of the wave state affect the slope distribution in complex ways, and this distinguishes open ocean from coastal regimes and lakes. Moreover, the along-wind and across-wind slope statistics are not identical. Proper integration of reflected, emitted, double-reflected and emitted-reflected radiance would require a three-dimensional model or statistical knowledge of shadowing and joint probabilities for slope-pairs within line-of-sight of each other. Lastly, as wind speed increases, water surfaces become partly covered with bubbles, whose reflectance and emissivity properties differ. While the full treatment of these surface-state and geometrical effects is not solved, it is likely that existing approximate treatments (Masuda 2006, Filipiak et al. 2008, Nalli et al. 2008]) are adequate to within the uncertainty of single-pixel observations for thermal and near infrared wavelengths. Measurements at sea indicate that the wind-speed dependence of the apparent infrared emissivity is smaller than indicated by the earlier models (Hanafin and Minnett 2005).

In addition to representing the effects of view-angle and wind speed (i.e., wave state), models of surface emissivity for use in the thermal infrared should account for the temperature and salinity dependencies of the complex refractive index. These dependencies are not entirely established in the literature (see Embury et al. 2011), although published information is probably adequate to support the required accuracies of sea and lake surface temperature estimation.

In the case of reflectance at wavelengths where there is significant penetration depth, volume scattering and absorption are important in addition to the surface (interface) reflection, and this is the subject of a vast literature related to the effects of turbid water components and biological scatterers (phytoplankton). Over much of the open ocean the concentration of volume scatterers is low but in coastal regions there is often a temporally and spatially high concentration and variability of absorbing material (e.g., Chromophoric Dissolved Organic Matter, CDOM) or scatterers (suspended sediments, plankton, land runoff) that can confound the algorithms used to derive atmospheric variables. In shallow waters, such as near coasts or over coral reefs, reflection from the sea-floor should also be taken into account, and this requires knowledge of the optical properties of the substrate, and the water depth (i.e., tides). The variability of the background water-leaving radiance can in turn render very difficult, but not impossible, the retrieval of some atmospheric properties, such as those of aerosols (Wang et al. 2005, Remer et al. 2005).

4.2.1.7 Profile and Surface Data Sets for Simulations

Clear sky

For state-of-the-art simulations of clear-sky TOA radiances for METimage in the solar channels at least an a priori knowledge of pressure, temperature and humidity profiles as well as some a-priori knowledge of the total columnar ozone content is needed. For the pixel under observation the total

atmospheric pressure is important since it determines both the Rayleigh scattering optical depth of the column and the reflectance signal in the O_2 A-band channel. For atmospheres containing aerosols and clouds as well as for spectral surface albedo and surface skin temperatures CIRC (Continual Intercomparison of Radiation Codes, http://circ.gsfc.nasa.gov/; Oreopulos et al. 2011) provides a catalog of well-defined cases which can be used for radiative transfer code evaluation.

For the simulation of clear-sky transmittance at infrared wavelengths, the aerosol-free atmosphere can be well approximated as a non-scattering medium, thereby rendering radiative transfer simulations manageable, and a key issue is the proper sampling of the full variability of meteorological parameters (temperature and water vapour profiles, together with air-surface temperature difference). Profiles from NWP models are useful for this purpose, subject to taking care of certain aspects. An example is the profile sets of Chevallier (2002) and Chevallier et al. (2006). For clear-sky simulation, it may be appropriate to exclude from such a set those profiles with 100% cloud cover (or relative humidity above some threshold such as 95%), to reduce a humidity bias relative to observed clear-sky locations. Also, what surface temperature is appropriate to associate with the profile depends on the application (e.g., for the sea surface temperature application in sea-ice areas, see Embury et al. 2010). To represent the spatial distribution of relevant atmospheric variability, output from the analysis fields of NWP models can be used.

A second key issue for clear-sky simulation in the infrared and solar channels is specification of trace gas concentrations and profiles. Depending on the channel, the trace gas and the application,and the level of detail to which the trace gas profile needs to be specified may vary from the global mean annual average (for a long-lived trace gas with a small impact on brightness temperature variability, e.g., CO_2 for the 11 μm channel) through inclusion of some seasonal and/or latitudinal variability, to fully sampling variability in association with meteorological variability (surface pressure, total columns of water vapor and ozone). MIPAS reference atmospheres (Remedios et al. 2007) are useful where only generic/typical trace gas profiles are required. Similarly, atmospheric profiles can be selected from NWP models such as the 83 profile subset of a comprehensive ECMWF profile dataset assembled by Chevallier et al. (2006), which is used in the RTTOV context.

Clouds

The main issue for a realistic treatment of the cloud's influences on the radiation field is to cover the variance at pixel level (this is sufficient if considered as independent).

The major impact of clouds is demonstrated in the absorbing wavelength range (IR). Dominant cloud properties in this spectral region are cloud temperature and particle size (e.g., Nakajima and King 1990).

The VIS part of the spectrum is most affected by the total optical thickness. Nevertheless, cloud composition, variations in cloud height, particle phase (and mixing ratio), geometrical thickness, size spectra and multiple cloud layers must be taken into account.

A general difference of radiation fields at absorbing and non-absorbing wavelengths is the penetration depth. While 'non-absorbing beams' are able to sense the entire cloud layer, reflected or emitted IR beams carry no information from deeper cloud areas.

As mentioned in chapter 4.2.1.2 cloud pixels are not independent. Thus, to make a database even more realistic (i.e., three dimensional), it should cover surrounding pixels and their variations also. Since there is a physical coupling between neighbouring pixels, the degree of freedom can be reduced here. Unfortunately, there are no direct observations of 3D cloud fields. However, cloud models (see chapter 4.2.1.2 or model supported observations (e.g., Evans and Wiscombe 2004) provide pseudo-realistic fields with all required optical parameters available. A compilation of tools to generate various 3D cloud fields can be found at

http://i3rc.gsfc.nasa.gov/Public_codes_clouds.htm.

3D cloud fields generated by models are also a suitable source for cloud optical parameters at the single column level; however, with growing horizontal inhomogeneity and associated net horizontal energy transport the comprehension of adjacent columns becomes more important at higher spatial resolution.

Directly related to the need for a realistic and detailed cloud database is the need for proper validation possibilities. Here the ground based validation suffers from probing different volumes (upward looking instruments feature in contrast to their downward looking counterparts an upside down-cone and, if not the whole depth of the cloud is permeated, there might be no overlap in the probed volumes of the groundbased and the spaceborne instrument) and bad colocation rates for polar satellites. A setup of a polar platform with active instruments (LIDAR/RADAR) in an appropriate orbit would solve these problems.

The success story of Cloudsat (with the nadir looking radar CPR onboard) and CALIPSO (carrying CALIOP a nadir looking lidar) represent a useful example here. For the first time these platforms allowed for a sound and comprehensive validation of cloud products based on polar orbiting satellites. They did not only raise the bar for validation, they also opened possibilities for new probabilistic cloud-mask algorithms. Additionally, the instruments capabilities of providing in-depth knowledge of the cloud vertical structure, enables training and validation of multi-layer cloud detection algorithms.

Unfortunately, there will be no overlap in operation time of METimage and these two active instruments. Therefore, to exploit the potential of METimage, there is an urgent need for a follow-up mission with comparable active instruments.

Aerosols

The specification of aerosol properties in simulations requires several pieces of information. Assuming that the individual aerosol particles are homogeneous spheres, the wavelength dependent real and imaginary parts of the refractive index (RI) and the aerosol particle size distribution (PSD) need to be specified. For the PSD one typically assumes log-normal type laws (mono-, bi- or multi-modal for which each mode is defined by the modal radius r_m and its variance σ.

Commonly, different aerosol types are defined such as maritime, continental, urban, desert-type and stratospheric aerosols using the information assembled in the OPAC database of Hess et al. (1998) based on input data from Shettle and Fenn (1979) and others. For biomass burning cases additional information on their optical properties needs to be taken into account (Dubovik et al. 2002, Hungershoefer et al. 2008). Note that for the simulation of the single-scattering properties of aerosols the so-called internal and external mixing of different aerosol components can be employed.

A further piece of information required is the vertical distribution of the aerosol particles for which information can be taken from existing datasets of the satellite-borne aerosol lidar CALIPSO, the future ESA Earth Explorer Missions ADM-Aeolus as well as EarthCARE, the planned Franco-German MERLIN lidar climate mission or similar planned future missions.

For example, a global atmospheric database in preparation for ESA's ADM-Aeolus mission has recently been compiled by using CALIPSO night-time total attenuated backscatter data plus additional meteorological parameters from the ECMWF model (Marseille et al. 2011). This database has a full global coverage, covers all seasons and provides vertical information for the characterization of aerosols and clouds from the surface to 40 km altitude.

Aerosol vertical profile information from ground-based lidar observation networks such as the European EARLINET network, is also very valuable. For example, EARLINET data include

profiles for the particle backscatter coefficients (including errors) for one or more wavelengths (355, 532, 1064 nm). In addition, EARLINET operates several Raman-lidars, which can directly provide aerosol extinction coefficient profiles for one or two wavelengths.

Land surface

Contrary to homogenous surfaces (e.g., ocean) land surfaces show a high diversity. Based on the underlying geology and climatic zone the topography, surface and vegetation coverage differs on a local and regional scale and show a high temporal variability. Hence, the emissivity, spectral reflectance and broadband albedo depend on precise knowledge of surface type and orientation etc. Strugnell et al. (2001) were among the first using an improved BRDF parameterization to produce global albedo maps derived from AVHRR data. A global land cover classification and some field measurements of surface directional reflectance were the basis for their developments. They assigned the BRDFs to land cover classes and used the RossThick-LiSparse Reciprocal (RTLSR) model (Li and Strahler 1992, Wanner et al. 1995) to invert the measurements. After the successful launch of Terra/MODIS the focus shifted away from AVHRR to develop enhanced algorithms for land use applications (Friedl et al. 2002, Schaaf et al. 2002). Jin et al. (2003b) and Shuai et al. (2008) investigated the quality of the MODIS BRDF/Albedo product for different biomes and confirm their applicability except for snow and ice-covered areas in Greenland, which underlines the need to monitor cryospheric objects.

Validation data sets for simulation: MODIS land surface products should be used to simulate radiation for METimage channel configuration. The ESA Sentinel-2 satellites / sensors could provide overlapping information at high spatial resolution with a spectral configuration similar to SPOT and Landsat. The matchups between Post-EPS and future satellites depends on the launch dates and life time of sensors, respectively.

Cryosphere

Snow extent (cover): on a global scale or at least for hemispherical coverage information about snow cover/extent will be available from NOAA and/or NSIDC. More details (snow grain size, impurities) are needed for reliable modelling of snow reflectance which will be only acquired for regional investigations. One may consider point measurements of national weather services in combination with snow models (e.g., DISORT-iscrete ordinate radiative transfer code, Stamnes et al. 1988; or SAFRAN-CROCUS, Météo France). It is expected that ESA's Sentinel missions will contribute to snow cover monitoring and expand the data sets generated in the frame of ESA Globsnow project (based on AATSR and AVHRR; validated with Landsat TM and ground measurements).

Snow albedo: modeling the forward scattering (reflectance) of snow covered areas requires detailed information of the snow layer (snow grain size, impurities, density, depth, liquid water content) and of the sensor-sun-surface geometry. Several codes (e.g., MODSCAG—MODIS Snow-Covered Area and Grain size, Painter et al. 2009) are available but the quality of the calculated reflectance relies on proper knowledge of the surface parameter obtained during ground truth campaigns.

Glacier: as mentioned in chapter 4.2.1.5 , the spatial resolution of the Post-EPS mission is not sufficient to map mountain glaciers but ice fields in the Himalaya-Hindu Kush or Patagonia. WGMS did a great effort during the last years (and continues its work in the frame of ESA GlobGlacier and CCI project) to monitor the glaciers of the world. These data are available to simulate reflected radiation from glaciers. However, the surface of glaciers shows a high variability (fresh snow, impurities, glacier ice, debris, etc.), which make it almost impossible to gather all required data to model surface reflectance.

Sea ice: in addition to the temporal change of surface properties (e.g., melt ponds, grain size) sea ice is floating forced by ocean currents and wind stress. Cryosat-2 (or any follow-up mission) data can be used as a source for simulation but due to the high dynamic of sea ice only simultaneous nadir observations (SNO) can be considered for validation. There are chances that Sentinel-2 will deliver some of the needed data during summer time.

Water surfaces

The primary oceanic variable to be derived from METimage data is SST. In the infrared the emission comes from the electromagnetic skin layer on the aqueous side of the air-sea interface, and which has an emission depth (reciprocal of the absorption coefficient in Beer-Lamberts Law) of several μm (e.g., Bertie and Lan 1996). The electromagnetic skin layer is thinner, or comparable in thickness, to the thermal skin layer that results from heat flow between the ocean and atmosphere being facilitated by molecular conduction. The sign of the temperature gradient in the thermal skin layer is nearly always such that the surface is cooler than the underlying water as the conductive heat flow supplies energy for the heat loss to the atmosphere, both the radiant (net infrared) heat loss and the sensible and latent heat losses. Thus the temperature derived from infrared radiometers is generally lower than that at a depth of a millimetre or so, which is referred to as the sub-skin temperature. Conventionally, the temperature beneath the thermal skin layer is called "bulk temperature" as is measured by thermometers in the "bulk" of the water, but given that temperature gradients can exist in the uppermost several metres of the water column, especially in conditions of low wind speed (Böhm et al. 1991, Soloviev and Lukas 1997, Ward 2006, Gentemann et al. 2008, 2009) it is better to refer to these measurements as "temperature at depth" (T_z), where the depth of the measurement, *z*, is given explicitly. These distinctions are developed more fully elsewhere (https://www.ghrsst.org/ghrsst-science/sst-definitions/).

As they propagate through the atmosphere the infrared photons from the sea surface may interact with molecules in the atmosphere, through absorption and emission, with the net result that the equivalent temperature they represent when measured by a spacecraft radiometer is lower than the skin SST. Water vapour is the main atmospheric component that influences the atmospheric infrared radiative transfer, and because of the large temporal and spatial variability of water vapour, an atmospheric correction algorithm must be applied on a pixel-by-pixel basis. The atmospheric effect is wavelength dependent and can be corrected by the combination of bore-sighted measurements taken at different wavelengths, i.e. in different spectral bands of the radiometer (McMillin 1975, Walton et al. 1998, Merchant et al. 2008).

Sensor model

To simulate the data from specific spacecraft instruments, a model of the sensor is needed that characterizes the way the instrument properties influence the measurements. The most important characteristic is the relative spectral response function of each of the sensor spectral bands, and this should include the "out-of-band" response to permit the simulation of spectral cross-talk, if it exists. Other characteristics include the reflectivity of optical surfaces, specifically dependences on wavelength an angle of incidence on the mirror surfaces, polarization sensitivity, detector noise levels and sources of stray light.

4.2.2 Radiative Transfer Modelling for METimage

Radiative transfer (RT) models are required for simulating radiances for all METimage channels in a mathematically and physically consistent manner. The interaction of radiation with atmospheric constituents (trace gases, aerosols, and clouds) as well as with spectrally varying surface reflection and emission properties has to be fully taken into account. The different subtopics are elaborated in more detail below. An overview of radiative transfer models (RTM) for remote sensing can be

found at http://esaslight.libradtran.org/internal/Wiki/doku.php?id=rtmodlestable.

4.2.2.1 Line-by-line Models

Line-by-line RTMs can be considered as the most accurate approach for simulating atmospheric radiative transfer in different geophysical scenarios. In certain METimage channels the spectroscopic features absorbing and emitting trace gases like water vapour, ozone, carbon dioxide and others have to be considered for accurately prescribing the transmission properties of the clear atmosphere. Line-by-line RTMs are the starting point for developing fast RTMs, which rely on certain approximations and parameterizations, cf. for treating absorption and emission by trace gases.

Due to the computational challenges of line-by-line modelling, in particular when multiple scattering processes have to be simulated as well, widespread use of this approach has been possible only in the more recent past. The FASCODE model has been one of the first publicly available line-by-line codes (Clough et al. 1988). A further development of FASCODE has led to LBLRTM (Clough et al. 2005). Other line-by-line RTMs to be mentioned are GENLN2 (Edwards 1988) and RFM (Dudhia et al. 2002).

Line-by-line RTMs require as input spectroscopic databases, such as the HITRAN (Rothman et al. 2009) or the GEISA (Jacquinet-Husson et al. 2008) databases, for specifying absorption line parameters (such as line position, line strength, lower state energy, half-widths for air and self broadening, pressure-broadening parameters) for the most relevant atmospheric trace gases.

Further capabilities of line-by-line RTMs are:

- calculation of radiances for multiple gases and multiple ray paths;
- implementation of various line shape functions and band models;
- representation of continuum absorption (cf. water vapour continuum);
- allowance for various observation geometries;
- incorporation of the spectral instrument response function.

4.2.2.2 Radiative Transfer Models Including Multiple scattering

Multiple scattering processes play an important role for radiative transfer in clear-sky, aerosol-loaded and cloudy atmospheres. In connection with surface reflection, multiple scattering is responsible for producing the directional characteristics of reflected solar radiation in the Earth-atmosphere system. For thermal radiation, water and ice clouds give rise to spectrally dependent characteristic reflection patterns.

As a starting point, the most accurate mathematical treatment of RT including multiple scattering is required. In most cases the so-called discrete ordinate method or variants thereof, have reached a mature state, are well validated and widely accepted within the community. Despite the fact that polarization will not be measured by METimage, it is mandatory for some of spectral bands to employ RTMs incorporating the Stokes vector for providing polarization corrections to METimage instrument responses via look-up tables (LUTs), for example, for cirrus clouds or for aerosols located over anisotropic reflecting surfaces. It should be mentioned that polarized radiative transfer is significantly more expensive than scalar models. A recent study by (Emde et al. 2010) showed that Monte Carlo algorithms – which are usually considered very time consuming – might actually be faster than deterministic RT codes.

The accurate simulation of radiances in cloudy situations requires a proper treatment of the scattering phase functions. Usually one considers a Fourier expansion to separate off the azimuthal

dependence of the radiance field. For the remaining zenith dependence of the radiative transfer equation a sufficiently high number of radiative streams has to be chosen (Levoni et al. 2001).

Certain approximations for RTMs such as two-stream, four-stream or six-stream models are commonly employed, so that the computational effort for treating multiple scattering processes can be further reduced. These simplified models are still accurate enough to provide the basis for radiative budget simulations but may lack in details, essential for advanced retrieval algorithms.

A particular importance is to be attributed to the description of the spectrally and directionally dependent surface reflectance properties. Any state-of-the-art atmospheric RTM should be capable of treating both realistic anisotropic surface BRDFs as well as simplified (Lambertian) surface reflectivities. In the thermal infrared region, the directional dependence of the surface emissivity needs to be considered in an appropriate manner as well. This is in particular important in case of rough terrain with irregular heating pattern (e.g., Jakosky et al. 1990).

4.2.2.3 3-D Radiative Transfer Models

Three-dimensional radiative transfer effects need to be taken into account if any atmospheric or surface component exhibits strong horizontal variations at the scale of the photon transport through the atmosphere. This is usually the case for clouds, in particular for broken clouds or inhomogeneous clouds like stratocumulus (see Figure 7). Under clear sky conditions, 3D effects play a minor role. Traditionally three-dimensional effects have been neglected for practical reasons and the atmosphere was assumed horizontally homogeneous, or pixels we supposed radiatively independent from their adjacent counterparts which greatly facilitates the solution of the radiative transfer equation and allows closed numerical approaches like the discrete ordinate method described above. In that sense, “homogeneous plane-parallel clouds may not exist in nature but they are the only ones for which we know how to solve the radiative transfer in a small amount of computer time." said Anthony Davis more than a decade ago. This is no longer true. Not only has computational power increased by several orders of magnitude since then, but also 3-D Monte Carlo codes have been improved considerably. The majority of codes to tackle 3D radiative transfer problems are based on the Monte Carlo technique (e.g., House and Avery 1969). This method takes advantage of the stochastic nature of scattering and absorption. Here the paths of single photons are simulated explicitly. The distribution of optical properties within the model domain has minor impact on the performance. The accuracy achieved by this method is a function of the number of calculated test-beams and hence a function of calculation time. One major drawback of this method is that the general differences of photon sources in the short and long-wave spectral areas require different treatment. This is in particular a problem in channels (like the 3.7 μm) where solar and terrestrial contributions are expected. The MYSTIC model (Mayer 2009) is one example of such models, which allows inclusion of arbitrarily complex clouds and horizontally inhomogeneous surface albedo, BRDF and topography (Mayer et al. 2010). Simulations are performed in fully spherical geometry, enabling calculations for low sun or low satellite viewing angle (Emde and Mayer 2007). Polarization is fully included (Emde et al. 2010) and the model runs very efficiently due to a number of sophisticated variance reduction methods (Buras and Mayer 2010, Emde et al. 2011). The most prominent alternative to the Monte Carlo technique in 3D radiative transfer modelling is the SHDOM by Evans (1998). SHDOM is an iterative procedure combining elements of the Spherical Harmonics (e.g., Zdunkowski and Korb 1974) and of the Discrete Ordinate Method (e.g., Stamnes and Swanson 1981). Distinct spatial inhomogeneities or pronounced anisotropic scattering phase functions do have negative impact on the calculation speed. A sound overview of common 3D radiative transfer codes together with the (older) results of a comparative study can be found on the page of the Intercomparison of 3D Radiative Transfer Codes I3RC (Cahalan et al. 2005; http://i3rc.gsfc.nasa.gov/I3RC-intro_new.php).

Three-dimensional radiative transfer is certainly a feasibly approach for end-to-end simulations for

METimage, as will be shown in 4.2.2.7 . Such simulated satellite scenes are one possible way to optimize sensor characteristics as well as to develop and test remote sensing algorithms.

Cloud retrieval algorithms for practical reasons usually assume that clouds are plane-parallel and homogeneous within a pixel; and that individual pixels may be considered independent of each other. Neglecting horizontal inhomogeneity by these two assumptions has been shown to affect cloud remote sensing algorithms in two ways. Firstly, the variation of cloud properties within the instantaneous field of view of the sensor causes the so-called plane-parallel bias (increasing with pixel size) which, due to the shape of the reflection function (versus optical depth) leads to an underestimation of the pixel-averaged optical thickness of the cloud. Secondly, neglecting the net horizontal photon transport between adjacent pixels causes the independent pixel error, which may be positive or negative (Cahalan et al. 1994). Zinner and Mayer (2005) showed that these errors can be considerable for the typical pixel sizes of 0.5 – 5 km, usually employed in cloud remote sensing. This error (absolute value) increases generally with decreasing pixel size. It is strongly dependent on solar and observation angles. Thus, is it possible to reduce this kind of error with inclined model columns (Tilted Independent Pixel Approximation, TIPA, Varnai and Davis 1999). This accounts more properly for the geometry of the direct solar beam. Nevertheless, only few attempts have been made to date to consider three-dimensional effects quantitatively in a retrieval and these methods are usually computationally very expensive (e.g., Zinner et al. 2005).

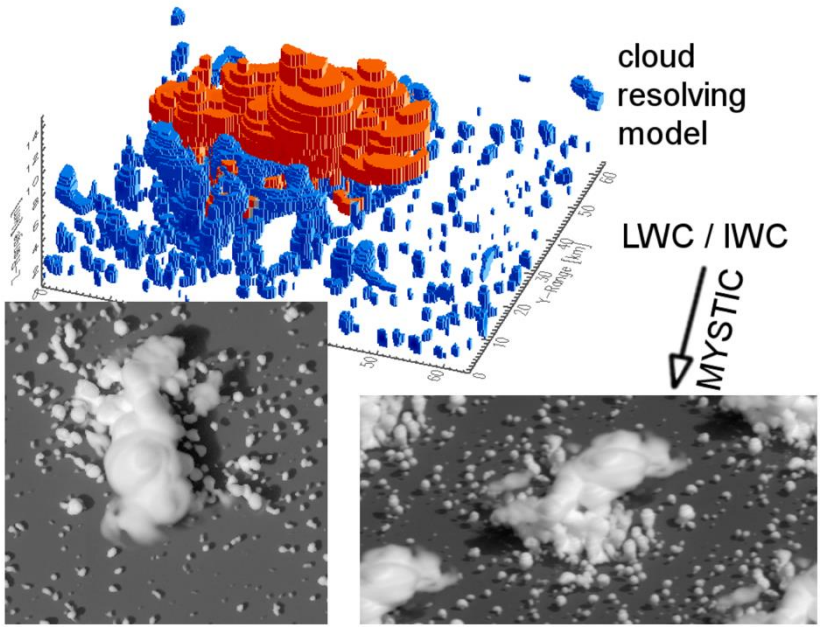

Figure 7. Output of a cloud-resolving model (top); liquid water is shown in blue, ice water in red; (bottom) simulation at 550 nm of a high-resolution nadir-view of the cloud (left) and an oblique view (60° viewing angle, right), similar to Buras and Mayer (2011). Note the eminent 3D effects (like shadowing) due to the cloud structure.

4.2.2.4 Fast Radiative Transfer Models

In view of the computational challenge of lbl RTMs including multiple scattering, fast radiative transfer models have been developed for use in operational geophysical retrieval algorithms and for data assimilation. Depending on wavelength, the METimage channels vary in width from 10 nm in the visible up to several 100 nm in the thermal infrared. For example, radiative transfer codes such as 6SV1 (Kotchenova et al. 2006), MODTRAN (Berk et al. 2005), RT3 (Evans and Stephens 1991)

and SHARM (Lyapustin 2005) are employed for generating the LUTs used in the MODIS aerosol retrieval and atmospheric corrections schemes. These RT codes employ correlated-k or exponential-sum fitting of transmissions techniques for treating the absorption process of trace gases in particular sensor channels.

Band models have been developed since the early days of RT modelling in meteorology and astrophysics. In the more recent decades, exponential sum-fitting (Wiscombe and Evans 1977) and correlated-k distribution methods (Lacis and Oinas 1991) have been utilised, which account for the typical temperature and pressure ranges in which a particular trace gas absorbs or emits radiation. These parameterizations have to be optimised for a certain METimage channel by exploiting lbl RTMs to derive the relevant parameters for the exponential sums or k-distributions. Usually, the most general radiative transfer code (cf. DISORT or Doubling and Adding) is used to perform the radiance computations for these fast RTMs.

Apart from the trace gas input, optical properties of aerosol and clouds have to be tailored to the various METimage channels. In certain cases (assimilation methods, non-linear inversion methods), linearised versions of the radiative transfer codes are required. At least two options are available to compute functional derivatives for retrieval algorithms: i) the numerical finite differences approach, or ii) algorithmic or analytic differentiation (Spurr 2006, Doicu and Trautmann 2009). Due to the high spatial resolution of METimage, multidimensional approaches to RT are required for accurately simulating radiance fields in multi-layer partially cloudy scenes.

In the thermal infrared RTTOV is commonly used and continuously developed, version 10 having been released in 2010 (Saunders et al. 2011), and version 11 in 2013. Compared to earlier versions, RTTOV is now capable of simulating reflected solar radiance, which is important for channels around 4 μm in day time, and can be relevant in sunglint conditions even around 11 μm for high precision retrievals such as SST. At the time of writing, exploitation of this capability is in its early stages. In addition, a more sophisticated and flexible surface emissivity module (Seeman et al. 2008) is inbuilt.

4.2.2.5 Surface Reflectivity and Emissivity Models

The use of a commonly accepted solar flux spectrum in all efforts related to research in general, and calibration/validation purposes in particular, appears to be quite important. For example, for sensor simulations with the help of radiative transfer models it is necessary to use a standard exo-atmospheric spectral solar irradiance (SSI) spectrum. Since several spectral solar irradiance data sets and models had been derived and used in the past, there is a need to recommend a "standard calibrated spectrum" for general use.

An intercomparison of several SSI spectra in the wavelength range from 350 to 1200 nm was presented by Shanmugan and Ahn (2007). Here SSI spectra from Neckel and Labs (1984), Kurucz (1993), Wehrli (1986), the so-called ASTM E-490 spectrum for zero airmass (ASTM International, 2000), Thuillier et al. (2003) and from other data sources were analyzed. It is noted that in 2006 CEOS WGCV experts (Committee on Earth Observing Satellites, Working Group on Calibration & Validation) recommended the composite SOLSPEC spectrum as published by Thuiller et al. (2003) for standard SSI spectrum use. This spectrum has become the *de facto* standard for solar spectral irradiance in the 400 to 2400 nm range (Harder et al. 2010).

Such a standard SSI is used to compute the band-integrated solar input for each sensor channel. For example, on NASA's ocean color site (http://oceancolor.gsfc.nasa.gov/) band-pass averaged quantities based on the SSI spectrum of Thuillier et al. (2003) can be found for several sensors (MODIS-Aqua, MODIS-Terra, POLDER and others).

SSI data sources for the mid-wave infrared region (3-4μm) have been discussed by Platnick and

Fontenla (2008). Here it appears that, despite the ubiquity of 3.7 μm channels in optical remote sensing, absolute solar spectral irradiance data in this spectral region are rather scarce. Since for day-time measurements solar and thermal components have to be separated, uncertainties in the 3.7 μm band-averaged SSI may lead to uncertainties in the retrieved cloud microphysical products.

Water-surface infrared emissivity models should account for view angle, wind speed (with wave state in equilibrium), temperature and salinity dependence. Asymmetry with respect to wind direction, surface bubbles and surfactants seem to be possibly neglected. For coastal and inland water locations, the influence of fetch could be marginally important; this could usefully be assessed, and possibly addressed using an effective wind speed for low-fetch locations. The water-surface emissivity model will give an effective emissivity at the view angle. For the reflection of downwelling atmospheric radiance, different models have proposed reflection of radiance calculated at an effective (non-specular) angle, or effective reflectivity at the specular angle. It is not clear at present which is preferable. Appropriate infrared emissivity models for use on water surfaces are provided by Masuda (2006), Filipiak (2008) and Nalli et al. (2008).

Land-surface infrared emissivity models have to be strongly based on empirical observations, rather than on modelling of surface processes. Land surface emissivity is not generally as dynamic in time as for water bodies, but is significantly more variable overall. Exceptions are where precipitation (new snow cover or water-logging) can modify emissivity rapidly. On longer timescales, emissivity evolves with vegetation (seasonal growth and vegetation stress). The UWiremis model is based on MODIS and laboratory measurements (Seeman et al. 2008), and is implemented as a database in RTTOV10 and higher versions. High spectral resolution observations from, for example, the Infrared Atmospheric Sounding Interferometer (IASI), will continue to improve the knowledge of spatial and temporal climatology of surface emissivity, and need to be accounted for.

4.2.2.6 Spectral databases

Many applications require information on the spectral behaviour of land coverage. During the last years some data bases (spectral libraries) were compiled to support modelling reflectance from different surfaces for a wide spectral range but mainly for visible and near infrared wavelengths. The libraries contain measurements of various qualities based on single campaigns or dedicated sampling of many spectra for vegetation / soils / rocks using different field spectrometers or goniometers (3-D measurements of spectral reflectance values). The following spectral libraries are available and open for public access:

- The United States Geological Survey (USGS) Digital Spectral Library; http://speclab.cr.usgs.gov/spectral-lib.html. The UV to mid-infrared 0.2-150 μm library (splib06; 2007) contains over 1300 spectra including mid-infrared data as well as spectra from splib05a and additional visible and near-infrared spectra. The library includes many more minerals, organic and volatile compounds, vegetation, and man-made materials than the previous libraries. The database is compiled based on over 6000 web pages, figures and sample images and data listings. Some additional information on terrestrial studies and publications can be found at: http://speclab.cr.usgs.gov/earth.studies/earth-is.html.
- Vegetation Spectral Library (VSL); http://spectrallibrary.utep.edu/. This library has been developed by the Systems Ecology Laboratory (SEL) at the University of Texas at El Paso (UTEP) in cooperation with colleagues at the University of Alberta and contains many spectra for different vegetation types.
- Vegetation and snow spectra; http://specchio.ch/index.php. The data are sampled by Remote Sensing Laboratories, Department of Geography, University of Zürich, Switzerland and compiled in the data base SPECCHIO. The spectral library does not only contain spectrometer measurements but also 3-D spectra derived from field and lab goniometer.

- The web page “Hyperspectral.info” (http://www.hyperspectral.info/) contains spectral libraries, documents and links to their geographical distribution provided via Google Earth. The network link http://database.hyperspectral.info/map/specmap.kml can be added to Google Earth to get access of the spectral data base and their geographic attributes. (Ferwerda et al. 2006).
- Spectral library of DLR, Oberpfaffenhofen; http://cocoon.caf.dlr.de/intro_en.html. Measurements made during different field campaigns and to support sensor developments. The data base contains 152 spectral libraries with 1609 spectra (July, 2012).
- ASTER spectral library: http://speclib.jpl.nasa.gov/ The ASTER spectral library is one of the most comprehensive libraries and contains more than 2400 spectra of natural and man made materials but includes also many spectra of the USGS spectral library (Baldridge et al. 2009).
- Airborne campaigns are underway (in 2013 and 2014) in support of the development of the NASA Hyperspectral Infrared Imager (HyspIRI) (http://hyspiri.jpl.nasa.gov/airborne) mission. HyspIRI is a hyperspectial visible and multi-spectral imager being developed to meet the recommendations of the NASA Decadal Survey (National Research Council 2007). The NASA ER-2 research aircraft will be used with the hyperspectral Airborne Visible/Infrared Imaging Spectrometer (AVIRIS) and the multispectral MODIS/ASTER Airborne Simulator (MASTER). These measurements can be used to enhance spectral libraries.
- Thermal spectra (http://speclib.asu.edu/); The purpose of this page is to allow easy and flexible access to thermal infrared spectra of a variety of materials, including minerals, rocks, soils and manmade objects. Each spectrum is accompanied by descriptive ancillary information, including physical and compositional information, sample quality, spectral analysis data and other comments.
- The NASA JPL Joint Emissivity Database Initiative (JEDI) will create a unified land surface emissivity Earth System Data Record (ESDR), defined as a long-term consistent and calibrated dataset valid across multiple missions and satellite sensors for a given parameter of the Earth system. Emissivity products are derived from measurements of NASA sensors in low earth orbit including MODIS on the Terra and Aqua satellites, AIRS on Aqua, ASTER on Terra, and VIIRS on Suomi NPP, all having different spatial, spectral and temporal resolutions, See http://emissivity.jpl.nasa.gov/.
- SPECMIN™ (http://www.pimausa.com/specmin2.html) is a mineral identification system for SWIR spectroscopy that includes an extensive and dynamic library of reference spectra for minerals and includes information on physical properties of each species in the database, and literature references for the infrared active mineral phases. Over 1000 spectra showing over 150 infrared active mineral species are included in the library. The data base contains also chemical formula, occurrences of minerals and their chemical compositions, etc of the spectra.
- RTTOV 11: the spectral library for VIS and IR is based on a representative set of hyperspectral surface reflectance spectra obtained by selecting 126 spectra (100 spectra for soils, rocks, and mixtures of both and 26 spectra for vegetation) from the USGS hyperspectral laboratory measurements database (Clark et al. 2007).

4.2.2.7 Cloud models

To assure a sound and realistic radiance image at TOA, the profile data, surface data and especially the cloud and aerosol data should be consistent. Particularly, the composition of cloud and aerosol

particles is crucial. A risk behind this approach lies in implicit assumptions (e.g., shape of ice particles). These assumptions translate into radiation fields. If algorithms are based on or tuned to these results, such assumptions become part of the retrieval scheme.

In principle any cloud resolving model could work to produce cloud-fields as long as these fields provide all the necessary optical properties. Large eddy simulations (LES) are powerful tools for the simulation of high resolution, 3D cloud structures (e.g., Smolarkiewicz and Margolin 1997). The consistency of atmospheric composition depends mainly on the set-up parameters and the model physics. Inter-comparison studies like that provided by Xu et al. (2002) may ease the decision.

By now limited area versions of general circulation models run at cloud resolving spatial resolution. They are generated to be nested in large scale models such as the one of the Deutscher Wetterdienst (DWD) model chain and fetch boundary conditions. The system is designed to keep close contact with reality, but the spatial resolution may still not cope with all requirements.

In situ measurements and adapted analysis schemes build a third possibility for the generation of realistic, high resolution cloud fields. Schmidt et al. (2007) showed that these so called cloud generators are capable of reproducing 3D cloud fields and corresponding irradiance fields on the basis of aircraft measurements.

Figure 8 shows as an example a simulated satellite image covering an area of 1000 × 1000 km^2 over central Europe. The simulation was done with the 3D RTM MYSTIC (see section 4.2.2.3). The input was taken from a prediction of the operational high-resolution DWD COSMO-DE model. The model output resolution was 2.8 km which was downscaled by a statistical method to a resolution of 560 m, appropriate for the 3D radiative transfer calculation. Bugliaro et al. (2010) discussed a possible testing or validating of cloud remote sensing algorithms on the basis of such simulations. The simulation provided was done similarly as in this paper but the radiative transfer here was fully three-dimensional rather than in one-dimensional approximation. Three-dimensional effects are obvious e.g. in the smoothing of the features of the low cloud by the cirrus layer above.

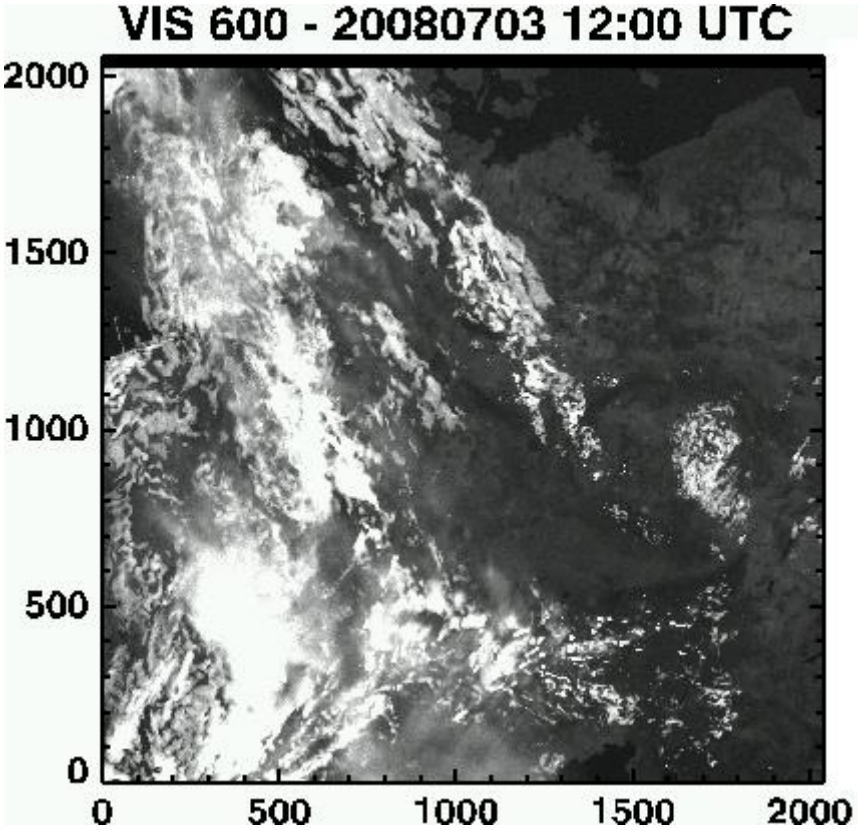

Figure 8. Simulated satellite image; visible channel (centered at 650 nm) of a high-resolution (560 m) satellite instrument, based on the output of a numerical weather prediction model COSMO-DE; data were generated by Faure, Buras, and Mayer in the framework of the EUMETSAT fellowship of Françoise Faure.

Of particular importance for the simulations of 3D cloud fields is the prediction of ice crystal habits in the cloud starting from the modelling of the detailed cloud microphysical structure. The University of Wisconsin has recently advanced in this direction with the Spectral Habit Ice Prediction System, (SHIPS, http://cup.aos.wisc.edu/group/research/Microphysics/Microphysics2.html) (Hashino and Tripoli 2007, 2008, 2011a,b), which represents a continuous-property approach to microphysics simulation in an Eulerian cloud-resolving model (CRM). Verifications of the model simulations have demonstrated how crucial is the accurate description of the ice hydrometeors habits to determine the radiative, microphysical and dynamic property of the cloud system also casting doubts on what is commonly accepted in the literature.

4.2.2.8 Aerosol models

In atmospheric radiative transfer models the interaction of light and aerosol particles is considered as independent and thus the scattering and absorption properties of an aerosol can be calculated from the properties of the single aerosol particle by a simple weighted (scattering/absorption efficiency and relative frequency) mean. The interaction of light with a single particle can be described by the Mie theory, as long as the particle is spherical. The effort for non-spherical particles is much higher: discrete dipole approximations (DeVoe 1986), t-matrix (Mishchenko et al. 1996), ray-tracing (Macke 1995).

In any case, these algorithms calculate the scattering properties of a single particle from:

- complex refractive index;
- shape (spherical or something else).

Knowing the

- composition (relative number or mass), and
- size distribution for each component,

the scattering properties of an aerosol can be calculated.

There has been an enormous increase of knowledge of aerosol optical properties in the last 20 years. For simulating synthetic measurements for desert dust events the spherical assumption may not be adequate anymore. Here at least rotationally symmetric particle should be used whose features - as compared to classical Mie spheres - have been explored in many scientific papers during the last two decades (Mishchenko et al. 1996, Kahnert et al. 2005, Dubovik et al. 2006, Rother 2009). In order to create Look-Up-Tables (LUT) for the aerosol inversion the use of a benchmark scattering database (Schmidt et al. 2009) for the optical properties of spheroidal particles may strongly ease the computational burden.

As for radiative models, there are a number of widely used and validated software tools to calculate the optical properties of particles such as the codes by Wiscombe (1996) or implementations of Bohren and Huffman (1998) for spherical particles, and the T-matrix (Mishchenko 1996, Macke 1995, DeVoe 1964, Yurkin and Hoekstra 2007) for non-spherical particles.

Equally important is the knowledge of the occurrence and distribution of different aerosol types, their related size distributions and shapes. The currently most comprehensive data source is available from AERONET measurements (Holben et al. 1998, Smirnov et al. 2009). This should be used as a basis for remote sensing algorithms as well as for correcting algorithms.

For some applications (in the TIR, e.g. SST) it is sufficient to assume the Henyey–Greenstein (Henyey and Greenstein 1941) approximation for the scattering phase function, i.e.to describe aerosol scattering properties parameterised by the asymmetry parameter, g.

4.2.2.9 Needs for Radiative Transfer Model Inter-Comparison

A variety of validation studies on RTMs have been performed. Since these studies were focusing on a certain wavelength range or on specific atmospheric conditions, the problem is to pick the right one.

In general, validation is done by an inter-comparison of different models. An absolute validation (comparisons with the “truth”) is only possible in case of idealised and simplified atmosphere. Realistic atmospheres do not allow for analytic solutions.

For the solar bandwidth (0.28 to 5 µm) 16 1D radiative transfer models have taken part in such a study (Halthore et al. 2005). The atmospheric variations taken into account cover clear sky, aerosol and cloudy conditions.

The more realistic 3D cases were studied in a comprehensive survey, started in the 90s. In two phases 23 models (10 in the first phase, 13 in the second) were tested under conditions of varying complexity (Cahalan et al. 2005). One of the key finding is that 3D radiative transfer is dominated by SHDOM (Evans 1998) and Monte Carlo models.

Well calibrated thermal infrared observations in window channels over the ocean can compare to within a few tenths of K with simulations driven by numerical weather prediction fields such as those from ECMWF, assuming that the SST is close to the truth. This amounts to a simultaneous validation of instrument characterisation, NWP profiles and radiative transfer model

4.3 Retrieval of Geophysical Parameters

Note the text here is just a summary of the retrievals. More detail will be given later in the ATBD. The text here should at least give an indication of the maturity of the techniques wrt state of the art and where we want to be in 2020. Any deficiencies or research needs should be clearly identified and indicated in the summary tables below.

4.3.1 Atmosphere

4.3.1.1 Clouds

Cloud products

Cloud Top Height: Most algorithms for passive instruments use the cloud top temperature (CTT) to assign (via predicted or climatological profiles, constant lapse rates) a cloud top height (CTH). This is straight forward in case of opaque clouds and the brightness-temperature in the 11µm region (which is close to real, thermodynamic temperature), but difficult for broken or semi transparent clouds. The signal of the latter may be contaminated by contributions from the surface or underlying clouds. Today these problems are handled by analysis of larger segments or optimal estimation methods (Watts et al. 1998). Moreover, the problem of two-layer cloud properties is largely untouched given its inherent difficulty; multispectral methods are being conceived and validated against A-Train data (e.g., see

Figure *9*).

Cloud Type: Here the methods depend to a large extent on the segmentation of cloud classes. In general, information on cloud height is needed as well as cloud phase and structure. Thus, it is common to assign a class at the end of a multi threshold-cascade (e.g., Dybbroe et al. 2005a,b). The atmospheric state is normally needed for these methods to run and it is taken either from a NWP model, if available, or from a climatological dataset.

Cloud Optical Thickness: The cloud optical thickness (τ) is often derived together with the effective radius at cloud top. The reflection of visible light is mainly determined by the cloud optical thickness. Nakajima and King (1990) took advantage of this fact and derived an algorithm, which is still used in a more or less unmodified manner. Algorithms from this family are vulnerable to overestimations caused by bright surfaces or sunglint (if visible through the cloud). Because of the logarithmic shape of the reflection curve, the achievable accuracy decreases dramatically with increasing optical thickness.

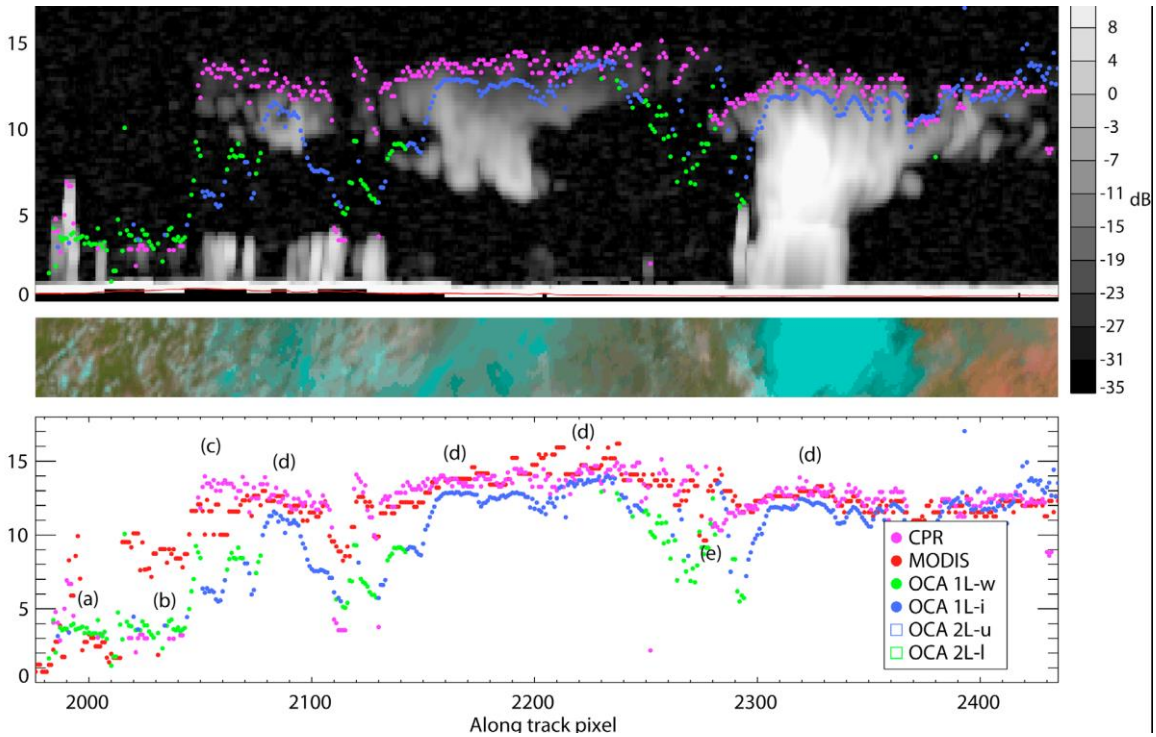

Figure 9. Tropical section of CloudSat overpass 1735. (top) CloudSat Profiling Radar (CPR) reflectance image with symbols indicating cloud top height (CTH) from CPR (white), SEVIRI water (green), and SEVIRI ice (blue). (middle) The daytime "true" colour SEVIRI image along the track (centre). (bottom) The CTH from MODIS. The scale on the left refers to height (km, top) and CTH (km, bottom). (from Watts et al. 2011, courtesy of American Geophysical Union)

Effective Radius: It is often derived together with cloud optical thickness (see above) by a Nakajima and King (1990)-like algorithm. The particle size has a major impact on absorption in correspondence to absorbing wavelengths. Absorptivity increases with particle size. Additional influence is pronounced for the particle phase so that this must be taken into account. One of the major problems with particle size algorithms is that the penetration depth decreases with increasing absorption (Kokhanovsky 2004). The thickness of the probed layer varies with wavelength and the same is true for the sensitivity to cloud top microstructure, and surface and 3D effects (e.g., Rosenfeld et al. 2004).

Cloud screening

Cloud Mask: Naturally, the cloud masking stands at the beginning of any further analysis of atmospheric or surface properties. There is a wide variety of principles in use to distinguish cloudy and non-cloudy pixels. They range from threshold over neural network-based to optimal estimation algorithms. However, the general strategy is to find signatures that are unique for clouds or cloud-free observations. Unfortunately, there is no such feature.

Common imagers work within the solar and the IR spectral ranges. In the reflectance of solar radiation, clouds appear brighter than the Earth surface most of the time, but this is not true for sunglint areas, deserts, snow or ice covered regions. In the IR clouds are generally colder than the surface except for the Arctic, the Antarctic or highly elevated regions. Most successful algorithms include a certain amount of auxiliary information like the forecast surface temperature or snow and ice maps to handle these problems.

One established approach to separate the signal from noise is to use thresholds on channel

differences. The split window technique (using a difference in channels around 11 and 12 µm) is a classic example (Inoue 1987). This channel difference is powerful in detecting thin cirrus (Inoue 1985) and works under almost every condition. Another prominent channel combination aiming at the same target is the difference of the 3.7 µm and 12 µm channel. It provides better contrast but during daytime the 3.7 µm channel will be contaminated by sunlight, which makes it difficult to apply such tests during daytime. A compromise is the use of a newer channel between 8.5 and 8.7 µm. It provides a better contrast than the classic split window channels and is not affected by sunlight.

Cloud property databases

Cloud properties derived from space-based instruments are extremely valuable for climate studies and model evaluation. However, the statistics of some of the cloud properties is affected by inherent instrument capabilities and/or the adopted retrieval methodology. The Global Energy and Water Exchanges (GEWEX) Project Assessment of global cloud datasets from satellites (Stubenrauch et al. 2012, 2013) has recently shown how cloud properties are perceived by instruments measuring different parts of the electromagnetic spectrum and how cloud property averages and distributions are affected by instrument choice as well as some methodological decisions.

EUMETSAT's Cloud Retrieval Evaluation Workshop (CREW, http://www.icare.univ-lille1.fr/crew/index.php/Welcome) is a recently established research initiative to evaluate the strengths and weaknesses of the most important algorithms that retrieve cloud properties from passive imager instruments onboard both polar and geostationary satellites (SEVIRI, AVHRR, and MODIS). METimage will clearly contribute to maintaining the heritage products in the various databases and add observational capabilities to the constellation in orbit.

4.3.1.2 Aerosols

Aerosol optical thickness (AOT)

Aerosol optical thickness is given by the total vertical column extinction for a range of wavelengths in the solar domain. Retrievals will be performed globally in daylight conditions except in the presence of clouds or bright surfaces. Separate retrievals are performed over land and ocean due to the different background reflective properties using channel sets that maximise the contrast between the aerosol and background. For example, over a dark ocean background, aerosols appear bright when viewed with red and NIR channels whilst over land blue channels can give a better contrast. Retrievals over land are inherently noisier and require good knowledge of the spectral albedo shape of the underlying surface.

Statistical retrievals are performed using LUTs of aerosol models. The observations are inverted using the aerosol models and the model exhibiting the best fit to the observations is taken as the retrieved AOT. There is strong heritage of such retrievals from MODIS (Remer et al. 2006) and similar retrievals are planned operationally for VIIRS (VIIRS ATBD, 2010).

Aerosol optical depth measurements over bright surfaces (e.g., snow) are possible but are still more a subject of research and require a very accurate snow/cloud mask.

Aerosol altitude

Aerosol altitude is retrieved using reflectance ratio measurements from the two channels within and just outside the oxygen-A band. For a given surface reflectance, relationships between reflectance ratios and aerosol altitude are made as a function of viewing geometry and atmospheric conditions. Experience with POLDER and MERIS has demonstrated retrievals of aerosol altitude to within 0.2 km accuracy for MERIS and 0.5 km for POLDER (due to the poorer spectral resolution)

(Dubuisson et al. 2009). Retrievals are only accurate over dark surfaces with high single layer aerosol loads (multi-layers will not be resolved).

Aerosol particle effective radius

Aerosol size parameters can be derived from the Ångstrøm coefficient which itself is simply calculated from the optical thickness in two different channels. Larger particles exhibit a higher sensitivity of optical thickness as a function of wavelength thus allowing particle size information to be derived.

Aerosol size information is also retrieved alongside with optical thickness through the use of the aerosol model. Different models exist for coarse and fine modes and the effective particle size can be determined by the model that produces the best fit to the inverted observations. Furthermore, coarse and fine modes can be combined with relative weights in order to match the observed aerosol (Remer et al. 2006).

Aerosol type

Aerosol type classification is obtained through the use of aerosol models used to retrieve the AOT and are usually classified into five main types: urban aerosol, sea salt, dust, volcanic emissions and smoke.

4.3.1.3 Water Vapour

Water molecules absorb and emit electromagnetic radiation in a very broad spectral range from microwave to visible wavelengths. Accordingly, a number of different methods have been developed during the past decades, using emitted radiance in MW measurements (e.g., SSM/I - Schlüssel and Emery 1990), mid- and long-wavelength IR spectral range (e.g., AIRS - Susskind et al. 2003, or IASI - Pougatchev et al. 2009) or using the absorption of water vapour in the visible (e.g., GOME, SCIAMACHY - Noël et al. 2002, 2004) or near infrared spectral range from MERIS or MODIS (e.g., Bennartz and Fischer 2001, Gao and Kaufman 2003, Albert et al. 2005, Guanter et al. 2008, Lindstrot et al. 2012). Above ocean, MW and IR techniques have proven to be superior, due to the well-known emissivity and temperature of the ocean surface. Over land, the water vapour signal at these wavelengths is blurred by the uncertain emissivity of the surface, limiting its main applicability to the sensing of upper-air humidity by using strongly absorbing bands. In the VIS and NIR spectral regions, the situation is reversed as the brighter land surfaces allow water vapour retrievals with a high accuracy. The existing retrievals for the VIS /NIR are various, but all use the fact that the amount of absorption is related to the amount of water vapour. For monochromatic radiation, neglecting scattering processes, assuming non-saturated and constant absorption in the path of light, the mass of the water could directly be related to the transmittance (inverting Lambert Beers law). Accordingly, for the wide channels of METimage, multiple scattering in the atmosphere (in particular the scattering scaling height) and finally the temperature and pressure dependency of the water vapour absorption baffle a simplified estimation of the water vapour column. Instead the algorithms are based on precise radiative transfer calculations (incorporating some or all of these properties), which are either inverted by regressions, look up tables or by more sophisticated inversion methods (Lindstrot et al. 2012). The related uncertainties depend in a complex manner on all properties, but mainly on the surface brightness and on the uncertainty of the ancillary data (Diedricht et al. 2013). The METimage algorithm shall quantify this on a pixel basis.

4.3.1.4 Earth Radiation Budget

METimage is not designed to make observations of Earth Radiation Budget (ERB) parameters. However, in the absence of Clouds and the Earth's Radiant Energy System (CERES) or Total Solar

Irradiance Sensor (TSIS) follow-on missions, METimage observations can contribute to observations of SW cloud reflectance, Earth surface albedo and emissivity.

4.3.2 Surfaces

Monitoring of surface properties relies on precise cloud detection and atmospheric correction. For near real time (NRT) applications remaining cloud free pixels are the basis to deduce further information or products from land surfaces or ocean. If the temporal resolution is not essential (e.g. climate related investigations), a clear sky mosaicking approach could improve derivation of parameters from land surfaces. The process of mosaicking is based on the usage of subsequent images covering the same area during a short time interval of approximately 7 or 10 days. Appropriate methods improve cloud screening, cloud shadow detection and result in a clear sky mosaic (Luo et al. 2008).

4.3.2.1 Land surfaces

Land surface temperature: The derivation of land surface temperature is based on multichannel approaches located in the atmospheric windows. The wavelength depended attenuation caused by atmospheric constituents is considered in the widely used split-window method to improve the quality of land surface temperature (LST) products. Atmospheric profiles and RTMs (RTTOV12, MODTRAN, etc.) improve the derivation of the regression coefficients. The emissivity of natural surfaces in the thermal spectra can be approximated using emissivity libraries and land use / land cover maps. The resulting static values can be improved to employ the current characteristics of the surface taken into account e.g. the normalized difference vegetation index (NDVI). The main remaining uncertainties are subpixel land coverage which distorts the proper assignment of the emissivity and the dynamic scaling. In addition, imprecise land use / land cover maps lead to doubtful allocation of emissivity values. Furthermore, undetected subpixel clouds are still a source of error for all land surface applications. Quality flags indicating the probability of cloud coverage are mandatory to improve the final product.

Fire detection: The essence of fire detection is to locate pixels that have a higher temperature than the surrounding background. The non-linearity of the Planck function means that there is a much higher sensitivity to fires at 3.9 µm than at 10-12 µm making the channel at 3.9 µm ideally placed to identify even smoldering sub-pixel fires.

For cases where the fire signal at 3.9 µm is too small for detection using this channel alone, the difference between the 3.9 and 10.7 µm channels can be used. Even for small cooler fires the resulting BT difference provides a detectable signal compared with the surrounding pixels (Giglio et al. 2003). The detection of sub-pixel fires, particularly on a regional scale, remains an active area of research. Smoke detection is also used to detect very small cool fires that cannot be detected by thresholding alone (Xie et al. 2005).

Satellite data from different sensor systems are used in experimental and operational mode to map and monitor active fires as well as burned vegetation. Roy et al. (2008) investigated the performance of the MODIS burned area product (MCD45) in comparison with the MODIS active fire product (MOD14). Depending on the selected area (South America, Africa, Northern Eurasia, etc.) and land cover/ leaf area the undetected areas in both products can exceed 60% of the burned area. In open shrublands and sparsely vegetated areas the quality of the MOD14 product increased by 17% (Roy et al. 2008). Chuvieco et al. (2005) improved the results using AVHRR and MODIS data in the Iberian Peninsula. Depending on the used technique, burned scars were detected if the cloud coverage was low. A forest fire data set was compiled from Pu et al. (2007) based on AVHRR data. This time series of 12 years covering entire forested North America shows the importance of daily available data to detect active fires and burned areas. The fire detection

capability of SPOT-VEGETATION (1 km spatial resolution) was investigated by Fraser and Li (2002) for boreal forests in Canada. An improved compositing technique using the minimum reflectance in the NIR spectrum improved the results in comparison to maximum composite techniques. For instance, the coarse resolution border of the burned scars was in good agreement with a validation data set based on Landsat-TM imagery (30 m resolution). Based on statistically improved methods, Kalpoma et al. (2006) achieved promising results for fire detection in Japan using NOAA-AVHRR data.

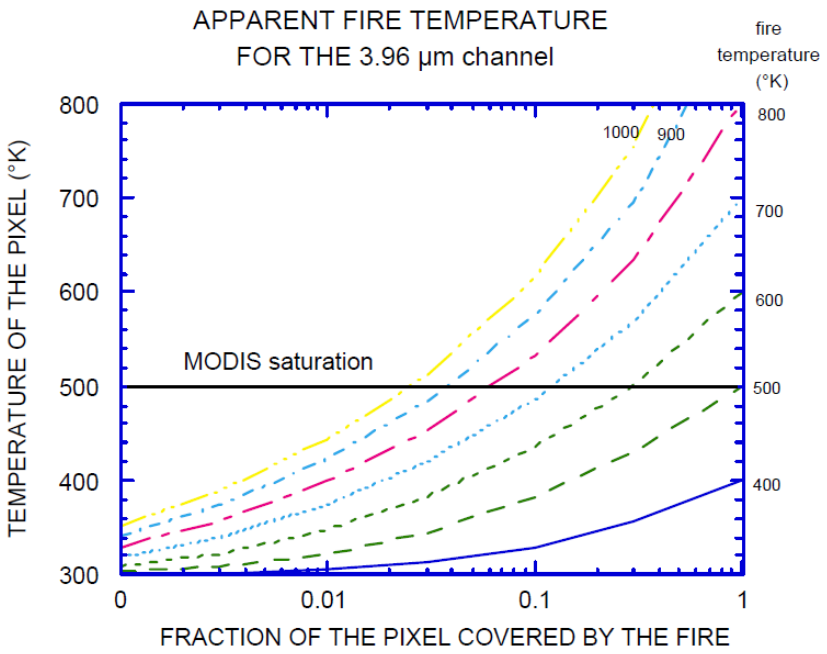

Figure 10. The apparent temperature of the pixel at 3.96 µm, as observed by MODIS, for a single fire as a function of the fraction of the pixel covered by the fire and its temperature. [Source: MODIS FIRE PRODUCTS; (Version 2.3, 1 October 2006); (EOS ID# 2741): atbd_mod14.pdf. Figure: page 10]

Leaf Area Index (LAI): The leaf area index describes the ratio between the area of foliage to the ground surface (m^2 m^{-2}). Numerous methods exist to derive LAI from any combination of different spectral reflectance values mostly based on a linear assumption between NDVI and LAI or on adapted versions of the Beer's law. Dense vegetation / tree canopies may lead to saturation effects (increased NDVI does not result in an increased LAI). RTM can improve the results but rely on precise information of leaf type, leaf amount, leaf orientation, state of leafs, etc. Monitoring of LAI based on medium resolution sensors will be an approximation especially at a global scale.

Normalized Difference Vegetation Index (NDVI): NDVI is based on the reflectance in the RED and NIR spectra taken into account the behavior of green vegetation to reflect less in RED in comparison to NIR. Changes in chlorophyll and water content in the cells result in distinct modification of reflectance values. NDVI is a robust method indicating vegetation dynamic and due to the normalization the effect of shadow on vegetation is minimized.s. A complete atmospheric correction (Rayleigh / Mie scattering (ozone, oxygen, aerosol) and absorption e.g. water vapour)) of the RED and NIR channels avoid a bias of the NDVI values. Most of the available products do not consider an aerosol correction leading to doubtful NDVI values in regions with high pollution.

Vegetation coverage: Vegetation coverage is an essential product for many land surface applications. Mapping is based on classification approaches (supervised classification) considering

NDVI. Neural networks can improve the classification results but require a careful and time-consuming training. Detection of sparse vegetation with medium resolution sensors is prone to errors especially in Northern latitudes due to frequent cloud coverage.

Photosynthetic active radiation (PAR): A significant part of the irradiance in the shortwave (0.4 – 0.7 µm) is absorbed by green vegetation for photosynthesis. RTMs are needed to calculate the absorbed term based on atmospherically corrected surface reflectances and consider detailed information of vegetation coverage and canopy structure. Solution of the three-dimensional radiative transfer problem is time consuming and requires an iterative procedure. LUTs enable fast processing and make NRT applications feasible. Existing methods show a high level of maturity (MODIS FPAR; MODIS_ATBD 1999) to approximate the photosynthetic active radiation but the generation of precise values on a global scale requires further effort.

Fraction of photosynthetic active radiation (FAPAR): see PAR

Vegetation type: approach of supervised classification based on clear sky mosaics and appropriate training areas will enable the generation of vegetation type coverage. A classification of the main biomes is feasible with the channel configuration of METimage, however it is not sufficient to distinguish between different species (e.g., ash tree versus maple). METimage data can be used for an update of the COoRdinate INformation on the Environment (CORINE) database or the ESA Globcover product.

Albedo: retrieval of albedo requires the correction of the bidirectional reflectance distribution. Hence, monitoring of ground pixels with different viewing geometries on a short period (days – week) is mandatory to provide sufficient measures for kernel-based models. The MODIS BRDF/Albedo operational product MCD43A considers kernel-based models and relies on cloud-free, atmospherically corrected surface reflectances from a 16-day period. The final 8-day albedo/BRDF product is produced in NRT and the accuracy is better than 5%. The quality of the correction (and therefore of the albedo product) depends on the number of observations per period. A high revisiting period or many satellites with the same sensor aboard (e.g., AVHRR) improve the quality of the retrieval.

4.3.2.2 Cryosphere

Sea ice: threshold methods considering the NDSI are in operational use for MODIS to provide the user community with sea ice information during day light. The methods rely on reflectance measurements in the SW and NIR spectra. Additional surface temperature is used as an indication for the occurrence of sea ice. Quality of sea ice monitoring relies on precise cloud masking and considering also subpixel clouds. During polar night only methods based on MW data (passive or RADAR) are suitable for sea ice detection using not only the brightness temperature or backscatter coefficient but also polarization (V-H) and gradient (channels) ratio. In addition, emissivity differences of channels in the thermal window may be used to distinguish between sea ice and open water during polar night but no mature algorithm is in operation so far.

Glacier / ice shields: spatial resolution of METimage is not sufficient for glacier monitoring but can be used for ice shield mapping; threshold methods show high level of maturity if the ice sheet is snow covered or pure ice. Problems occur with debris and impurities on surface reducing the reflectance values significantly.

Snow cover: threshold methods are in NRT use; The quality relies on precise cloud masking and good knowledge of land use/land cover to find approbriate modifications for thresholds. Problems with snow in (dense) forests are still a matter of research but transmissvity maps might be one solution as shown in the ESA Globsnow project.

Snow grain: There are some methods available (e.g., Nolin and Dozier 2000, Painter et al. 2009)

but not for real-time application with sufficient accuracy; snow grain size is an essential parameter to calculate albedo but liquid water on snow surface or impurities hamper the derivation on snow grain size. In addition, subpixel snow coverage leads to reduced reflectance values and may result in wrong snow grain size retrievals.

Snow temperature: The split-window approach (described for SST and LST) can be used to retrieve snow surface temperature with known emissivity but these values are modified due to liquid water on the snow surface. The mixed pixel problem for patchy snow fields prevents the determination of precise snow temperature, especially during the accumulation phase in early winter.

4.3.2.3 Water surfaces

For a well-characterised spacecraft infrared radiometer, with good in-flight calibration, a major source of inaccuracies in the retrieved SSTs is the effectiveness with which the consequences of the intervening atmosphere are corrected. Cloud droplets and ice crystals scatter the infrared radiation so the surface emission measured at satellite height cannot be detected to derive SSTs in the presence of clouds, even optically thin clouds or small clouds that occupy a small fraction of the IFOV. Thus, it is vitally important that the presence of clouds be identified and contaminated pixels be flagged so that values resulting from the retrieval algorithm are not interpreted as surface temperatures. Aerosols pose a similar problem, and depending on their properties, may be less easily identified in the satellite measurements. For some optically thin aerosol layers, an SST can be derived, with reduced accuracy, and the correction for aerosol effects is a current area of research (e.g., Merchant et al. 2006).

The propagation of infrared radiation through a cloud-free atmosphere is subject to absorption and emission, even in the spectral intervals where the atmosphere is most transparent (atmospheric windows), where the satellite measurements are made for surface temperature retrievals. Since the atmosphere is generally colder than the surface, the temperatures derived from inverting Planck's function, the brightness temperatures, are lower than the surface temperature. The main atmospheric constituent that interacts with the infrared radiation in the atmospheric windows is water vapour and this is very variable in its time-varying spatial distribution. The effects of other, well-mixed gases are generally smaller and being less variable, are less difficult to correct for.

Multi-spectral observations in atmospheric windows contain information about both surface temperature and atmospheric absorption/emission to support SST estimation, since the effect of atmospheric gases on the propagation of infrared radiation is wavelength dependent. Thus, the brightness temperature measured in the same IFOV at different wavelength intervals (spectral channels or bands) is different. By using measurements at different bands that have similar wavelengths, Planck's function and the radiative transfer equation can be linearized and a weighted combination of the brightness temperatures in different bands has often be used as an estimate of SST (McMillin 1975). The operational algorithm currently applied in the Ocean and Sea Ice SAF (OSI-SAF) for METimage class instruments is a Non-Linear SST (NLSST) formulation with an additional correction step based on fast radiative transfer modelling informed by NWP forecast fields. The form of the OSI-SAF NLSST algorithm is:

$$SST = a_o + a_1 T_i + \left(a_{21} + a_{22} SST_{guess} + a_{23}(\sec\theta - 1)\right)(T_i - T_j) + a_3(\sec\theta - 1)$$

where SST is the derived SST and T_i, T_j are the brightness temperatures in channels i, j (typically at ~11 and ~12 μm wavelengths), SST_r is a reference SST (or first-guess temperature), and θ the zenith angle to the satellite radiometer, measured at the sea surface (Walton et al. 1998, Minnett and Barton 2010). The coefficients are derived by regression analysis of radiative transfer simulations (using RTTOV) of brightness temperatures against SSTs used as input in the simulations.

Experiments at the OSI-SAF have shown developing benefits from physical inversion approaches (e.g., Merchant et al. 2013). Physical inversion is likely to be standard in the time frame of METimage operations, and will rely on simulation of METimage brightness temperatures to the level of ~0.1 K. Since this is well beyond the 0.5 K calibration specification of the thermal channels, effort will be required on bias adjustment of observed relative to simulated BTs may be necessary in order to gain the benefits to SST products of physically based approaches. Cross-calibration of METimage BTs to other instruments (IASI-Next Generation - IASI-NG, Sea and Land Surface Temperature Radiometer -SLSTR) may also help in this regard, and is discussed in section 4.5.1.2

METimage will also have two more spectral bands at 3.959 and 4.05 μm in the atmospheric transmission window. At these wavelengths there is significant scattering of solar radiation and so these bands are used primarily for night-time SST retrievals. Various variants of the NLSST algorithm, with or without the SST_r value, have been used with similar bands on MODIS, yielding high accuracy SSTs.

4.3.3 Summary

Product	Retrieval scheme(s)	Level of Maturity		Auxiliary data	Means of validation	Ongoing activities and gaps	
		Operational	Scientific			Operational	Scientific
Imagery	True and false colour composites	High	High	None	Inter-comparison	New channel combinations for enhanced information	New channel combinations for enhanced information
TCWV	1D-var, multi-dimensional (non-) linear regressions	High	High	Surface characterisation and first guess atmospheric profile	RAOBS, MW and GPS inter-comparisons	Fast RTM development /parameterisations needed to replace look-up tables	Deficiency in spectroscopy REF Lindstrot
Cloud mask	Multiple methods e.g. thresholding, Bayesian and NN.	High	High	Variable from none to real model outputs depending on method	Inter-comparison, ground observations, synop, aeronet	Ongoing characterisation of accuracy of methods Deficiency for detection of warm clouds above cold surfaces and handling of fractional cloud cover	Effect of cloud detection on level 3 products. Improvements to detection schemes.

Table 19: Summary of retrieval of cloud products

Product	Retrieval scheme(s)	Level of Maturity		Auxiliary data	Means of validation	Ongoing activities and gaps	
		Operational	Scientific			Operational	Scientific
Cloud type	Threshold algorithms	High	High	Atmospheric and surface properties	Intercomparisons, ground observations	Requires also structural information from surrounding pixels	Result of structural analysis is scale dependent Requires also structural information from surrounding pixels
COT	Nakajima & King like algorithms, optimal estimation	High	High	Surface reflectivity, atmospheric profile	Intercomparisosn, ground observations	Problems over bright surfaces, reduced accuracy for larger τ.	
CTH	Assignment of temperature to height via profile or lapse rate	High	High	Atmospheric profile or climatology of lapse rates	Intercomparisons with active instruments	Dependency on profiles is a problem.	Transition zone of lapse rate to profile could still be an issue.
CTT	Multiple algorithms, e.g. direct measurement of Tb, CO2 slicing	High	High	Atmospheric profile, information on opacity	Intercomparison	Arc-approach for semitransparent clouds requires relative large 'homogeneous' areas	Problems with multilayer clouds not yet solved.
Cloud drop R_{eff} at cloud top	Nakajima & King like algorithms, optimal estimation	High	High	Cloudtop temperature, atmospheric profile, cloud phase	Intercomparison, in situ measurements		Different wavelengths have different penetration depths
Cloud ice R_{eff} at cloud top	Nakajima & King like algorithms, optimal estimation	High	High	Cloudtop temperature, atmospheric profile, cloud phase	Intercomparison, in situ measurements		Different wavelengths have different penetration depths
Multi-layer cloud detection	Different approaches, e.g. optimal estimation	Low	Developing	First guess atmospheric state, surface properties	Intercomparisons with active instruments		

Table17: Cont.d.

Product	Retrieval scheme	Level of Maturity		Auxiliary data	Means of validation	Ongoing activities and gaps	
		Operational	Scientific			Operational	Scientific
Aerosol altitude	Reflectance from O_2-A band channels	Low	High	Cloud mask, aerosol models and surface spectral albedo maps	Validation using lidar (CALIPSO, EARLINET)	Consolidated spectral albedo databases lacking	Retrievals over other surfaces
Aerosol optical depth	Statistical retrieval with LUTs derived from aerosol models	High	High	Cloud mask, aerosol models and surface spectral albedo maps		Consolidated spectral albedo databases lacking	Retrievals over bright surfaces
Aerosol effective radius	Either from Ångstrøm coefficient or derived from AOT model	Low	High	Cloud mask, aerosol models and surface spectral albedo maps		Consolidated spectral albedo databases lacking	
Aerosol type	Derived from AOT model	Low	High	Cloud mask, aerosol models and surface spectral albedo maps		Consolidated spectral albedo databases lacking	

Table 20: Summary of retrieval of aerosol products.

Product	Retrieval scheme	Level of Maturity		Auxiliary data	Means of validation	Ongoing activities and gaps	
		Operational	Scientific			Operational	Scientific
Land surface temp	Split-window	high	high	Emissivity / land use; cloud masks	Ground measurements, air temp. incl. RT	Emissivity in NRT	Aerosol type and concentration influencing thermal emission of atmosphere
Lake surface temp	Weighted combinations of BTs	low	low	Cloud masks, water/land masks (ideally time-varying for some inland waters)	In situ, buoy data (rare)	Temperature difference (skin – buoy) modelling for validation. Water/land masking, especially for small and variable water bodies. Ice on/off detection.	Continental aerosol effects of surface temperature estimation. Cloud detection optimised for smaller water bodies.

Table 21: Summary of retrieval of land surface products

Product	Retrieval scheme	Level of Maturity		Auxiliary data	Means of validation	Ongoing activities and gaps	
		Operational	Scientific			Operational	Scientific
Fire detection	Brightness temp at 4µm and difference between 4 and 11 µm	high	high	Emissivity / land use; cloud masks	TBW	Improve detection small fires	Aerosol type and concentration influencing thermal emission of atmosphere
Fire fractional cover	Brightness temp at 4µm and difference between 4 and 11 µm	high	high	Emissivity / land use; cloud masks	TBW	Improve detection small fires	Aerosol type and concentration influencing thermal emission of atmosphere
Fire temp	Brightness temperature at 4 µm	high	high	Emissivity / land use; cloud masks	TBW	TBW	TBW

Table 22: Summary of retrieval of fire products

Product	Retrieval scheme	Level of Maturity		Auxiliary data	Means of validation	Ongoing activities and gaps	
		Operational	Scientific			Operational	Scientific
LAI	Beer's law or linear approach, RT	medium	medium	NDVI, land use/land coverage LULC, vegetation type; cloud mask,	Single campaigns	Full atmospheric correction including aerosol	Improvement of RT
NDVI	NIR/RED combination	high	high	Cloud mask, atmospheric state		Full atmospheric correction including aerosol	
Fraction of vegetated land	Unmixing?, endmember selection of 100% and 0% coverage	medium	medium	LULC	High resolution satellite data.	Full atmospheric correction including aerosol	
Vegetation type	Classification, thresholds, neural networks	high	high	LULC,	High res. Satellite data (spatial and spectral)	Full atmospheric correction including aerosol	

Table 23: Summary of retrieval of vegetation products.

Product	Retrieval scheme	Level of Maturity		Auxiliary data	Means of validation	Ongoing activities and gaps	
		Operational	Scientific			Operational	Scientific
PAR	RTM driven by spectral radiance	medium	medium	LULC, cloud mask	Single campaigns; comparison with PAR derived from hyper-spectral airborne data	Full atmospheric correction including aerosol	
FPAR	RTM driven by spectral radiance	medium	medium	LULC, cloud mask	Single campaigns; comparison with FPAR derived from hyper-spectral airborne data	Full atmospheric correction including aerosol	

Table 21: Cont.d.

Product	Retrieval scheme	Level of Maturity		Auxiliary data	Means of validation	Ongoing activities and gaps	
		Operational	Scientific			Operational	Scientific
Albedo	Linear kernel-based semi-emperical models	high	high	Cloud mask, snow mask, atmospheric correction (aerosols, air pressure), DEM	Ground measurements; satellite products	improvement of the needed auxiliary data	Improvement of kernels for reduced amount of data of angular reflectances

Table 24: Summary of retrieval of surface albedo

1 Product	2 Retrieval scheme	3 Level of Maturity		4 Auxiliary data	5 Means of validation	6 Ongoing activities and gaps	
		Operational	Scientific			Operational	Scientific
Snow detection	Thresholds, NDSI, aggregated ratings	high	high	Cloud mask	Point measurements, high res. Satellite data	Improved cloud mask	Snow in forest
Snow cover	Thresholds, NDSI	high	high	Cloud mask		Improved cloud mask	Snow in forest
Snow surface temp	Split window	High; being part of land surface temp.	high	Pure snow cover		QF to avoid mixed pixels	Emissivity change with water on snow
Snow albedo	BRDF-model (forward scatterer)	medium	medium	Grain size, impurities; elevation model	Goniometer measurements	Simultaneous derivation of grain size, impurities and albedo	Influence of liquid water on grain size / albedo
Glacier cover	Thresholds	high	high	Coverage of glacier (snow, debris, etc.)	High res. Satellite data	Glacier inventory ongoing	Automatic delineation of glacier edges

Table 25: Summary of retrieval of snow and ice products.

Product	Retrieval scheme	Level of Maturity		Auxiliary data	Means of validation	Ongoing activities and gaps	
		Operational	Scientific			Operational	Scientific
Sea surface skin temp	Multi-channel (radiative-transfer based NLSST with bias adjustment, or physical inversion)	High	High	Numerical weather prediction fields of atmospheric state, for radiative transfer. Land/sea mask. Cloud and ice detection.	Comparison with ship-board radiometer data, withheld buoy data with skin-layer correction	Continuing improvement being sought	Improved algorithms to replace NLSST atmospheric correction
Sea surface temp at depth	As skin temperature, plus models for skin-depth adjustment	Low	Moderate	Numerical weather prediction fluxes determining skin-depth physics	Comparison with withheld buoy data	Continuing improvement being sought	Continuing improvement being sought
Sea Ice surface temp	Multi-channel atmospheric correction (NLSST or derivative)	Medium	Medium	Few validation data	Few validation data	Continuing improvement being sought	Continuing improvement being sought

Table 26: Summary of retrieval of sea surface temperature products.

Product	Retrieval scheme	Level of Maturity		Auxiliary data	Means of validation	Ongoing activities and gaps	
		Operational	Scientific			Operational	Scientific
Polar AMVs	Target tracking from successive acquisitions using cross correlation.	High	High	Scene analysis, cloud mask, CTH, NWP forecast variables.	Comparisons against FC fields and Radiosonde observations.	Use of additional channels (e.g. 1.24, 3.7 and 8.5 µm)	Combination with other instruments

Table 27: Summary of retrieval of polar atmospheric motion vectors.

4.4 METimage Instrument and Ingest processes

It is helpful when describing instrument and ingest processes to follow the information flow first in form of photons through the optical system down to conversion to electrical signals, then to follow these signals through the analogue electronic chain down to conversion to digital sample values, and finally to follow these values through the digital processes both onboard and inside the ingest section of the Ground Segment down to the deliverable level 1 data.

The first process of METimage is the collection of light emitted from the Earth-atmosphere along directions given by the scanning geometry and its transport through the radiometer toward the detectors. METimage is a cross-track scanning radiometer. Successive scans are continuous at nadir enabling global coverage in 12 hours from a 817 km orbit using a swath width of ~2800 km. During each scan, METimage acquires 38 individual lines of data for the 500 m channels, enabled by the large field-of-view optics and therefore allows for a slower scanning speed, larger integration time and improved radiometric performance. Each scan line includes over 3000 Earth views (from +/- 55 degrees from nadir) and views of the calibration targets and cold space.

The METimage telescope, which initially receives the incoming photons, consists of an in-plane scanner and de-rotation optics. After passing through the scan assembly, light is focused onto the detector plane by the cooled secondary optics. Both an aperture and a field stop minimise stray light and radiative intrusions for the thermal channels and a beam splitter divides the visible and thermal components onto separate focal planes. The MWIR and LWIR focal planes are actively cooled to cryogenic temperatures whilst the VNIR focal plane is operated at ambient temperature.

The spectral separation of individual channels is performed by in-field separation, where the scanning motion successively moves the image over the detectors for each spectral channel located side-by-side in the focal plane. Detector rows can be duplicated to increase integration time and therefore improve the signal to noise ratio (time-delayed integration). The spectral resolution is achieved by placing filters in front of the detectors, which control the spectral shape and resolution for each channel.

To complete the optical process, detection of photons is performed using three focal planes: VIS/NIR, detector for the solar channels for wavelengths up to 914 nm, SWIR/MWIR for wavelengths 1.24 – 4.05 µm and LWIR/VLWIR for wavelengths 6.725 – 13.34 µm. State of the art readout integrated circuits (ROIC) are employed with integration stages and amplifiers and are directly mounted on to the focal plane arrays. 16-bit digitisation is used for the analogue to digital conversion within the front end electronics (FEE) following which the data is provided to a data

formatting module.

It is recommended to keep on-board processing as minimal as possible. If necessary, it must be fully reversible to allow for re-processing later on. If data compression is applied on-board, it must be lossless and checksums at both ends must be met to ensure the data is faithfully reconstructed. Another compression method that could be applied is data thinning where "duplicate" data from overlapping swaths is discarded (as done with VIIRS). However, the option to override this and download the full data set could be useful over very heterogenous targets (albeit over Nyquist frequency). Furthermore, the extra data can be useful for calibration purposes over uniform targets (such as Antarctica Dome C) to perform inter-spatial homogeneity checks. After recording in the spacecraft mass storage system, the data are down-linked to the EPS receiving stations. After separation of the data flows from the different instruments, the METimage data enter the level 1 processing system, which converts the incoming raw instrument source packets to level 1 products. Level 1 data radiances are fully radiometrically calibrated and geographically localised.

4.5 Level 1 Processing

This section describes the level 1 processing beginning with generic requirements before moving on to describe the main tasks for generation of level 1b data (calibration and geolocation).

It is imperative for users to have access to all parameters required for the level 1b processing as reprocessing dictated by new findings, corrections, improvements etc will be needed. The level 1b data should therefore be "self-contained" with respect to the parameters and housekeeping data required for processing up to level 1b. Full traceability of processors, observation data and auxiliary data should be maintained so that all level 1b data generated can be pin-pointed to specific versions/collections. Historical auxiliary data should also be available to users, particularly for climate applications where sudden updates in calibration coefficients disrupt trend monitoring and re-processing must be possible in order to rectify the analyses. Full transparency of level 0 to level 1b, including instrument model corrections, is required in order users can perform this.

4.5.1 Calibration

For the solar channels, the radiometric calibration method has to deliver calibrated radiances at level 1b with an accuracy of 3-5 % according to the specification (see 3.2.2) over the entire dynamic range and life time of the instrument.

For the thermal channels, the method should deliver calibrated radiances with an accuracy better than 0.5 K over the entire dynamic range and lifetime of the instrument. Additionally, the radiometric calibration should account for the following:

- the radiometric calibration should be performed at the detector element level;
- it is necessary to verify the spatial uniformity of the detector element radiance response with an accuracy better than 0.1 K in order to meet the medium term stability.

The proposed approach shall utilise on-board calibration in order to provide autonomous and timely calibration of the measurements suitable for operational use. The specified radiometric accuracy of the calibrated radiances/brightness temperatures shall be reached with on-board calibration alone although vicarious calibration techniques can be used to periodically monitor the instrument response and any degradation with time against other known reference sources.

4.5.1.1 On-board calibration

Solar diffuser calibration

On-board calibration using a solar diffuser (SD) will serve as the baseline form of calibration, to be performed once per day. The main purpose of the on-board SD is to provide a uniform scene of known irradiance that can be used to provide absolute calibration of the optic-detector chain and to verify the spatial uniformity of the detector elements of the same spectral channel. In order to achieve this, the bidirectional distribution factor of the diffuser shall be fully characterised prior to the launch. The diffuser should also be used to verify the short-term temporal stability, i.e., between successive acquisition cycles. However, due to the degradation of the SD with time, absolute radiometric calibration derived from the on-board diffuser should be confirmed by a second diffuser used periodically to monitor the in-orbit degradation of the primary diffuser.

The diffuser calibration method uses two reference points: the radiance from deep space and the solar radiance using the diffuser to establish the radiometric calibration slope. This 2-point calibration mechanism does not allow the linearity of the radiometer response to be verified, nor the spectral calibration, i.e., any displacement in the sensor spectral response function. Therefore, it is important that linearity and spectral stability are ensured by design.

Black body calibration

METimage will be equipped with an internal black body. A black body at a temperature close to instrument temperature will be inserted into the optical path to allow an end-to-end calibration of the instrument together with the deep-space view. While the accuracy of 0.5 K will apply over the whole dynamic range, at scene temperatures close to the black body temperature, much better accuracy is required and can be expected. The black-body and space-view measurements allow a determination of the linear term in the calibration of each of the infrared detectors. The characterisation of any instrument non-linearity will be performed on-ground for each of the detector elements. A change to this non-linearity cannot be detected by the use of the internal black body and deep-space calibration with only two fixed temperatures, but can be estimated post launch by either contolled cycling of the temperature of the blackbody calibration target or by systematically varying the integration times. For the MODIS instruments, this has been done every three months and the pre-launch off-set and non-linearity terms are adjusted as needed (Xiong et al. 2005).

4.5.1.2 Stability monitoring and vicarious calibration

In order to validate the absolute calibration and monitor the stability over the mission lifetime, independent vicarious calibration techniques can be employed. These are particularly valuable for assessing any in-orbit degradation of the instrument that cannot be identified using the on-board calibration, such as scan mirror reflection versus scan angle (RVS) changes, SD stability and spectral calibration. The vicarious calibration techniques used in the past have used radiosondes, RTMs and cross-calibration with other instruments. However, a major problem concerns the size of the targets available, which are often an order of magnitude smaller than the METimage swath. Thus a complete detector array radiometric calibration is not possible from a single target. Due to this, lengthly vicarious calibration campaigns are often needed in order to characterise the full swath and the resulting absolute accuracy is often insufficient for the needs of the mission. Therefore, vicarious calibration can never substitute on-board calibration. Nevertheless, with good stable targets they can be extremely valuable for stability monitoring, where the absolute accuracy is not so important, and for validation of the calibration against known sources.

Vicarious calibration using Earth targets

By viewing stable and homogeneous Earth targets of known reflectivity/emissivity, the absolute

radiometric calibration of the instrument can be independently monitored. The method can largely be based on SEVIRI heritage (Govaerts et al. 2001) that currently has an accuracy of around 5%, using selected surface calibration targets and adding deep convective clouds as additional calibration targets to:

- provide an absolute radiometric calibration value to confirm the on-board calibration value through radiative transfer simulation over well characterised targets;
- monitor the radiometer degradation, e.g. diffuser stability or scan mirror RVS changes;
- perform spectral calibration; applicable for channels close to spectrally variable regions (e.g. absorption bands) whereby under certain known conditions, TOA radiance can be precisely modelled and used to correct for spectral deviations, e.g. surface pressure over cloud free elevated areas.

The radiometric calibration reference is composed of spatially "uniform" targets over sea, bright desert and deep convective clouds. In light of the stringent radiometric calibration requirements and different spectral characteristics of the METimage channels, the following changes need to be implemented with respect to heritage missions such as SEVIRI:

- there is a need to re-define stable and uniform targets, using recent surface reflectance data sets to reduce the error of the surface reflectance characterisation;
- atmospheric characterisation needs to be improved, in particular for the non-window spectral channels;
- deep convective clouds should be added as radiometric calibration targets to better cover the full dynamic range of the instrument;
- polarisation should be taken into account for radiance simulation of the spectral channels in the visible domain.

The presence of the multi-spectral, multi-viewing, multi-polarisation (3MI) imager on-board the same platform offers the opportunity to significantly improve knowledge of the anisotropy of the atmosphere and associated polarisation effects.

Lunar calibration

Experience from the SEVIRI Spectral Channel Calibration (SSCC) has shown that vicarious calibration provides reliable drift estimation only after several years of exploitation. Additionally, an on-board diffuser might also be subject to aging. It is therefore recommended to include additional mechanisms to monitor accurately the solar channel calibration stability, using the Moon (U.S. Geological Survey Robotic Lunar Observation (USGS ROLO), http://www.moon-cal.org/index.php) as stable calibration reference for spectral channels with wavelength shorter than 2.5µm.

There are significant complications to using the Moon as a radiometric standard source, primarily resulting from the variegation of the surface albedo, the constantly changing lunar phase and librations, and the strong dependence of the surface reflectance function on phase angle. However, the lunar surface reflectance properties are extremely stable, and therefore knowable to high precision. In practice using the Moon for instrument radiometric calibration requires the use of a model that can predict the lunar brightness for the precise geometry of illumination and view of the instrument. Such a model, once established, is valid for any observation of the Moon within the geometry range, including those made in the past.

The use of the Moon as calibration reference for METimage is subject to some constraints such as:

- The Moon is seen only by a limited number of detector elements; the method can be used only on the integrated lunar value. This implies that the method can only be used for the radiometric calibration of equalised data.
- There is a need to apply the method frequently to minimise the effect of the uncertainty resulting from changes due to viewing geometry, lunar phase, and librations.

Lunar calibration has proven to have a positive impact on SeaWiFS stability monitoring (Eplee et al. 2012). The proposed method is based on monthly views of the moon to monitor the relative sensor degradation (Eplee et al. 2011). When the Moon is used as an absolute calibration reference, differences between SeaWiFS radiance and the USGS ROLO radiance vary between 7 to -1%. Difference between MODIS and the ROLO lunar model is in the range of 7 to 9%, which is in agreement with the lunar model estimated accuracy of about 5 to 10% (Stone 2008). Hence, the Moon can be used to monitor the relative sensor degradation, but not as an accurate absolute calibration reference. Lunar calibration is most effective when the following guidelines are adhered to (Stone 2011):

- Observe the moon as often as possible. Although viewing at constant phase angle is preferable in terms of model error, the instrument measurement error outweighs the model error and therefore more measurements lead to improved calibration accuracy.
- During commissioning, obtain as many lunar views as possible in order to get a stable calibration baseline.
- Do not change the frequency to which the SD is used and deep the exposure constant throughout the mission. This makes modelling the SD degradation far easier (smoother degradation function and therefore easier to work with the measurement noise).

Cross-instrument comparison

Level 1 observations could also be inter-calibrated with collocated observations from other satellite instruments following the concepts of the Global Space-based Inter-Calibration System (GSICS). Cross-calibration is best performed with instruments from the same platform to avoid temporal variations of the atmosphere (assuming similar viewing geometry). Else, simultaneous nadir overpasses (SNO) can provide a means to calibrate an instrument with another instrument of "known performance". Hyper-spectral sounders, such as IASI-NG to be flown on the same spacecraft, are particularly useful for this. They allow the radiances within the METimage spectral channels to be simulated by convolution of their observed spectrum with METimage SRFs. Given IASI's high calibration accuracy and stability, this should allow any radiometric biases to be monitored over time. If necessary, the radiometric calibration can be adjusted to ensure consistency with other instruments. The spectral range of IASI-NG extends only to about 3.7 µm at the short wavelengths and so does not cover the full spectral interval of the channel of METimage centered at 3.7 µm. Therefore a more sophisticated approach will need to be developed to monitor the long term stability of the 3.7 µm METimage channel, e.g., extrapolation of the spectrum using radiative transfer. In general, a "Clareo class" instrument flying at the time would provide further beneficial precise radiometric correction and stability monitoring.

Cross calibration of window channels used for SST retrieval will be a required part of the exploitation of METimage. The 0.5 K accuracy specification on brightness temperatures is not adequate for the estimation of SST by other than empirical means (regressing brightness temperatures to in situ measurements), since brightness temperature biases tend to be amplified in the process of inversion to surface temperature. If cross calibration can demonstrate stable radiometric accuracy of order 0.15 K for clear-sky ocean-scene brightness temperatures, physically based methods will be possible that confer several advantages (Merchant et al. 2008). Cloud

detection exploiting brightness temperature simulations is found to be more discriminating for difficult cases such as low uniform cloud banks at night (Dybbroe et al. 2005; Mackie et al. 2010), but relies on adequate agreement between the sensor and the forward model. Likewise, formulations of the inverse problem that explicitly use simulated brightness temperatures and/or their partial derivatives can deliver improved precision and SST sensitivity relative to regression-based formulations (Merchant et al. 2013). In addition to the potential cross calibration with IASI, linkage to the Sea and Land Surface Temperature Radiometer (SLSTR) on Sentinel-3 would be of benefit. SLSTR has been designed to a threshold and goal accuracy target of 0.2 K and 0.1 K, respectively. Sentinel 3 should be operational before the METimage mission, and with an anticipated second SLSTR on a second Sentinel 3 satellite, which would provide overlap though the METimages mission. The dual view capability of SLSTR, like (A)ATSR, will allow useful cross-calibration using multi-sensor match-ups when the satellite viewing angle of the cross-calibrated sensor is in the range between the SLSTR view angles (roughly nadir and 55°) (Merchant et al. 2003). Such cross-calibration approaches account for sensors' spectral differences using radiative transfer simulations, the residual systematic effects being attributable to SRF and calibration error.

Sensor to sensor calibration can also be used to monitor the spectral response function of the METimage channels. Hyperspectral instruments such as the UVNS with much higer spectral resolution can be used to monitor shifts in the METimage spectral response functions. Similar comparisons have been made between MERIS and SCIAMACHY (Casadio and Colagrande 2003), detecting wavelength shifts of the order of 0.01 nm.

4.5.1.3 Calibration Frequency

The frequency of the recommended METimage calibration vary from once per swath to once per months. Most frequent calibrations, once per swath, are needed for the deep space and internal blackbody views. Calibration of short-wave channels by means of solar diffuser calibration has to be done once per day. If these measurements disrupt the nominal calibration mode they should be done in "remote areas", such as Antarctica for the time intervals as small as possible, preferably < 1 minute in order to minimise the outage of Earth-view measurements. Vicarious calibration using Earth targets using the normal measurement mode should be done at time intervals of about once per month, depending on visibility of well characterised calibration targets. Cross-calibration with other instruments on the same spacecraft can be done routinely and should be performed once per day. For the monitoring of the long-term stability of the solar channels, the calibration using the stability monitor and a lunar calibration should be done around once per month, preferably without interrupting the normal Earth-view measurement mode. The frequency of the stability monitor and lunar calibrations should stay fixed for the lifetime of the mission (with the exception of commissioning during which as many calibrations as possible should take place).

The frequency and modes needed for the METimage calibration methods are summarised in*Table 28*

Type of Calibration	Frequency	Instrument Mode
Solar Diffuser	Once per day	Solar Calibration Mode
Lunar/VIS stability	Monthly or less	A special mode may be needed to image the moon
VIS/NIR Vicarious	Monthly	Earth view, no outage
Deep Space	Every Swath	Space view, no outage

Black Body	Every Swath	BB view, no outage
IR Vicarious (RTM models)	Monthly	Earth view, no outage
VIS/NIR/IR Vicarious (cross calibration)	Daily with METOP-SG instruments –IASI-NG, S5	Earth view, no outage

Table 28: Recommended METimage calibration frequency and modes

4.5.1.4 Role of instrument pre-launch calibration and characterisation

Pre-launch calibration and characterisation is essential to achieve the required radiometric performance of the instrument. The success of the radiometric conversion of measured counts to radiances depends on accurate knowledge of several instrument properties including polarisation sensitivity (full Müller matrix), cross-talk (including memory effects), stray light and RVS. To ensure good lifetime performance, the in-orbit stability of these effects should be met by design where possible to reduce the need for further in-orbit monitoring.

Concerning RVS, these are caused by a dependence of the reflectivity of a rotating mirror on the angle of incidence, which is also wavelength dependent. As the reflectivity decreases, the contribution of the emission from the mirror increases, the correction of which requires knowledge of the mirror temperature. If uncorrected, or incompletely corrected, RVS errors contaminate channel difference values and variables derived from these. The problem was initially severe with MODIS on *Terra*. The RVS is not removed by on-board calibration as the calibration measurements are taken at fixed angles on the mirror. Experience with MODIS shows:

a) Some progress was made with quantifying the problem and deriving a correction based on the asymmetry of the angle on the scan mirror about the nadir point.

b) A major brekathough was achieved when the Terra MODIS went into a safe-hold mode with the earth aperature door closed, but with the mirror rotating and data being collected. Assuming the temperature of the interior of the door to be uniform, the main source of the signal was then attributable to changes in the RVS of the mirror.

c) Definitive measurements were made by a pitch manoeuver on the eclipse part of an orbit so that the earth-view sensors measured deep space. The signal measured across the swath is then just the emission from the optical surfaces, and the RVS component readily identified.

The optical design of METimage, which consists of a scanner and derotator, is such that the range of incidence angles on the scan mirror throughout a scan is significantly reduced compared to MODIS. This means that RVS issues should to some extent be avoided by design.

Pre-launch characterisation of the calibration targets is also essential in order to reach the calibration accuracy. For example, care should be taken to ensure that the solar diffuser BRDF is characterised over the full operational angular range. Pre-launch characterisation must also be representative of the in-orbit environmental conditions.

In order to be able to verify the performance of the instrument, an instrument model capable of simulating all processes that affect the output signal is needed. This model is also needed for the conversion from detector output to calibrated radiances including any instrument artefacts that may arise during the mission lifetime. Such artefacts include RVS errors, stray light, polarisation, cross-talk and instrument ageing effects. Exhaustive ray tracing should be performed where necessary. This model is essential for any artefact correction from level 0 to level 1b.

4.5.2 Geolocation and Remapping

A precise knowledge of the location of every pixel is needed for all applications. If this is not given, quantitative remote sensing of the land surface is prone for errors, especially for climate related studies. The level 1 processing of the METimage data includes the geolocation of individual pixels. The geolocation of imagery follows three steps.

Starting from orbital elements with a corresponding orbit propagation model the spacecraft coordinates relative to an Earth fixed coordinate system will be determined as function of time. Adding information on spacecraft attitude, instrument alignment, and instrument scan parameters allows the calculation of geodetic pixel coordinates on the Earth surface. These will be as accurate as about 1 to 5 km, depending on the scan angle.

Higher accuracy of the geodetic pixel coordinates is needed (Requirement MRD_VII.310), and can be achieved by landmark navigation. This is done by correlating small reference images (of size about 64 × 64 pixels) with salient features of known coordinates to the real images of the instrument, in order to obtain for each reference image a linear displacement of the real image. Interpolation of the displacements from different reference images allows the determination of correction of locations for all real image pixels.

Following the landmark navigation, the influence of topography on the pixel position has to be removed. The satellite projection has to be transferred to a parallel projection to make the satellite image comparable with map projections. As auxiliary data an elevation model with a spatial resolution better than the sensors resolution is needed. The satellite position and satellite zenith angle are known. With these parameters and the elevation model the ortho-shift can be corrected to have proper co-registration between image and GIS layers especially in mountainous areas, which is mandatory to avoid artefacts in climatic related time series.

Experience with the navigation of the AVHRR data from Metop shows that the operational landmark processing requires the specification and use of about 500 globally distributed reference images. For MODIS, the accuracy achieved by the landmark processing following the initial coarse navigation is 50 m at nadir (Wolfe et al. 2002).

In order to achieve geolocation performance and establish the line of sight of each pixel within the focal plane, a series of instrument and engineering data are required. These include time tagged spacecraft position, velocity and attitude, scan parameters and co-ordinate transformation matrices. Once a line-of-sight (LOS) is established, intersection with the World Geodetic System 1984 (WGS84) ellipsoid is calculated to obtain latitude and longitude in the absence of terrain height modelling (often performed for ocean surfaces). For land applications, surface rectification is imperative and a digital elevation model such as the Science Data Processing Toolkit (SDPTK) is used to evaluate the appropriate terrain elevation and calculate the geodetic latitude and longitude. Cloud parallax correction may be required for certain applications, e.g location of thunderstorms, tornadoes and polar atmospheric motion vectors.

In terms of the data output, the presence of latitude and longitude for each pixel can help reduce processing complexity at user sites. For cases where the data volume is simply too large, tie point interpolation can be used. However, care is needed in order to avoid problems at co-ordinate boundaries and the Poles. A 2D tie point interpolation scheme has been used by EUMETSAT for the VIIRS regional service in order to reduce the data volume of the original VIIRS product. This scheme applies the interpolation on a flat geoid with no surface rectification.

4.5.3 Level 1b data output

This section outlines some guidelines for the content of the level 1b data. In order to enable the generation of scientific products to the required accuracy for all levels of processing and application

areas, it is imperative that all information required to process up to level 1b is encapsulated in the level 1b data itself. This information ranges from platform navigation and attitude data (NAVATT), relevant housekeeping and telemetry data (HKTM) to appropriate quality and control data (flags, sanity checks, calibration status, dead pixel and bad line info, etc.). Aside from the data itself, it is also necessary to log and propagate all calibration and processor versions through the various data levels such that full traceability of the data processing and calibration is achieved. This is imperative for climate applications where the back processing might be necessary for continuity of data records. Off-line updates to calibration parameters (e.g., ageing of the solar diffuser) should also be traceable to specific calibration campaigns for these purposes. Preservation of the time stamp throughout the processing levels is also imperative.

The preferred output of the level 1b science data is often application dependent. For example, users of solar data often want reflectances, while users of thermal data want brightness temperatures. For a multi-purpose instrument like METimage, which covers both visible and thermal spectral domains, it is often preferred to output radiances which can then be used across both spectral domains with appropriate conversion factors to perform band averaged radiance to reflection/brightness temperature conversion. To preserve the accuracy of the products, it is essential to provide consistent reference data (e.g., solar radiance spectrum) and conversion factors appropriately scaled to the instrument spectral response function. Clear documentation of these procedures is essential.

Concerning the geolocation, it is preferable that latitude and longitude is availbe for all pixels to avoid problems when interpolating tie points over mountainous regions or over the Poles. Of prime importance for the level 1b data is geolocation accounting for the actual relief using a DEM.

4.6 Level 2 Processing

Level 2 processing involves the retrieval of geophysical products beginning with calibrated level 1b radiances. As such and given the large number of products to be retrieved from METimage, discussion of the level 2 retrieval here is kept generic with respect to level 2 operational processing and the details for retrieval of each algorithm deferred to the individual algorithm theoretical basis documents (ATBDs).

Level 2 processing for METimage must be based on proven operational techniques. The operational processors themselves must ensure full transparency of all processor and data versions and propagate all version histories of algorithms, auxiliary data and calibration coefficients throughout all data levels. This is imperative for tracking the evolution of the processor performance and for re-processing data to ensure continuity for climate applications. Processors themselves are best kept modular to enable easy update of specific algorithms in a plug and play fashion. The ability to easily update the processor is advantageous for the incorporation of new findings, corrections and for optimisation purposes. Extensive validation considering the whole bandwidth of all relevant atmospheric states and land coverage has to be well documented and discussed in the science community before a re-processing of products is scheduled.

Prototype processors are essential for testing the operational processor and for providing a platform for developing and testing new retrieval methods. Furthermore, they play an essential role in pre-launch characterisation and in-orbit verification. A prototype processor must be used in conjunction with the on ground testing to ensure the accuracy of the products at all levels. This must be further used in-orbit to confirm that he same performance is achieved in orbit and that the instrument is functioning as expected before handing over to the operational processor. In this sense, end-to-end processors beginning with TOA radiances through to instrument source packets and then level 0 to level 2 processing are required. Aside from an instrument data simulator (evolved from instrument

performance models), appropriate test data capable of capturing the full variability of the geophysical radiances to be observed in orbit must be available in order to not only test the retrieval algorithms but to ensure the robustness of the ground processor.

Each level 2 product imposes a specific requirement on instrument performance (e.g., ISRF, SNR, polarisation, out-of-band response). These parameters must be available at least one year before launch (characterisation performed in vacuum) in order to prepare for the product retrievals. The performace of an instrument may or may not meet these requirements and algorithms and test harnesses need to be in place to monitor and if necessary compensate for these deficiencies, e.g. monitoring of spectral stability of oxygen A band channels, stray light corrections, striping, sanity checking of data and flagging is therefore an important part of the pre-processing in order to highlight the cases where degraded data is to be expected.

In addition to processor and instrument validation using test data, validation using in-situ measurements is also necessary. This is described in more detail in the next section.

4.7 Monitoring and Validation of METimage Data and Products

Monitoring and validation will be important activities for METimage. They will require significant pre-launch preparatory activities and substantial routine effort after launch. Separate and more detailed plans will be required for:

- Monitoring, quality control and optimisation (continuous quality control of instrument performance and retrieval algorithms) – to included sanity checking, flagging etc;
- Validation of level 2 products.

This section describes the most important issues that must be addressed in these plans. Recommendations on the monitoring and validation of Level 1 (radiances) and Level 2 (geophysical parameters) are provided.

4.7.1 Monitoring, Quality Control and Optimisation

4.7.1.1 Instrument Monitoring

Instrument performance must be continuously monitored beginning with pre-launch characterisation and continued throught the in-orbit lifetime. Any changes in performance such as degradation of mirror reflectances, focal plane temperature changes, spectral shifts in channels must be indentified and reported appropriately as these effects often impact the calibration and therefore the product quality. Instrument parameters necessary for calibration are key factors that must be continuously monitored as they impact the quality of the Earth view calibration (e.g., black body temperature readings).

Experience with heritage missions has shown that in-orbit monitoring has been vital for following the instrument health throughout the mission lifetime and that relying on pre-launch characterisation is not sufficient to guarantee the product quality. Lunar calibration has been particularly successful for monitoring solar diffuser degradation, cross-talk, channel co-registration and reflection versus scan angle changes. During commissioning, it should be possible to perform sufficient checks to verify the initial performance of the instrument. These data will then serve as a baseline to future monitoring procedures. In particular, lunar calibration should be performed during commissioning as this serves as a baseline for monitoring the decay of the solar diffuser.

4.7.1.2 Product Quality

Quality control of products is imperative throughout all stages of the level 0 to level 2 processing for exception handling within the processor itself (e.g., if data is corrupt or missing) and that users are aware of degraded output and the cause of the degradation. Flags should be suitably designed such that the nature of the problem can be logically propagated throughout the data levels and not lost within the processing chain. Furthermore, it is important that the quality assessment metrics are concise and transparent. Quality variables should be simplistic with as few categories as possible (e.g., yes/no, usable, not useable etc.), consistent over time and require little or no post-processing in order to be of use.

At level 1, the sorts of checks that should be carried out include sanity checks of data (bounds checking), checks for missing data, saturated pixels and invalid calibration data. Consistency checks must be performed at the start of the level 1 processing (e.g., time stamp continuity, radiance bounds checking) and then reporting flags set at the end of the level 1 processing to indicate the status of the level 1 products (e.g., Earth location successful/failed, unsuccessful calibration etc.).

At level 2, the nature of the flag setting and quality control becomes more specific to the product and type of use. The level of "fuzziness" that a user might tolerate varies between applications, e.g. the presence of thin cirrus clouds might render the data worthless for one application but not for another. Therefore, it is important that the flag setting protocol is appropriate for the needs of all applications.

4.7.1.3 Optimisation

Optimisation of product generation and data processing is directly linked to the process of continued validation. All products need a sound validation throughout the lifetime of the sensor/satellite to guarantee the best information on sensor stability and quality of level 2 products. The result of extensive validation processes may lead to an optimisation of algorithms for product generation and data processing related to accuracy and processing time.

4.7.2 Validation

Continuous validation of the METimage products needs to be sustained throughout the lifetime of the mission. Continuous validation gives valuable information on the geophysical retrievals, as described case by case in the section 4.7.2.3 below. Validation can and should also give feedback to activities monitoring and optimising the quality of level 1 radiances discussed in the previous section. This feedback is not automatic, and post-launch interactions need to be created between scientists working on product validation and instrumentation experts. Where artefacts and errors in derived products emerge that can be related to issues with instrument performance, it is ultimately preferable to solve these at level 1 rather than to implement level 2 fixes.

4.7.2.1 Constraints for Reliable Validation

Geophysical product validation implies the availability of *in situ* validation data. In most cases, validation data are not specifically collected for satellite validation, and those undertaking validation do not have control over the spatio-temporal sampling of the *in situ* measurements. Consideration should therefore be given in advance for each geophysical product identifying and implementing additional *in situ* measurement systems that will most usefully increase the reliability of validation activities. Past experience has shown that periodic intensive campaigns, often using specialized instruments deployed on aircraft and surface platforms, are very valuable in producing validation data for variables that are not widely measured in a routine fashion for other purposes.

4.7.2.2 Pre-launch Validation Studies

Geophysical retrieval algorithms will be defined prior to launch. The general principles and effectiveness of the retrieval methods should be validated in pre-launch studies. These generally take two approaches.

First, retrieval methods can be validated in pure simulation studies. The first step is typically the creation of realistic METimage level 1 simulations. These simulations use radiative transfer models informed by pre-launch instrument calibration and characterisation. The simulations are done for a range of sample geophysical situations relevant to the particular product. The geophysical parameter to be "retrieved" is specified in the simulation and perfectly known. For realistic validation of the retrieval method, appropriate levels of instrument bias and noise should be randomly added to the simulations, before the retrieval algorithm under test is applied. The "retrieved" geophysical parameter can be compared to that specified in the simulation, to validate retrieval performance and understand its limitations. The strength of this approach is that the performance of the retrieval method itself can be cleanly diagnosed in the absence of complications arising from unexpected instrument performance. The limitation is that the results are only as comprehensive and realistic as the radiative transfer model and simulation scenarios that are assumed. For example, retrieval performance under conditions where radiances are contaminated by unidentified cloud will not be validated unless this scenario is specifically included in the simulation.

Second, retrieval methods can be validated using heritage instruments with similar channels. The strength of this approach is that the method is tested across a range of real world situations. The limitations are: algorithms using new channel combinations cannot be implemented in this mode; and generally there is some ambiguity in interpreting whether any poor performance arises intrinsically from the retrieval method, or from the necessary adaptations of the method to the heritage instrument. Nevertheless, the use of pre-launch synthetic data streams is a valuable tool to test the validation procedures, including specialized software.

4.7.2.3 Post-launch Validation of Level 2 Products

The intensive validation activities that follow launch are vital to the initial assessment of the instrument performance. These should begin as soon as feasible after launch, even during the commissioning phase, but the major thrust would be once the instrument is placed in a stable configuration that is intended for use through the lifetime of the sensor. Given the long lead time for the use of some validating instruments, such as those deployed on ships and aircrafts, it is frequently not feasible to shift deployments to accommodate launch delays. Since it is expected that the instrument will exhibit some performance degradation with time, the L2 validations should be sustained throughout the satellite missions.

As discussed above, the validation process requires the generation of "match-up data bases" that include the satellite measurements coincident and simultaneous (within some acceptable limits that are determined by the properties of the variable) with the validating measurements; additional information, such as from other sensors or from modelled fields are sometimes required. Of course it takes time to populate the matchup data bases to sufficient numbers that an analysis yields a statistically meaningful result. This time is largely determined by the availability of the validating instruments. Given the likely variations of the retrieval uncertainties on season and shorter timescales, regional and shorter length scales, and dependences on other variables, such as weather features, the time to sample the natural variability in a match-up data base may be several years. Indeed, a multi-year data base is desired to ensure that seasonal cycles and interannual variations are properly sampled. To provide useful information within shorter periods after launch, match-up data bases can be generated that use other, established and validated, satellite-derived fields. In this

way a very large number of matchups can be generated in a short time. However, the lack of independence of the two (or more) satellite fields renders this approach insensitive to errors that are correlated due to the similarity of the measurement types or the processing algorithms, and is therefore not a long-term substitute to the match-up data bases generated with independent validating measurements.

Within Europe, the established SAFs will have important roles to play in the validation of the METimage L2 products.

In the following sections, aspects of the validation activities that are specific to particular products are presented and discussed.

Cloud products

In general, it is difficult to compare products derived from different sensors. If they feature different pixel sizes or shapes, the results are sensitive to inhomogeneities. In cases where instruments differ substantially (like for imagers and LIDARS) only scenes should be selected, where clouds are rather homogeneous in the magnitude of the larger pixel.

The most reasonable set of 'truths' for intercomparisons of cloud products is generated by active instruments like LIDAR or/and RADAR. This concept has been proven manifold by the instruments onboard Cloudsat and CALIPSO, both part of the A-Train (e.g., Sassen and Wang 2008, Kubar et al. 2011, Behrangi et al. 2012). Ground based observations suffer from probing different volumes and low sampling/co-location frequencies. Lidar and optical-drum ceilometers are largely used although their use is limited by the representativeness of their measurements, however, they are very instrumental to validate satellite-based products (e.g., Joro 2010). Unfortunately, there will be no overlap in operation time of the cloud radar or CALIOP and METimage. From a scientific point of view, it would be extremely helpful, to have a follow-up mission in space. Otherwise it would become very difficult to keep the continuity in quality control.

Cloud Mask

For the validation of the cloud mask, generally the most sensible instrument is selected as a reference. CALIOP has established as a trustworthy source during the last years.

However, a direct comparison is not fair, since an active optical laser is much more sensitive to cloud particles than any passive instrument can possibly be. Karlsson and Johansson (2013) suggest that clouds with an optical thickness less than 0.3 should not be taken into account for a validation because this marks the theoretical limit of detection of AVHRR-like passive instruments. The validity of this threshold for METimage should be subject of future investigations. Supersaturation could become an issue only for cloud mask profiles. This can be solved by a combination of RADAR and LIDAR datasets (e.g., DARDAR).

Cloud Type

The assignment of types to clouds is a more descriptive procedure. Cloud type can depend on many different parameters like cloud height, cloud phase or cloud history. This makes this feature hard to validate. A common method to check at least for outliers is to sort cloud types into classes (like all types that are associated to high elevations) and check for this specific attribute. It is more a sanity check than a full validation.

Cloud Top Height

Most algorithms for passive instruments derive the cloud top height on the base of cloud top temperature and an atmospheric profile. The cloud top temperature is calculated after the application of an atmospheric correction from observations in the IR, preferably in the 11 µm

region.

Active instruments like the spaceborn LIDAR CALIOP are able to derive - directly via runtime measurements - the distance to the uppermost backscattering particles.

It is obvious from the different approaches that even under optimal conditions the passive algorithm will detect lower heights since it has to handle signals also from the lower parts of the cloud, an artefact most pronounced for optically thin clouds. This can be taken into consideration by removing a thin layer of a certain optical thickness (Karlsson and Johansson 2013).

Liquid Water Path (LWP)

The cloud liquid water path is the vertically integrated content of liquid cloud particles. Up to now, the most reliable products of the LWP are derived from observations of emissions in the microwave spectral range. One of its pros is that it depends on fewer assumptions than possible for observations in the VIS or IR region. To keep the absorption coefficients in the valid range, rain contaminated pixels have to be excluded. Due to complex contributions from land surfaces, microwave-based LWP products are only applicable if the footprint is completely over water bodies. For the time being, proper validation is possible over sea pixels only, because LWP products loose their reference character over land (Deeter and Vivekanandan 2006).

Ice Water Path

For the validation of the cloud ice water path comparisons with data derived from spaceborne RADAR instruments (like Cloudsat) are useful. A RADAR receives a distinct signal from the bigger solid parts of the cloud. Problems may be caused by large raindrops or supersaturation in case of substantial ice contents.

Cloud phase

Information on the dominant phase of cloud particles are provided by cloud LIDARs. If it is (as it is for CALIOP now) on a level base, only cases with a certain homogeneity in the upper layers should be taken into account. This is because passive instruments can not distinguish between layers and receive signals from several heights.

Aerosols

In absence of clouds, aerosols become more important in terms of modifying the signal detected by satellites. The aerosol load within an atmospheric column is characterized mainly by its optical thickness, Angstrom exponent, and backscatter ratio. The most feasible instrument that would work as a reference for validation, would be a spaceborn LIDAR. The AERONET network is also another validation source, however ground observations often suffer from too few observation matches and probing different volumes. But heavy loads (like in case of forest fires or dust storms) may lead to a saturation of the LIDAR signal even for aerosols.

Validation of METimage aerosol products may use a combination of i) AERONET data for total optical depth and the Angstrom exponent, ii) cross-satellite comparison with aerosol products from VIIRS on the Joint Polar Satellite System (JPSS) or similar imaging sensors, iii) a comparison with ground-based (cf. EARLINET lidar network) lidar aerosol products, and iv) the exploitation of future spaceborne backscattering lidar instruments.

Water vapour

The total column water vapor can/shall be validated over land against various sources of reference data, namely: radiosonde data (e.g., GUAN or follow-on), sun-photometer measurements (e.g., AERONET), microwave radiometer (e.g., ARM) observations and ground-based GPS water vapour

monitoring data. Each of these reference data sets delivers accuracies better or equal to the envisaged accuracy of METImage. AERONET and ARM additionally deliver information about cloud cover.

Accuracy shall be quantified in terms of bias, root mean square deviation, the Pearsons correlation coefficient and the offset and slope of the linear best fit. From experience with MERIS (Lindstrot et al. 2012) we expect root mean square deviations better than 3 mm and bias less then 1 mm. The total column water vapor can/shall be validated over sea surfaces against satellite based microwave data (AMSR/GPM). Significant lower accuracy is expected over land.

SST

Sea surface temperature validation post-launch will be against in situ sources matched in time and space. Guidance on effective windows for such validation can be obtained from recommendations of the Group for High Resolution SST (GHRSST).

Consider validation of accuracy (bias) and precision (dispersion). Here, the principle is to reconcile observed satellite-in situ discrepancies with expected satellite SST retrieval uncertainties and known uncertainty characteristics of validation data. If the uncertainty budget cannot be reconciled, this may be evidence that the retrievals are not fully understood and can be improved or the validating data are contributing more error than expected. If discrepancy statistics depend systematically on factors such as wind speed, column water vapour in the atmosphere, satellite zenith angle, etc, these dependencies point to the nature of problems in the retrieval. Note that such comparisons need to be made against validation data not used in defining the SST retrieval (which is intrinsically the case if the retrieval is based on radiative transfer) such as using a set of comparisons that were withheld from the algorithm generation.

Direct validation of skin SST is possible against ship radiometer measurements, which match the same geophysical quantity. Ship radiometer measurements presently are available from commercial vessels (such as cruise ships and ferries) but often in limited geographical areas, and from oceanographic research cruises (which often cover areas of scientific interest). Their uncertainty is generally of order 0.1 K at their point (or line) of measurement. Spatial variability of the skin SST can add uncertainty to the comparison which may be comparable in magnitude. To within these uncertainties, comparison with ship radiometer measurements offers traceability of the satellite retrievals to international SI standards. Skin SST can also be validated relative to drifting buoys by accounting for the skin effect (skin being ~0.2 K than subskin SST) and near surface stratification often caused by diurnal heating (not always present). An effective approach is to use matches at night and/or in moderate wind regimes under which conditions, skin to drifter-depth differences in SST can be accounted for with an uncertainty also ~0.1 K. However, drifting buoys at present are calibrated only to ~0.2 K, and any inferences about satellite SST accuracy and precision should account for this source of uncertainty. There are efforts underway to improve signficantly the accuracy of the thermometers in the drifting buoys, and by the period of the METimage it is expected (and highly desirable) that the uncertainties in the buoy temperature measurements will be closer to the GHRSST requirement of 0.05 K. Depth SST should be directly comparable to drifting buoy and mooring SSTs without adjustment, at least under conditions where near-surface stratification is limited (wind speeds exceeding ~4 m s^{-1}) or where the validation data depth matches the target depth for the satellite estimate.

Other aspects of SST quality should also be validated. SST retrieval performance under conditions of atmospheric aerosol (e.g., desert dust) should be isolated and assessed. Stratification of satellite-in situ discrepancies against proximity to cloud may reveal issues related to cloud detection. Retrieval quality should be characterised as a function of quality flags. Ideally, the relative precision of nearby SSTs (or, equivalently, the local sensitivity to true SST change) should be validated

against in situ transects across SST frontal gradients, something that is not generally done at time of writing. The long-term stability of SST retrieval (the constancy of accuracy over time) should be monitored against suitable validation data (ship-board radiometers that have thier internal calibration systems periodically checked using SI-traceable laboratory facilities, well calibrated moorings and uppermost measurements of Argo profiling floats, especially those that take near-surface measurements using un-pumped sensors).

Conventionally, and correctly, the satellite SSTs are validated at Level2, whereas for some applications interpolated L4 fields are used. The generation of the L4 fields introduces additional errors and uncertainties beyond those determined at L2, and assessment of these should be considered part of the overall validation exercise.

Finally, note that, if properly approached, not only the SST product is validated via the above activities, but also the uncertainty information in the SST product is validated. For an increasing number of applications (e.g., numerical weather prediction using coupled atmosphere-ocean models), the quality of the uncertainty estimate attached to each SST will be as important as the quality of the SST itself.

Land products

EUMETSAT SAFs should play a leading role to validate products derived from METImage. During the last years the SAFs developed many procedures and algorithms to validate products retrieved from AVHRR and SEVIRI to improve product quality and guarantee long term stability. The knowledge and experience of the different SAF-teams (e.g., LSA-SAF, H-SAF, CM-SAF, etc.) should be the basis for validation of any land product. Furthermore, extensive data bases are compiled considering ground measurements, satellite products and auxiliary data (DEM, land use, etc.), which are applicable for the validation of METImage products. In addition, the developed and proofed methods for the validation of land parameters (some are also named ECVs by GCOS) are an excellent basis to ensure a proper validation process for the future METImage products.

A similar experience and knowledge is available at JRC (Ispra) related to vegetation products. During the last years they developed RTMs and different algorithms to retrieve vegetation products but also to validate MODIS products. Data of many validation sites around the globe were used to compare ground measurements of different biomes and satellite products. This knowhow should be used to tailor a validation procedure for METImage vegetation products.

Cryosphere

Validation of all cryospheric parameters need reference data sets aquired almost simultaneously with METimage data due to the high variability in time and space of the retrieved products (snow extent, sea ice, etc.).

Validation of snow extent products is a process to assess the product's accuracy by means of a comparison to some reference data. Due to the different types of reference data (high-resolution satellite SE, gridded snow data and ground truth snow depth, snow fraction)), different validation methods had to be applied. All validation steps refer to *daily* snow products with temporal coincidence of SE-product and reference data and restricted to confidential clear-sky conditions (comparison against snow course data and European Climate Assessment & Dataset (ECA&D) weather station data).

The snow surface reacts fast on changes of the atmospheric conditions but the snow extent is more stable in time depending on snow height. Validation of snow extent product can be done using either satellite data with a higher spatial resolution to proof the quality of the retrieval algorithms for different land use / land cover or to use point measurements of snow depths considering a certain snow height of 5 to 10 cm. The retrieval of snow grain size depends on pixels fully covered by snow and precise reflectance values. Hence, a validation requires simultaneous overflights of hyper spectral sensors (air-borne or satellite) or ground measurements using spectrometers (goniometers). In addition, the measurements (grain size, impurities, density, temperature) of regular snow and avalanche surveys can be used to model the expected spectral reflectance with RT (DISORT or similar).

Sea ice distribution can be monitored by METimage only during Sun light conditions (± summer). During time of melting the ice surface changes its condition from day to day resulting in changes of spectral reflectance. Validation needs simultaneous over-flights (SNO) of sensors with higher spatial resolution and proofed algorithms to detect and monitor sea ice.

In relation to sea ice and snow cover ice sheets are stable objects and, due to their size, they are detectable by METimage. To validate the retrieved ice sheet edge higher resolution imagers are needed but a comparison with some days/weeks offset should not be problematic.

Information about permafrost, glaciers, snow height and snow water equivalent can not be retrieved by METimage. Hence, no process of validation is required.

A remaining critical issue for monitoring of the cryosphere and validation of the different products

is a reliable cloud mask. It is recommended to mask the clouds in a conservative mode to avoid pixels affected by clouds and sub-pixel clouds.

Vegetation (NDVI, LAI, FAPAR, etc.)

Validation of vegetation products relies mostly on comparison with other satellite products, which are extensively validated by means of ground measurements. A problem is the required representativeness of the ground measurements for the pixels to be compared with satellite retrievals. Only a limited amount of validation sites is available which fulfil these requirements. This leads to the development of RTMs considering the shape, size and spectral behaviour of plants to model the radiative transfer between vegetation and atmosphere. NDVI is a simple measure of vegetation activity considering the red edge with high absorption in the solar spectra and increased reflectance values in the near infrared. Validations of NDVI rely mostly on NDVI retrieved by other airborne or satellite sensor data or RTM runs. Due to the strong increase of reflectance in the NIR the spectral bandwidth and center wavelengths of the sensors used for comparison need careful consideration because this changes the numerical value of quantity. Very often NDVI is the basis to retrieve other vegetation related products (e.g., LAI, FAPAR, etc.) but also RTMs are used. Therefore, validation should also consider information about spectral and spatial resolution of the used sensor and the resulting uncertainty of the reference product. The validation should be undertaken for diverse biomes in different climatic zones to guarantee consistent quality of the retrieval for different types of land use / land cover. A simultaneous overflight is not needed but the reference data should be not older than a week to avoid strong changes of vegetation dynamic (e.g., drought, foliation, etc.) during the validation process.

Land surface temperature

Validation of land surface products needs simultaneous ground measurements or SNOs. If the observed region is homogenous, products (temperature and emissivity) from geostationary satellites can be used to fulfil the requirements of the NRT overpass. High precision of ground measurements require huge efforts to install and maintain the measurement devices for different climatic regions of the world. In addition, comprehensive knowledge is needed to process reference data at high quality. The needed expertise is available at Land-SAF and their partners (e.g., IMK Karlsruhe, Germany).

Albedo

The bidirectional reflectance distribution determines the retrieval and quality of broad band albedo. This leads to a validation process, which requires precise ground measurements of the incident and reflected radiation for different surfaces and topography with limited availability. Hence, most of the times the validation relies on measurements made by local authorities (e.g., weather services) but only for grass cover. In addition, products (blue -, black or white sky albedo) from other satellite systems (e.g., MODIS) are used for comparison and validation. A high quality of reference satellite product requires good sensor stability and many observations of the same pixel with different sun-view geometries to reproduce the bidirectional reflectance distribution. This leads to 8- or 16-day products due to frequent cloud cover preventing ground observations with the needed angular variety.

4.8 Reprocessing for Climate

An important outcome of the longer-term validation of METimage variables that correspond to the Global Climate Observing System (GCOS) Essential Climate Variables is a quantitative assessment of the performance of the instrument and the algorithms that should be fed-back to the instrument monitoring and algorithm development teams. Revising the instrument model and the algorithms to

compensate for time dependent changes in the behavior of the instrument and algorithms is a vital step in ensuring such artefacts are not erroneously interpreted as a climate change signal. Reprocessing of the entire data stream is expected to be necessary to remove the potential corruption of the ECV time series by extraneous effects.

For revisions of the instrument model, reprocessing of the L1 data will be necessary, followed by regeneration of all downstream products. Revisions of algorithms for the generation of L2 products may only require the geophysical retrievals to be reprocessed. It is likely that both may be done as a single event. Experience with the MODIS instruments indicates that reprocessing is necessary every 18-24 months.

It is anticipated that the Satellite Application Facility on Climate Monitoring (CM-SAF) will play a leading role in reprocessing METimage data for climate applications.

4.9 Applications of METimage Data and Products

4.9.1 Operational Meteorology

METimage is designed to provide high quality imagery including many relevant parameters for both NWP and NWC, with highest benefit in Polar regions where space-borne imagery data from geostationary satellites are not available.

4.9.1.1 Numerical Weather Prediction (NWP)

Numerical Weather Prediction (NWP) will benefit from a number of geophysical parameters to be derived from METimage, which will be assimilated into the forecast models. With the evolution of NWP towards utilisation of rather high spatial resolution (< 10 km) an improved representation of atmospheric processes encompassing the whole Earth system (including land and ocean) will be required. Hence, the role of geophysical variables such as clouds and aerosols as well as surface parameters such as vegetation, and surface temperature will play an increasing role in a skilful weather forecast.

The success of any numerical environmental model highly depends on the estimation of the initial field, the control vector, when starting the simulation. Satellite data as a data source which is available on the global scale with comparable quality plays an important and further increasing role in the assimilation schemes of the weather prediction centers. In 1969 temperature profiles derived from measurements of the temperature sounder SIRS-A were the first space borne data assimilated into a NWP model (Ohring et al. 2002). Nowadays 90% of the data amount assimilated into the ECMWF model (and other models) are radiances of space borne instruments, another 5% of the data are geophysical properties derived from satellite data.

As already mentioned, the spatial resolution of NWP models is continuously increasing and global models have almost reached the resolution of the current and planned spaceborne sounders. In the future, the relatively high resolution of the imagers will be necessary to get the additional high resolution information on a global scale, which leads directly to the need for polar orbiting satellites and imagery missions.

Sounding data, such as the MW sounder AMSU or the IR sounder IASI is heavily relied upon in NWP. For a long time, these data could only be used in cloud free conditions. To assimilate cloud affected data is a quite recent topic of research (e.g., Vukicevic et al. 2006, Pincus et al. 2011, Polkinghorne and Vukcevic 2011). Today regional NWP models have reached a spatial resolution that requires the use of cloud resolving physics instead of parametrisations and a concludent assimilation of cloud physical properties has become more and more important. Data of multi-

channel, high resolution imagers will be used in two different ways to support this. On the one hand, imager data will be used to derive cloud physical properties itself (see later chapters), either inside or outside the NWP models. On the other hand, the high resolution data will be used for cloud masks that will be used as auxillary data for the sounder data with a relatively sparse spatial resolution. Related problems in this context are the assimilation of aerosol data that directly influence cloud physics as well as radiative transfer in the atmosphere, and volcanic ash properties.

The first kind of imager data that were used for assimilation were wind vectors, used for the first time in 1973 with data of the geostationary GOES. Atmospheric motion vectors (AMV) are particularly valuable in polar regions (e.g., Bormann and Thépaut 2004), where no access to such products from geostationary satellites is available. As shown by several studies (e.g., Goerss et al. 1998, Tomassini et al. 1999, Rohn et al. 2001, Rabier 2005, Cherubini et al. 2006, Zapotocny et al. 2008) the assimilation of AMV even from the polar regions of the southern hemisphere has a positive impact on NWP results over the northern hemisphere. Bedka and Mecikalski (2005) have also shown that high-density, satellite-derived AMVs can be derived that contain both synoptic-scale and mesoscale flow components associated with and induced by cumuliform clouds. AMVs have also a positive impact on the forecast skill of tropical cyclones (Leslie et al. 1998), but with higher performance of geostationary satellites.

Last but not least, there is a strong request to have current information about the surface as the lower constraint of the NWP model (or upper constraint for ocean models). There is a long list of parameters that can be derived from imager data, again either outside or inside the NWP model by assimilating radiances. For example, sea surface temperature (SST) has a large impact on the heat fluxes and heating rates. A fast RTM is available for AVHRR data (Liu et al. 2009). For derivation of SST outside the model, the IMAPP package can be used for MODIS data. The visible channels are used to derive information about vegetation (Los et al. 2000). Variables like fraction of PAR, NDVI, leaf area index or vegetation cover fraction are important for the energy cycle and necessary to make assumptions about the emissivity spectra. Scatterometer data and microwave imager data can be used to derive information about soil moisture. Another important parameter for the energy cycle is the snow cover (Pullen et al. 2011) that can be derived from imager data.

4.9.1.2 Nowcasting (NWC)

Nowcasting heavily relies on the utilisation of cloud imagery, which is the most important satellite measurement in the related applications. Depending on his/her field of interest (or duty), the forecaster, who has to predict the near future weather and to give out corresponding warnings, is mainly interested in topics like:

- Exact location and evolution of areas with fog or other situations where ths visibility is significantly decreased thus inducing a danger for almost all kind of traffic systems, as well airborne, on land as on sea. This includes also dust storm areas, which not only reduce the visibility but also threaten the functionality of ship engines.
- Location of areas with the potential for heavy convection (stability indices) at high spatial resolution.
- In areas with convection, the location and movement of the most active cells, together with an estimation of the amount of precipitation.
- The wind field, including the location of jet stream axes.
- For marine forecasting, the location of ice on the ocean.
- As the eruption of Icelandic volcano Eyjafjallajökull in 2010 showed, the location of areas with a significant amount of volcanic ash is an essential knowledge for aviation. A global

monitoring at high spatial resolution can be done only with satellite imagery, constrained by ground based measurements and numerical propagation models.

The design of METimage allows to attain this information. While in midlatitude regions one main focus is increasing the spatial resolution of the geostationary satellites, at high latitudes the polar orbiting satellites are the only source of information. Combination of these data (also from other orbiting platforms) allows for a satisfying temporal resolution.

Combining some of the data channels to one multichannel image can give a quick overview to the trained forecaster on several topics. With the current satellites, there are several recommendations for such images. Depending on which channels are combined one can get information about cloud height and physics (e.g., for fog detection, to discriminate between water and ice phase of clouds or to localize the position of the strongest updraft inside convection), about vegetation (in the framework of nowcasting especially in combination with fire detection) or the location of jet stream axes or cyclogenesis (with a combination of the window channels and the ozone channel). These multichannel images are (in most cases) far from any natural colour scheme and the forecaster actually needs some training prior operational use, since all such images have to be interpreted by the forecaster.

These imagery data can be supported by objective products. There are several products available and in the framework of EUMETSAT one has to mention the NWC-SAF as an important developer of such products. The interpretation work of the forecaster is taken over by an objective scheme. This must not only use the imagery data but can also add data from other instruments or e.g. NWP output. Examples for such products are cloud type, cloud top pressure, cloud top height, cloud top temperature, stability indices, convective precipitation rate, precipitable water content or an image interpretation. See http://www.nwcsaf.org/HD/MainNS.jsp or the IMAPP project (http://cimss.ssec.wisc.edu/imapp/).

4.9.2 Climate Monitoring

Why observe the climate? Climate observations have a value in themselves as a mean for the monitoring of the biosphere under changing conditions. However, this fundamental question was asked by Goody et al. (2002) introducing the societal need for a greater confidence in long-range climate projections that necessarily requires consistent and systematic high-quality observations as a basis for testing the predictive capabilities of climate models. This is particularly true for long-term studies of global change where exact variables in the climate model projections need to be clearly defined (Pielke 2008). When needing to compare between observations and predictions the variables need not be conventional. Any physical quantity that can be computed from the output of a climate model, and that can be measured, can also be considered as a climate variable. Moreover, the variables need not to be just state variables, but fluxes are needed to properly characterize the climate system (Ackerman 2005). This would lead to a rather long list of variables. With the intent of providing support to the work of the United Nations Framework Convention on Climate Change (UNFCCC) and the Intergovernmental Panel on Climate Change (IPCC) the Global Climate Observing System (GCOS) of the World Meteorological Organization (WMO) introduced the list of the Essential Climate Variables (ECV) deemed technically and economically feasible for systematic observation. These variables are currently 44 with soil moisture being recognized as an emerging ECV (*Table 29*)

Domain	**Essential Climate Variables**

Atmospheric (over land, sea and ice)	**Surface** [1]: Air temperature, Wind speed and direction, Water vapour, Pressure, Precipitation, Surface radiation budget. **Upper-air** [2]: Temperature, Wind speed and direction, Water vapour, Cloud properties, Earth radiation budget (including solar irradiance). **Composition**: Carbon dioxide, Methane and other long-lived greenhouse gases [3], Ozone and Aerosol supported by their precursors [4].
Oceanic	**Surface** [5]: Sea-surface temperature, Sea-surface salinity, Sea level, Sea state, Sea ice, Surface current, Ocean colour, Carbon dioxide partial pressure, Ocean acidity, Phytoplankton. **Sub-surface**: Temperature, Salinity, Current, Nutrients, Carbon dioxide partial pressure, Ocean acidity, Oxygen, Tracers.
Terrestrial	River discharge, Water use, Groundwater, Lakes, Snow cover, Glaciers and ice caps, Ice sheets, Permafrost, Albedo, Land cover (including vegetation type), Fraction of absorbed photosynthetically active radiation (FAPAR), Leaf area index (LAI), Above-ground biomass, Soil carbon, Fire disturbance, Soil moisture.

[1] Including measurements at standardized, but globally varying heights in close proximity to the surface.

[2] Up to the stratopause.

[3] Including nitrous oxide (N_2O), chlorofluorocarbons (CFCs), hydrochlorofluorocarbons (HCFCs), hydrofluorocarbons (HFCs), sulphur hexafluoride (SF_6), and perfluorocarbons (PFCs).

[4] In particular nitrogen dioxide (NO_2), sulphur dioxide (SO_2), formaldehyde (HCHO) and carbon monoxide (CO).

[5] Including measurements within the surface mixed layer, usually within the upper 15m.

Table 29. GCOS Essential Climate Variables (ECV, updated 14 September, 2015) [http://www.wmo.int/pages/prog/gcos/index.php?name=EssentialClimateVariables]

Observations need to be global and their long-term continuity is to be ensured. Sensors onboard operational and research satellites are a key component of such a system (e.g., Asrar et al. 2001) for the production of Climate Data Records (CDR) that have the adequate degree of accuracy, longevity, and stability to facilitate credible climate monitoring (Robinson et al. 2004). In particular, Asrar et al. (2001) identified three major components of the physical climate system that serve the purpose of identifying significant changes. Such components involve different timescales: the atmospheric circulation (hours to weeks), the oceanic circulation (weeks to centuries), and the polar ice sheets (years to millennia). Forcing factors are solar radiation (the only source exterior to the Earth system), the greenhouse gases and the global carbon cycle, the aerosols. Finally, climate response and feedback mechanisms need to be considered such as 1) the water vapour, clouds and the planetary radiation balance, 2) the land surface hydrologic processes, 3) the impact of deep water formation on the ocean circulation and climate, 4) the ice sheet dynamics and the sea level rise. Last but not least there are obvious climate-weather interactions at all scales.

Not surprisingly, satellites are a crucial component of the climate observation system because of

their space-time coverage and observing capabilities. Their number has considerably increased over the past decades and so did the instrument variety, resolution and level of calibration. Their limitations consist basically on some basic facts: a) the temporal resolution is often inadequate and does not allow for monitoring the transient phenomena, b) the instruments are passive radiometers and this leads to all sorts of limitations when retrieving parameters due to heavy parameterizations and assumptions on the radiation field, c) the radiometers are not well suited to measure fluxes at the surface, d) the satellite instruments do not unambiguously measure climate processes because the measurements of key quantities are not often taken simultaneously in space and time, e) the accuracy and stability of the satellite observations are not always up to the ECV quality and in-flight inter-calibration can contribute to improve the quality.

This is why a system approach to observing the climate system is necessary (Trenberth et al. 2002, 2006) involving all ground, airborne and satellite components. Satellites should be launched in a sufficient number to enable the diurnal cycle to be adequately sampled. They should be launched prior the expected failure date of the satellite they will replace to ensure overlap of measurements that is essential for the CDRs. All instruments must be calibrated both prior to and post launch and an extensive ground truth validation should be sustained. Moreover, proper cross-calibration with previous instruments is a prerequisite.

In this context METimage enters the key category of the polar orbiting imagers with an important list of predecessors such as the Advanced Very High Resolution Radiometer (AVHRR), the Moderate resolution Imaging Spectro-radiometer (MODIS), the Visible and Infrared Scanner (VIRS), the Along Track Scanning Radiometer (ATSR) and several others. An impressive series of CDRs have thus been created and need to continue to be updated to which METimage will contribute through observation of several of the ECVs listed in *Table 29*. At the same time METimage's radiometric performances and space-time resolution introduce novel observing capabilities that will enhance the observation potential. These two aspects need to be harmonized in order to ensure continuity with the previous international efforts and reprocessing is another key contribution to accomplish this.

4.9.3 Research and Process Studies

4.9.3.1 Cloud radiative forcing and global energy budget

Already some time ago Wielicki et al. (1995) while introducing the new Earth Observing System (EOS) of the National Aeronautics and Space Administration (NASA) underlined the role of clouds in modifying the Earth radiation budget thus representing a key uncertainty in predicting climate changes. Key advances are still based on simultaneous observations of radiation budget and cloud properties and include cloud particle size and phase, improved detection of thin and multi-layered clouds, reduction of the ambiguities in partially cloud-filled satellite fields of view, improved calibration and stability of satellite-observed radiances, improved estimates of the radiative fluxes at the top of the atmosphere, at the surface and at levels in the atmosphere.

METimage data will help establish with sufficient accuracy the relationship between radiative properties of cloud systems and radiative fluxes at the top of the atmosphere. Kiehl and Trenberth (1997) estimate the annual global mean energy budget providing a description of the source of each component to the budget and Trenberth et al. (2009) give an update based on new observations and analyses. The role of the satellite observations is underlined in constraining the top-of-the-atmosphere (TOA) shortwave and longwave energy flux. METimage will contribute to the suite of LW and SW measurement instruments in orbit. In particular, changes in albedo from snow and ice cover changes are to be measured as well as a contribution can be foreseen in better determining changes over time and contributions from land and ocean.

As well as contributing to global climate datasets, such as those described by the GCOS ECVs, it is likely that exploitation of the high quality imagery data will allow more detailed studies of some of the physical aspects of the climate system that are yet poorly understood. In particular, it should prove possible to test some of the assumptions behind current theories of the absorption and scattering of radiation by cirrus cloud and also by WV in the window regions. The presence of cirrus cloud has a marked impact on the Earth's radiation budget. Understanding the interaction between IR radiation and the cirrus ice crystals is fraught with difficulty, however, because of the complexity of crystal shapes and sizes and no single theoretical/modelling approach has been found to be successful under all circumstances. As METimage is equipped with specific channels to observe cirrus clouds and water vapour, the resulting high spatial resolution observations of these fields will contribute to the understanding of these processes.

4.9.3.2 Cloud microphysics

The cloud horizontal and vertical structure is a key research topic that serves the purpose of understanding the mechanisms of hydrometeor formation, including aerosol-cloud interactions, and thus quantifying the cloud precipitation potential. Studies have recently demonstrated the capabilities of the VIS/NIR/IR to uncover the cloud temperature-effective hydrometeor size (Rosenfeld and Lensky 1998) so as to produce semi-operational systems for cloud-aerosol-precipitation analysis (CAPSAT, Lensky and Rosenfeld 2008). Comparisons between the different spectral channels have also shown their capabilities if used in synergy for cloud property retrievals (e.g., Rosenfeld et al., 2004). However, these tools are incomplete if the hydrometeor phase remains unknown and here is where research needs to concentrate (Drori and Lensky 2010, Riedi et al. 2010). The approach needs necessarily to be multi-sensor and involve synergies with polarized instruments (Goloub et al. 2000, Parol et al. 2004) like the EPS-SG 3MI and microwave imagers and sounders (e.g., Cattani et al. 2009), cloud radars (CloudSat; e.g., Mitrescu et al. 2010), and lightning detection sensors (e.g., Toracinta et al. 2002, Latham et al. 2004).

4.9.3.3 Water cycle

The role of clouds in the water cycle is another fundamental research topic devoted to untangle the links between water and energy cycles for developing better seasonal predictions of water and energy cycle variability through improved parameterisations encapsulating hydrometeorological processes and feedbacks for atmospheric circulation models (Sorooshian et al. 2005). The satellite component is essential (UNESCO 2009) especially for the large scale issues such as the mechanisms in action in the inter-tropical belt (Roca et al. 2010). The humidity distribution is a key open problem and satellite multi-sensor methods once more represent a way forward.

Although METimage is not specifically designed for aerosol monitoring, its channel characteristics make it suitable for aerosol detection as a heritage sensor in line with the Advanced Very High Resolution Radiometer (AVHRR) and the Moderate Resolution Imaging Spectroradiometer (MODIS) series (e.g., King et al. 2003). Retrieval problems are still to be registered as regards to aerosol optical thickness over land (e.g., Kokhanovsky et al. 2007) for a better quantification of climate forcings by natural and anthropogenic aerosols. As Stevens and Feingold (2009) have pointed out, the climatic effects of the aerosol remain largely controversial mainly due to the difficulty in establishing meaningful relationships among aerosol, clouds and precipitation. Comprehensive datasets are needed for documenting the behaviour of cloud regimes on timescales of days to seasons. Finally, the modification of precipitation regimes with climate changes are of utmost importance (e.g., Trenberth et al. 2003).

4.9.3.4 Land applications

The importance of forcing from the lower boundary is now recognised in all global models to

improve the representation of energy and momentum exchanges at the surface. Land surface temperature observations are crucial to describe surface fluxes (sensible and latent heat) and therefore observations of this type contribute to understanding the influence of the surface on the atmospheric processes and associated weather and climate patterns. Furthermore, large scale changes in land use can induce marked changes in the influence of the surface on the atmosphere (e.g., change in albedo, capacity to hold water). Although METimage is not designed to provide very high spatial resolution images (< 10 m) for land imagery per se, it will provide land imagery of high enough spatial resolution sufficient for monitoring and improving our understanding of lower boundary forcing.

Vegetation observations such as leaf area index and vegetation type are also important for weather, S&IA forecasts and climate models. In addition to influencing surface albedo and heat fluxes, knowledge of the type and amount of vegetation provides insight into evapotranspiration rates and thus water and CO_2 fluxes between the Earth and the atmosphere. This information is highly desirable for climate models and monitoring the carbon, hydrological and biogeochemical cycles and climate and global change. Satellite observations of vegetation are also of interest for a large variety of environmental applications beyond meteorology and climate such as deforestation, desertification and land use change. METimage will provide vegetation indices such as ***leaf area index*** (LAI); a chief observation that provides a measure of the photosynthetic surface available and thus the amount of evapotranspiration as well as fractional absorbed photosynthetically active radiation (FAPAR) which provides an insight into the canopy density and net carbon uptake by the ecosystem.

METimage will provide fire observations to enable the location and extent of fires to be determined. This is important since, aside from the direct threats to human life and property, the radiative effects of smoke particles both directly affect atmospheric thermodynamics and indirectly affect cloud microstructure and precipitation events. Fire and biomass burning contribute to atmospheric CO_2, smoke and aerosols, and hence are relevant issues for climate and air quality monitoring. Fires also dramatically change vegetation coverage and land use pertaining to large effects on the carbon and hydrological cycles. If equipped with a high saturation channel, METimage could also provide observations of fire temperature, which are important for the calculation of fire radiative energy from which the amount of biomass burnt and the quantity and type of aerosol released can be retrieved (Wooster et al. 2005).

4.9.3.5 Cryosphere

Higher latitudes, polar regions and mountain ranges are permanent or temporarily covered by snow and ice. The dynamics of snow accumulation and ablation is important for life in almost all regions dominated by the cryosphere. Depending on latitude, elevation and climate, water run-off, and therefore water supply for irrigation, tourism and power generation derives mostly from snow and to some extent from glaciers.

The high spectral albedo of snow in the short wave (0.4 – 0.7 µm) makes this coverage an important factor for weather forecast models and climate related investigations. Almost 80% of the short wave irradiance is reflected, which is an essential contribution and has to be taken into account in the energy balance. The high variability of snow coverage of the Northern hemisphere (summer: ≈ 5 Mio. km^2; winter: ≈ 50 Mio. km^2) and the remarkable difference of albedo between snow and barren / vegetation determines hemispherical climate and weather.

Many cryospheric processes are directly related to surface temperature, e.g. the onset of melt. Mapping of melting areas is an essential need for climate related studies. The maximum temperature of snow is 0° C resulting in a long wave heat flux of 214 W m^{-2}. The snow surface temperature can be as low as -60°C in the Northern hemisphere during the polar winter and even

colder in Greenland or Antarctica. Hence, the temperature range between 0 and -70°C should be detectable by thermal sensors.

METimage will support observation of the cryosphere through the provision of observations of snow detection, snow cover, snow surface temperature, snow albedo and to some extent glacier cover where the spatial resolution is sufficient. When coupled with observations from other missions, in particular microwave measurements, more detailed information on melting conditions, liquid water content and snow depth can be resolved.

4.9.3.6 Ocean studies

The primary conritbtion of METImage to the ocean mission is the accurate measurement of the skin sea-surface temperature (SST). This will build on the decades-long expreince with heritage line-scanning infreared radiometer, including AVHRR, MODIS and, most recently, VIIRS. The wide swath of METimage, and the heritage instruments, means the SST is sampled over all, or most, of the cloud-free ocean twice per day. Global SST felds are produced operationally (Donlon et al. 2012) and are needed for Numerical Weather Prediction (NWP) models, and ocean forecasting models (Bell et al. 2000). SST fields reveal structure in the ocean and atmosphere (Bjerknes 1964, Deser et al. 2010) as well as influencing both (Chelton and Xie 2010). SST is an Essential Climate Variable (see above), and when suitably validated can be a Climate Data Record (Minnett and Corlett 2012); and long time series of satellite-derived SST can be used to study the response of the climate system to changing radiative forcing (Allen et al. 1994, Good et al. 2007, Hansen et al. 2010).

METimage will also contribute to ocean applications through the provision of sea ice imagery. Ice plays a crucial role in air-sea interaction in Polar regions. The sea ice insulates the ocean from heat exchange with the atmosphere, modulates the thermohaline circulation of the world's oceans through deep-water formation, and insulates the Polar oceans from solar radiation by its high albedo. Satellite observations are the only source of continuous information about sea ice extent, type, thickness, and drift. Specific sea ice requirements pertaining to imagery include sea ice coverage, type, drift and melt pond fraction.

The retrevial of oceanic parameters from top-of-atmospehre infrared radiance measurements requires that the presence of clouds, including at the sub-pixel scale, be identified and their influence removed. This is usually done using a "cloud mask" and this latter may not necessarily be the same as that derived for other purposes, such as the derivation of cloud properties.

Although METimage will provide ocean imagery observations in the visible and NIR, the instrument is not tailored to ocean colour applications, which require measurements over specific narrow bandwidths and low scene radiances. For these data, the OLCI on the GMES Sentinel.3 missions are to be relied upon.

4.9.4 Support to other missions

4.9.4.1 Scene inhomogeneity determination for sounders

Several instruments in particular the infrared sounders require imagery information within the sounder field of view as any inhomogeneity within the scene changes the self-apodisation and thus modifies the spectral response. Clouds and surface variability are likely sources of such inhomogeneities that need to be known in order to correct for the changed spectral response and perform the atmospheric retrievals to the specified accuracy. For EPS, the operationally generated AVHRR (Advanced Very High Resolution Radiometer) scenes analyses are used to identify the surface or cloud types present in each IASI FOV (Phillips et al. 2005). For EPS-SG, METimage imagery data would serve as a main source for scene analysis data for the IASI-NG sounder in order

to perform similar corrections. Other EPS-SG instruments such as the UVNS would also benefit from the high spatial resolution cloud and surface imagery.

4.9.4.2 Image location

The high spatial resolution images provided by METimage can be used as a means to geolocate other instruments on board the EPS-SG satellite with lower spatial resolution. Since METimage data will be geolocated to within better than sub-pixel accuracy, the images can then be used as a geolocation reference for other lower spatial resolution instruments on board the same platform. For example, on EPS, IASI level 1b products are geolocated with the help of the IASI IIS (Intergrated Imaging Sub-system) and the AVHRR images. Validation of the geometric calibration is carried out frequently using scenes with high-contrast features (e.g., coastlines and rivers), giving a geolocation error to within 100 m with respect to AVHRR.

4.10 Needs of Direct Read-out Users

The temporal availability of data significantly affects the impact of METimage data on NWC. The lead time (time between observation acquisition and user reception) should be as short as possible, with highest priority for level 1 data. The availability of a direct data broadcast facility is considered mandatory for remote locations although the optimal solution for Europe might be through an optimised data dump system with a network of ground stations. However, given the volume of data for EPS-SG, local direct broadcast systems, which then require ground processors to level 1, might not be as efficient or as practical as a series of ground stations with fast data links to the users. Backup solutions in the event of a direct broadcast system failure should also be available.

Processing of the data should be continuous and available at the user premises (processed to level 1) within 5 minutes of acquisition. The oldest scan lines within a dump should not be more than 10 minutes old. The data dump should not block direct read-out. Direct read-out is for many users an effective way to fetch observations for the whole area of interest. Therefore, it is also important to get individual scans in independent parcels.

If direct read-out users receive the data stream at level 0, they need to perform the level 1b data processing chain from end-to-end in a timely manner. Both level 1b processing and ingest software is needed and should be simple, modular and transportable to various user platforms. It is anticipated that the approach to the processing will be generally based on the existing AVHRR local processing chain with modifications to account for the added performance of METimage. The data ingest and level 1b processing should be based as far as possible on the global processing including:

- Decommutation
- Decompression (if any)
- Calibration
- Navigation

5 Summary of Priorities for METimage Research and Development

Section 4 provides an overview of the scientific activities which need to be undertaken in preparation of the METimage mission in the frame of EPS-SG. The steps which are necessary to

process METimage data to geophysical products and to use data and products for different applications (operational meteorology, climate monitoring, hydrology, oceanography) have been discussed. Based on this discussion, and taking into account the current status of scientific activities within and outside the METimage SAG, priorities for further research and development have been identified. In this section, the needs for future research are summarised and prioritised (TBD). The priority is linked to the relevance of a scientific study for the development of operational processing chains for METimage data in the EPS-SG ground segment. Emphasis is also placed on studies which support the efficient exploitation of METimage data and products by the various user communities.

5.1 Spectral libraries for land surface

Many applications require information on the spectral behaviour of land coverage. During the last years some data bases (spectral libraries) were compiled to support modelling reflectance from different surfaces for a wide spectral range but mainly for visible and near infrared wavelengths. The libraries contain measurements of variable quality based on single campaigns or dedicated sampling of many spectra for vegetation / soils / rocks using different field spectrometers or goniometers (3-D measurements of spectral reflectance values). As a result, these libraries are often procured over a specific geographic location or are limited by the spectral range. In the near future the different data bases shall be homogenised and uncertainty measures should be added to provide the needed confidence interval for models simulating spectral surface reflectances. Furthermore, the gaps caused by missing geographical coverage and objects should be determined and closed.

5.2 Atmospheric correction algorithms for sea-surface temperatures

<<High priority>>

There are three aspects to correcting the effects of the intervening atmosphere that limit the accuracies of the SST retrieval: a) identifying clouds and reducing their effects; b) identifying the presence of aerosols and reducing their effects; and c) reducing the effects of the clear atmosphere. The heritage of each of these aspects is extensive, but there is scope for improvement in all.

The traditional approach to cloud detection relies on a series of threshold tests that serve to identify the presence of clouds in pixels through comparisons of the characteristics of cloudy and cloud-free pixels (e.g., Saunders and Kriebel 1988, Kilpatrick et al. 2001). More recent approaches involve a probabilistic (Bayesian) approach to the detection of cloudy pixels where the probability of clear sky for each pixel is estimated by applying Bayes' theorem using probability density functions for clear conditions calculated using infrared radiative transfer modelling and those for cloudy conditions obtained empirically (Merchant et al. 2005). Both approaches should be refined for the characteristics of the METimage sensor.

The effects of undetected aerosols on the derived SSTs can be significant and extensive. Well-known examples include volcanic aerosols which can girdle the globe and which, if undetected, can lead to large negative bias errors in infrared SSTs (e.g., Reynolds 1993, Blackmore et al. 2012). Less spectacular events such as the Saharan dust that episodically extends across the Atlantic Ocean and Mediterranean Sea can also introduce noticeable bias errors (e.g., Merchant et al. 2006, Díaz et al. 2011). The spectral radiative effects in the infrared of mineral dust, for example, are different from those of gases (mainly water vapour) in the clear atmosphere, and while it is important, first of all, to be able to detect the presence of aerosols, even if just to flag the SSTs as less accurate, it is also feasible to alter the atmospheric correction algorithms to better account for the presence of aerosols and reduce their effects. The identification of aerosols can be done using not only the METimage data from visible as well as infrared bands, but also using ancillary measurements from

other satellite sources (e.g., Díaz et al. 2011) including dual view SST radiometers (Blackmore et al. 2012).

The clear sky atmospheric effects are caused primarily by the absorption and re-emission of infrared photons by water vapour, and water vapour is very variable in its distribution over the oceans in both space and time. Given the small number of spectral bands available for the clear-sky atmospheric correction, the most successful approaches in wide-spread use today are statistical in nature involving linear or slightly non-linear combinations of the collocated brightness temperatures measured in different spectral bands (e.g., McMillin 1975, Walton et al. 1998). Improvements to the accuracies of the SSTs can be achieved by introducing information from modelling the infrared radiative transfer through the atmosphere (Merchant et al. 2008), but thus far a pure "forward solution" in which the SST is derived using radiative transfer simulations of the top-of-atmosphere brightness temperatures using an accurate representation of the atmospheric state at the time of the measurement remains an active research topic with very promising results (e.g., Merchant et al. 2008). In the period of the METimage missions this might become feasible thereby avoiding the inherent weakness of the statistical approach that results in larger SST errors when the atmospheric state departs from conditions close to normal (Minnett 1986, Barton 2011, Szczodrak et al. 2014).

5.3 Improved cloud mask

In general, a cloud mask product indicates whether a pixel is cloudy. However, there is not necessarily a unique cloud mask that suits all applications and derived products. This is because applications and derived products are differently sensitive to the presence of cloud contamination, and may require different trade-offs between accuracy and maximising coverage. As an example, it is noteworthy that for MODIS and VIIRS, the standard cloud masks were not adequate for the identification of pixels that include cloud radiances and their exclusion from the generation of skin SSTs. In particular pixels with small fractions of cloud cover, or optically thin clouds, can introduce unacceptable errors in the SST retrievals. Likewise for METimage, it may be necessary to have cloud masks targeted to particular products and applications.

The approaches to cloud masking and cloud classification can be very diverse ranging from simple empirical thresholding, bayesian techniques, neural networks and much more. All cloud detection techniques consider features which contrast between clear and cloudy conditions: reflectance (including whiteness), temperature, emissivity and/or spatial variability. Approaches for combining the knowledge from individual features include decision trees and Bayesian classification amongst others. Training data that represents the range of environmental conditions that will be encountered in METimage data is needed in addition to forward simulation of radiances (usually clear-sky radiances) to aid discrimination. Most of the time, ancillary information such as numerical model outputs or surface and upper air observations (e.g., temperature profile, sea ice extent) and land/ocean and snow/no snow flags, are required. Determination of the appropriate thresholds (decision tree) and probability distributions (Bayesian) can be achieved using radiative transfer modelling, and/or analysis of on-orbit data

Experience has shown that these thresholds are likely to be different for different products, and may require iterative refinement once they have been applied to the on-orbit measurements. Decision trees therefore change accordingly, depending on the specific application or the science behind the algorithm development. Different needs can be identified by different communities leading to specialized products that meet their expectations. The products can then be conceived for several application frameworks and a considerable number of datasets can then result with a variable level of complexity (e.g., Platnick et al. 2003). The accuracy of these products can also be variable depending on the satellite sensors involved or on the retrieval methods.

The available products range from simple yes/no classification to more sophisticated products including, like the one from the MODIS team (Ackerman et al. 1998, 2006; Frey et al. 2008), several categories: confident clear, probably clear, uncertain/probably cloudy, and cloudy. Another example of multi-categorical cloud mask is the one from EUMETSAT's NWC-SAF, which provides several information, such as the cloud mask itself, the quality of the product, the usage (or not) of ancillary NWP data, the illumination conditions of the pixel, the dust contamination (http://nwcsaf.smhi.se/ProductDescriptionCloudMask.php). A heritage algorithm stemming from operational algorithms run at NOAA, NASA and EUMETSAT was recently conceived for the Advanced Baseline Imager (ABI) (Heidinger and Straka 2013) based on multiple tests derived from spaceborne lidar and geostationary imager data.

Further scientific progress in this field is expected through the use of ancillary information from lidar and radar instruments on satellite as well as from better radiative transfer modeling. However, it is felt that the various available masks will continue to depend on their specific application.

Finally, the relatively high amount of available cloud masks prompts for adequate documentation being made available. This documentation will help the final user to correctly use the product within its validity limits. An example of such documentation is provided by Strabala (1998) for the MODIS cloud mask.

5.4 Aerosol retrieval over bright surfaces (TBC)

The total radiance received by a satellite sensor at the top of atmosphere is composed of an atmospheric term (scattered radiance mainly caused by aerosols and molecules) and surface contribution. If the spectral behavior of a surface is precisely known to determine the reflected proportion of the incoming solar radiation, the retrieval of aerosol optical depth is straight forward using a radiative transfer model (e.g. 6S) and knowing the radiative properties of the aerosols. Hence, the precise surface reflectance is a key variable in the retrieval process. This is of special importance for bright surfaces with its high reflectance values because the atmospheric term is low related to the high surface values. Small uncertainties in the determination of surface reflectance result in large errors in aerosol retrieval. Fortunately, a surface which appears bright in the visible spectrum (desert, urban areas) has a much lower reflectance in the UV. Therefore, the retrieval of aerosols over deserts or urban areas should be based on reflectance values below 440nm as it is applied for the Aerosol Index (AI) considering TOMS data (Hermann and Celarier, 1997), studies done with GOME data (Holzer-Popp et al. 2002; Kusmierczyk-Michulec and G. de Leeuw, 2005) or with data using MODIS (Hsu et al., 2004; Sorek-Hamer et al., 2015) and also planned for VIIRS. As shown in the cited references is the precise knowledge of the surface reflectance in the UV or in the blue range of the visible spectrum the critical term to retrieve aerosols with sufficient accuracy over bright surfaces. A static data base of the reflectance behavior of bright surfaces is a good starting point but it is not sufficient because it changes over time caused by spreading of cities, surface rearrangements (wind induced erosions), greening of deserts, etc. Hence, the surface reflectance should be retrieved simultaneously or with a slight delay of some days to guarantee a precise knowledge of the surface properties. Furthermore, the bidirectional reflectance distribution function of bright surfaces has to be considered because the surface term with its directional behavior is dominating the reflectance.

It can be concluded, that an aerosol retrieval over bright surfaces based on METimage data is feasible but there is some need for research to provide a data base of surface reflectance properties considering temporal changes and BRDF behavior. A simultaneous retrieval of aerosol optical depth and surface reflectance based on more than one channel as applied for MODIS can guarantee to minimize the error in the final product. However, the blue or UV-channels are the most relevant

for the retrieval over bright surfaces.

A3 Composition of the METimage SAG

Vincenzo Levizzani	Co-Chair	CNR, IT
Oliver Sievers	Co-Chair	DWD, DE
Bernhard Mayer	Member	DLR, DE
Christopher Merchant	Member	Univ. Reading, UK
Peter Minnett	Member	RSMAS Univ. Miami, US
René Preusker	Member	Univ. Berlin, DE
Ronald Scheirer	Member	SMHI, SE
Thomas Trautmann	Member	DLR, DE
Stefan Wunderle	Member	Univ. Bern, CH
Pepe Phillips	Secretary	EUMETSAT
Isabel Zerfowski	Secretary	DLR

A4 Terms of Reference

The METimage instrument will be part of the core payload of the EUMETSAT Polar System – Second Generation (EPS-SG). The first flight opportunity of the METimage instrument will be on the first EPS-SG satellite to be launched in 2020 and operated by EUMETSAT. METimage will contribute to primary mission objectives of the EPS-SG in the areas of operational meteorology and climate monitoring. The objectives of the METimage mission are those of the visible and infrared imaging mission as described in the document "Post-EPS Mission Requirements Document", prepared by EUMETSAT under the guidance of the Post-EPS Mission Experts Team.

For the scientific preparation of the METimage mission, DLR and EUMETSAT establish a METimage Science Advisory Group (SAG), composed of leading scientists in the areas of optical imaging of clouds, precipitation, aerosols, ocean, and large-scale land surfaces. The members of the SAG will meet in intervals of typically six months.

One of the primary tasks of this group is the preparation of a science plan to detail the scientific work which is needed to meet the METimage mission objectives. This plan will be prepared by the METimage SAG, guided by its two co-chairs, and supported by EUMETSAT and DLR. The science plan must especially establish the scientific requirements for the METimage related components of the EPS-SG ground segment. The plan will be used as reference for scientific activities to be undertaken within and outside the METimage SAG in the coming years.

In particular, the METimage SAG should:

- Provide a science plan to detail the scientific work which is needed in preparation of the METimage mission, especially also of the EPS-SG ground segment; update this plan when necessary
- Assist DLR and EUMETSAT in the selection of the most suitable methods to be applied for the EPS-SG PS ground segment, covering both the central processing at EUMETSAT and the de-centralised processing in the network of the EUMETSAT Satellite Application Facilities
- Advise DLR and EUMETSAT on requirements and methods for instrument calibration and post-launch validation activities
- Advise on the scientific requirements of the METimage system and instrument, taking into account constraints which are imposed by the status of design/development of the overall Post-EPS system and of the METimage instrument development
- Review the progress and the results of scientific projects initiated in support of METimage; provide recommendations to DLR and EUMETSAT on the direction and focus of further work to be pursued within these projects
- Review the progress of the METimage project by supporting technical reviews and advise on implications for mission and scientific objectives
- Provide recommendations for scientific studies which are needed to support the METimage project, in order to fulfil the requirements in the science plan and by assisting in preparation of work statements and by reviewing results of initiated studies
- Participate in the coordination of the METimage SAG activities with external science and user groups
- Contribute to the production of scientific reports and publications in the framework of the METimage SAG activities.

The meetings will be called jointly by DLR and EUMETSAT in agreement with the chairpersons. Electronic communication will be used as much as possible to exchange information and progress on the work between the meetings. The METimage SAG will accompany the METimage project at least to the end of the commissioning phase.

A5 Acronyms

3MI	Multi-viewing Multi-channel Multi-polarisation mission ESA-EUMETSAT)
AASTR	Advanced Along-Track Scanning Radiometer (ESA)
ABI	Advanced Baseline Imager (NOAA)
ACT	Across Track
ADM-Aeolus	Atmospheric Dynamics Mission-Aeolus (ESA)
AERONET	Aerosol Robotic NETwork (NASA)
ALT	Along Track
AMSR	Advanced Microwave Scanning Radiometer (JAXA)
AMV	Atmospheric Motion Vector
AOD	Aerosol Optical Depth
AOT	Aerosol Optical Thickness
ARM	Atmospheric Radiation Measurement network (DOE)
ASTER	Advanced Spaceborne Thermal Emission and Reflection Radiometer (NASA)
ASTM	American Society for Testing and Materials
ATBD	Algorithm Theoretical Basis Document
ATMS	Advanced Technology Micro-wave Sounder (NASA)
ATSR	Along-Track Scanning Radiometer (ESA)
AVHRR	Advanced Very High Resolution Radiometer (NOAA)
BRDF	Bi-directional Reflectance Distribution Function
CALIOP	Cloud-Aerosol Lidar with Orthogonal Polarization (CALIPSO, NASA-CNES)
CALIPSO	Cloud-Aerosol Lidar and Infrared Pathfinder Satellite Observations (NASA-CNES)
CAPSAT	Clouds-Aerosols-Precipitation Satellite Analysis Tool
CCI	Climate Change Initiative (ESA)
CCN	Cloud Condensation Nucleus
CDOM	Chromophoric Dissolved Organic Matter
CDR	Climate Data Record
CEOS	Committee on Earth Observing Satellites
CERES	Clouds and the Earth's Radiant Energy System (NASA)
CGMS	Coordination Group for Meteorological Satellites
CLARREO	Climate Absolute Radiance and Refractivity Earth Observatory (NASA)
CM-SAF	Climate Monitoring SAF (EUMETSAT)
CN	Condensation Nucleus
CNES	Centre National d'Études Spatiales
CNR	Consiglio Nazionale delle Ricerche
CORINE	COoRdinate INformation on the Environment database

COSMO	Consortium for Small scale Modelling
COT	Cloud Optical Thickness
CPR	Cloud Profiling Radar (CloudSat) (NASA-JPL)
CREW	Cloud Retrieval Evaluation Workshop
CRM	Cloud-Resolving Model
CTH	Cloud Top Height
CTT	Cloud Top Temperature
DARDAR	raDAR/liDAR project (LATMOS and Univ. Reading)
DEM	Digital Elevation Model
DISORT	Discrete Ordinates Radiative Transfer code
DLR	Deutsches Zentrum für Luft- und Raumfahrt
DOE	Depertment Of Energy
DMSP	Defense Meteorological Satellite Program (US Navy)
DWD	Deutscher Wetterdienst
EARLINET	European Aerosol Research Lidar Network (EC)
EarthCARE	Earth Clouds, Aerosols and Radiation Explorer (ESA-JAXA-NICT)
EC	European Commission
ECMWF	European Centre for Medium-range Weather Forecasts
ECV	Essential Climate Variable
EOS	Earth Observing System (NASA)
EPS	EUMETSAT Polar System
EPS-SG	EPS Second Generation (EUMETSAT)
ESDR	Earth System Data Record
EU	European Union
EUMETSAT	European Organisation for the Exploitation of Meteorological Satellites
FASCODE	Fast Atmospheric Signature CODE
FEE	Front End Electronics
FOV	Field of View
FAPAR	Fraction Absorbed Photosynthetically Active Radiation
FPA	Focal Plane Array
FWHM	Full Width Half Maximum
GCOS	Global Climate Observing System (WMO)
GEISA	Gestion et Etude des Informations Spectroscopiques Atmosphériques database
GEWEX	Global Energy and Water Exchanges Project (WMO)
GHRSST	Group for High Resolution SST
GIS	Geographic Information System
GMES	Global Monitoring for Environment and Security (EU)

GOME	Global Ozone Monitoring Experiment (ESA)
GPM	Global Precipitation Measurement (NASA) mission
GSICS	Global Space-based Inter-Calibration System (WMO-CGMS)
GUAN	GCOS Upper-Air Network (WMO)
HAM	Half Angle Mirror
HITRAN	High Resolution Transmission
HKTM	Housekeeping and Telemetry data
H-SAF	SAF in Support to Operational Hydrology and Water Management (EUMETSAT)
HyspIRI	Hyperspectral Infrared Imager (NASA)
IASI	Infrared Atmospheric Sounding Interferometer (ESA-EUMETSAT)
IASI IIS	IASI Integrated Imaging Sub-system (ESA-EUMETSAT)
IASI-NG	IASI Next Generation (ESA-EUMETSAT)
ICI	Ice-Cloud Imaging mission (ESA-EUMETSAT)
IFOV	Instantaneous Field of View
IGOS	Integrated Global Observing Strategy (UNESCO)
IMK	Institut für Meteorologie und Klimaforschung (Karlsruhe)
IPCC	Intergovernmental Panel on Climate Change
IR	Infra-Red
JEDI	Joint Emissivity Database Initiative (NASA-JPL)
JPL	Jet Propulsion Laboratory (NASA)
JRC	Joint Research Centre (EC)
LAI	Leaf Area Index
LSA-SAF	Land Surface Analysis SAF (EUMETSAT)
Landsat TM	Landsat Thematic Mapper (NASA)
LATMOS	Laboratoire Atmosphères, Milieux, Observations Spatiales
LBLRTM	Line-By-Line RTM
LEO	Low Earth Orbit
LES	Large Eddy Simulation
LIDAR	LIght Detection And Ranging
LOS	Line-Of-Sight
LST	Land Surface Temperature
LULC	Land Use/Land Cover data
LUT	Look Up Table
LWIR	Long Wave Infrared
MASTER	MODIS/ASTER Airborne Simulator (NASA)
MERIS	Medium Resolution Imaging Spectrometer (ESA)
MERLIN	MEthane Remote sensing LIdar mission (DLR-CNES)

MIPAS	Michelson Interferometer for Passive Atmospheric Sounding (ESA)
MODIS	Moderate Resolution Imaging Spectroradiometer (NASA)
MODSCAG	MODIS Snow-Covered Area and Grain size code
MODTRAN	MODerate resolution atmospheric TRANsmission
MRD	Mission Requirements Document
MTF	Modulation Transfer Function
MWI	Microwave Imaging mission (ESA-EUMETSAT)
MWIR	Mid Wave Infrared
MWR	Microwave Sounding mission (ESA-EUMETSAT)
MYSTIC	Monte Carlo code for the physically correct tracing of photons in cloudy atmospheres
NASA	National Aeronautics and Space Administration
NAVATT	Navigation and Attitude data
NDSI	Normalised Difference Snow Index
NDVI	Normalised Difference Vegetation Index
NICT	National Institute of Information and Communications Technology of Japan
NIR	Near Infrared
NLSST	Non Linear SST
NOAA	National Oceanic and Atmospheric Administration
NRT	Near Real Time
NSDIC	National Snow and Ice Data Center
NWC	Nowcasting
NWC-SAF	SAF in Support to Nowcasting and Very Short Range Forecasting (EUMETSAT)
NWP	Numerical Weather Prediction
NWP-SAF	SAF for Numerical Weather Prediction (EUMETSAT)
OLCI	Ocean Land Colour Instrument (Sentinel 3-ESA)
OPAC	Optical Properties of Aerosols and Clouds database
OSI-SAF	Ocean and Sea Ice SAF (EUMETSAT)
PAR	Photosynthetically Active Radiation
POLDER	Polarization and Directionality of the Earth’s Reflectances (CNES)
PSD	Particle Size Distribution
RADAR	Radio Detection And Ranging
Reff	Cloud Effective Radius
RFM	Reference Forward Model
RI	Refractive Index
RO	Radio Occultation mission (ESA-EUMETSAT)
ROIC	Readout Integrated Circuit
ROLO	RObotic Lunar Observation (USGS)

RSMAS	Rosenstiel School of Marine and Atmospheric Science (Univ. of Miami)
RT	Radiative Transfer
RT3	Radiative Transfer 3 (vector radiative transfer code)
RTLSR	RossThick-LiSparse Reciprocal model
RTM	Radiative Transfer Model
RTTOV	Radiative Transfer for (A)TOVS (TIROS Operational Vertical Sounder)
RVS	Reflection vs Scan angle
S5	Sentinel 5
S&IA	Seasonal and Inter-Annual forecasting
SAF	Satellite Application Facility (EUMETSAT)
SAG	Science Advisory Group
SCA	Scatterometry mission
SCIAMACHY	SCanning Imaging Absorption spectroMeter for Atmospheric CHartographY (ESA)
SD	Solar Diffuser
SDPTK	Science Data Processing Toolkit
SeaWiFS	Sea-viewing Wide Field-of-view Sensor (NASA)
SEL	Systems Ecology Laboratory
SEVIRI	Spinning Enhanced Visible Infra-Red Imager (ESA-EUMETSAT)
SHARM	Spherical Harmonics Atmospheric Radiation Model
SHDOM	Spherical Harmonic Discrete Ordinate Method
SHIPS	Spectral Habit Ice Prediction System
SIRS	Satellite InfraRed Spectrometer
SLSTR	Sea and Land Surface Temperature Radiometer (ESA)
SMHI	Swedish Meteorological and Hydrological Institute
SNO	Simultaneous Nadir Observations
SOLSPEC	SOLar SPECtrum spectrometer (LATMOS)
SPOT	Satellite pour l'Observation de la Terre (Airbus Defence & Space)
SSCC	SEVIRI Spectral Channel Calibration (ESA-EUMETSAT)
SSD	Spatial Sampling DIstance
SSI	Spectral Solar Irradiance
SSM/I	Special Sensor Microwave/Imager (DMSP)
SST	Sea Surface Temperature
SW	Short Wave
SWIR	Short Wave Infrared
S&IA	Scenario & Impact Analysis
TBD	To be defined
TBW	To be written

TCW	Total Column Water Vapour
TIPA	Tilted Independent Pixel Approximation
TIR	Thermal Infrared
TOA	Top of atmosphere
TRMM	Tropical Rainfall Measuring Mission (NASA-JAXA)
TRUTHS	Traceable Radiometry Underpinning Terrestrial- and Helio-Studies
TSIS	Total Solar Irradiance Sensor (NOAA)
UNESCO	United Nations Educational, Scientific and Cultural Organization
UNFCCC	United Nations Framework Convention on Climate Change
USGS	US Geological Survey
UTEP	University of Texas at El Paso
UV	Ultraviolet
UVNS	Ultraviolet Visible Near-infrared Shortwave mission
UWIREMIS	University of Wisconsin Global Infrared Land Surface Emissivity database
VII	Visible Infra-red Imaging mission (ESA-EUMETSAT)
VIIRS	Visible Infrared Imager Radiometer Suite (NASA)
VIRS	Visible and Infrared Scanner (NASA)
VIS	Visible
VLWIR	Very Long Wave Infrared
VNIR	Visible and Near-Infrared
VSL	Vegetation Spectral Library
WGCV	Working Group on Calibration & Validation (CEOS)
WGMS	World Glacier Monitoring Service
WGS84	World Geodetic System 1984
WMO	World Meteorological Organization
WV	Water Vapour

A6 References

Ackerman, T. P., 2005: The role of global observations for climate and other applications. DOE/SC-ARM/TR-067, 5 pp.

Ackerman, S. A., K. I. Strabala, W. P. Menzel, R. A. Frey, C. C. Moeller, and L. E. Gumley, 1998: Discriminating clear sky from clouds with MODIS. J. Geophys. Res., 103, 32141-32157.

Ackerman, S. A., R. Frey, K. Strabala, Y. Liu, L. Gumley, B. Baum, and W. P. Menzel, 2006: Discriminating claer-sky from cloud with MODIS – Algorithm Theoretical Basis (MOD35), Univ. Wisconsin-Madison, Cooperative Institute for Meteorological Satellite Studies 121 pp. [available at http://modis.gsfc.nasa.gov/data/atbd/atbd_mod06.pdf]

Albert, P., R. Bennartz, R. Preusker, R. Leinweber, and J. Fischer, 2005: Remote sensing of atmospheric water vapor using the Moderate Resolution Imaging Spectroradiometer. J. Atmos. Oceanic Technol., 22, 309–314.

Allen, M. R., C. T. Mutlow, G. M. C. Blumberg, J. R. Christy, R. T. McNider, and D. T. Llewellyn-Jones, 1994: Global change detection. *Nature*, 370, 24-25.

Anderson, G. P., S. A. Clough, F. X. Kneizys, J. H. Chetwynd, and E. P. Shettle, 1986: AFGL Atmospheric Constituent Profiles (0-120 km). AFGL-TR-86-0110, Air Force Geophysics Laboratory, Hanscom Air Force Base, MA, USA, 43 pp.

Anthes, R. A., B. Moore III, J. G. Anderson, S. K. Avery, E. J. Barron, O. B. Brown, S. L. Cutter, R. DeFries, W. B. Gail, B. H. Hager, A. Hollingsworth, A. C. Janetos, K. A. Kelly, N. F. Lane, D. P. Lettenmeier, B. D. Marcus, W. M. Washington, M. L. Wilson, M. L. Zoback, and S. W. Boland, 2007: Earth science and applications from space - National imperatives for the next decade and beyond. National Academies Press, 456 pp.

Asrar, G., J. A. Kaye, and P. Morel, 2001: NASA research strategy for Earth system science: Climate component. Bull. Amer. Meteor. Soc., 82, 1309-1329.

ASTM International, 2000: ASTM E-490 solar irradiance spectrum, http://rredc.nrel.gov/solar/spectra/am0/

Baldridge, A. M., S. J. Hook, C. I. Grove, and G. Rivera, 2009: The ASTER Spectral Library Version 2.0. Remote Sens. Environ., 113, 711-715.

Barton, I. J., 2011: Improving satellite-derived sea surface temperature accuracies using water vapor profile data. J. Atmos. Oceanic Technol., 28, 85-93.

Bedka, K. M., and J. R. Mecikalski, 2005: Application of satellite-derived atmospheric motion vectors for estimating mesoscale flows. J. Appl. Meteor., 44, 1761-1772.

Behrangi, A., T. Kubar, and B. Lambrigtsen, 2012: Phenomenological description of tropical clouds using CloudSat cloud classification. Mon. Wea. Rev., 140, 3235–3249.

Bell, M. J., R. M. Forbes, and A. Hines, 2000: Assessment of the FOAM global data assimilation system for real-time operational ocean forecasting. J. Marine Syst., 25, 1-22.

Bennartz, R., and J. Fischer, 2001: Retrieval of columnar water vapour over land from back-scattered solar radiation using the Medium Resolution Imaging Spectrometer (MERIS). Remote Sens. Environ., 78, 271-280.

Berk, A., G. P. Anderson , P. K. Acharya, L. S. Bernstein, L. Muratov , J. Lee, M. Fox, S. M. Adler-Golden, J. H. Chetwynd, M. L. Hoke, R. B. Lockwood, J. A. Gardner, T. W. Cooley, C. C. Borel, and P. E. Lewis, 2005: MODTRAN 5: A reformulated atmospheric band model with auxiliary species and practical multiple scattering options: update. SPIE, 5806, 662-667.

Bertie, J. E., and Z. Lan, 1996: Infrared intensities of liquids XX: The intensity of the OH stretching band of liquid water revisited, and the best current values of the optical constants of H_2O(l) at 25°C between 15000 and 1 cm^{-1}. Appl. Spectroscopy, 50, 1047-1057.

Bjerknes, J., 1964: Atlantic air-sea interactions. Adv. Geophys., 10, Academic Press, 1-82.

Blackmore, T., A. O'Carroll, K. Fennig, and R. Saunders, 2012: Correction of AVHRR Pathfinder SST data for volcanic aerosol effects using ATSR SSTs and TOMS aerosol optical depth. Remote Sens. Environ., 116, 107-117.

Böhm, E., S. Marullo, and R. Santoleri, 1991: AVHRR visible-IR detection of diurnal warming events in the western Mediterranean Sea. Int. J. Remote Sens., 12, 695-701.

Bohren, C. F., and D. R. Huffman, 1998: Absorption and scattering of light by small particles. J. Wiley & Sohns, New York, 530 p., ISBN 0471293407, ISBN 9780471293408 (2nd edition).

Bormann, N., and J.-N. Thépaut, 2004: Impact of MODIS polar winds in ECMWF's 4DVAR data assimilation system. Mon. Wea. Rev., 132, 929-940.

Bugliaro, L., T. Zinner, C. Keil, B. Mayer, R. Hollmann, M. Reuter, and W. Thomas, 2010: Validation of cloud property retrievals with simulated satellite radiances: A case study for SEVIRI. Atmos. Chem. Phys., 11, 5603-5624.

Buras, R., and B. Mayer, 2011: Efficient unbiased variance reduction techniques for Monte Carlo simulations of radiative transfer in cloudy atmospheres: the solution. J. Quant. Spectrosc. Radiat. Transfer, 112, 434-447.

Cahalan, R. F., W. Ridgway, W. J. Wiscombe, Harshvardhan, and S. Gollmer, 1994: Independent pixel and Monte Carlo estimates of stratocumulus albedo. J. Atmos. Sci., 51, 3776-3790.

Cahalan, R. F., L. Oreopoulos, A. Marshak, K. F. Evans, A. B. Davis, R. Pincus, K. H. Yetzer, B. Mayer, R. Davies, T. P. Ackerman, H. B. Barker, E. E. Clothiaux, R. G. Ellingson, M. Garay, E. Kassianov, S. Kinne, A. Macke, W. O'Hirok, P. T. Partain, S. M. Prigarin, A. N. Rublev, G. L. Stephens, F. Szczap, E. E. Takara, T. Várnai, G. Wen, and T. B. Zhuravleva, 2005: The I3RC: Bringing together the most advanced radiative transfer tools for cloudy atmospheres. Bull. Amer. Meteor. Soc., 86, 1275-1293.

Casadio, S., and P. Colagrande, 2003: Proceedings of MERIS User Workshop (ESA SP-549), ESA-ESRIN, Frascati, Italy. Editor: H. Lacoste. Published on CDROM., id.39.1.

Cavalieri, D., T. Markus, D. K. Hall, A. Ivanoff, and E. Glick, 2010: Assessment of AMSR-E Antarctic winter sea-ice concentrations using Aqua MODIS. IEEE Trans. Geosci. Remote Sens., 48, 3331-3339.

Chelton, D. B., and S.-P. Xie, 2010: Coupled ocean-atmosphere interaction at oceanic mesoscales. Oceanography, 23**,** 52–69.

Cherubini, T., S. Businger, C. Velden, and R. Ogasawara, 2006: The impact of satellite-derived atmospheric motion vectors on mesoscale forecasts over Hawaii. Mon. Wea. Rev., 134, 2009–2020.

Chevallier, F., 2002: Sampled database of 60-level atmospheric profiles from the ECMWF analyses. NWP SAF Report No. NWPSAF-EC-TR-004, 27 pp.

Chevallier, F., S. Di Michele, and A. P. McNally, 2006: Diverse profile datasets from the ECMWF 91-level short-range forecasts. NWP SAF Report No. NWPSAF-EC-TR-010, 14 pp.

CIRC (http://circ.gsfc.nasa.gov/; Oreopulos et al. 2011) in the framework of the Continual Intercomparison of Radiation Codes.

Clough, S. A., F. X. Kneizys, G. P. Anderson, E. P. Shettle, J. H. Chetwynd, L. W. Abreu, L. A. Hall, and R. D. Worsham, 1988: FASCOD3: spectral simulation. In IRS 1988: Current Problems in Atmospheric Radiation, J. Lenoble and J.F. Geleyn (Eds.), A. Deepak Publishing, 372-375.

Clough, S. A., M. W. Shephard, E. J. Mlawer, J. S. Delamere, M. J. Iacono, K. Cady-Pereira, S. Boukabara, and R. D. Brown, 2005: Atmospheric radiative transfer modeling: a summary of the

AER codes. J. Quant. Spectrosc. Radiat. Transfer, 91, 233–244.

Davies, A., A. Marshak, R. Cahalan, and W. Wiscombe, 1997, The Landsat scale break in stratocumulus as a three-dimensional radiative transfer effect: Implications for cloud remote sensing. J. Atmos. Sci., 54(2), 241-260.

Deeter, M. N., and J. Vivekanandan, 2006: New dual-frequency microwave technique for retrieving liquid water path over land. J. Geophys. Res., 111, D15209, doi: 10.1029/2005JD006784.

Deser, C., M. A. Alexander, S.-P. Xie, and A. S. Phillips, 2010: Sea surface temperature variability: Patterns and mechanisms. Annual Rev. Marine Sci., 2, 115-143.

DeVoe, H., 1964: Optical properties of molecular aggregates. I. Classical model of electronic absorption and refraction. J. Chem. Phys., 41, 393-400.

Díaz, J. P., M. Arbelo, F. J. Expósito, G. Podestá, J. M. Prospero, and R. Evans, 2001: Relationship between errors in AVHRR-derived sea surface temperature and the TOMS Aerosol Index. Geophys. Res. Lett., 28, 1989–1992.

Diedrich, H., R. Preusker, R. Lindstrot, and J. Fischer, 2013: Quantification of uncertainties of water vapour column retrievals using future instruments. Atmos. Meas. Tech., 6, 359-370.

Doicu, A., and T. Trautmann, 2009: Discrete-ordinate method with matrix exponential for a pseudo-spherical atmosphere: Scalar case. J. Quant. Spectrosc. Radiat. Transfer, 110, 146-158.

Donlon, C. J., M. Martin, J. Stark, J. Roberts-Jones, E. Fiedler, and W. Wimmer, 2012: The Operational Sea Surface Temperature and Sea Ice Analysis (OSTIA) system. Remote Sens. Environ., 116, 140-158.

Drori, R., and I. M. Lensky, 2010: Monitoring the evolution of cloud phase profile using MSG data. Atmos. Res., 97(4), 577-582.

Dubovik, O., B. Holben, T. F. Eck, A. Smirnov, Y. Kaufman, M. Kind, D. Tanre, and I. Slutsker, 2002: Variability and optical properties of key aerosol types observed in worldwide locations. J. Atmos. Sci., 59, 590–608.

Dubovik, O., A. Sinyuk, T. Lapyonok, B. N. Holben, M. Mishchenko, P. Yang, T. F. Eck, H. Volten, O. Munoz, B. Veihelmann, W. J. van der Zander, J.-F. Leon, M. Sorokin, and I. Slutsker, 2006: Application of light scattering by spheroids for accounting for particle non-sphericity in remote sensing of desert dust. J. Geophys. Res., 111, D11208, doi:10.1029/2005JD006619d.

Dubuisson, P., R. Frouin, D. Dessaully, L. Duforêt, J-F. Léon, K. Voss, and D. Antoine, 2009: Estimating the altitude of aerosol plumes over the ocean from reflectance ratio measurements in the O_2 A-band. Remote Sens. Environ., 113, 1899-1911.

Dudhia, A., P. E. Morris, and R. J. Wells, 2002: Fast monochromatic radiative transfer calculations for limb sounding. J. Quant. Spectrosc. Radiat. Transfer, 74, 745-756.

Dybbroe, A., K.-G. Karlsson, and A. Thoss, 2005a: NWCSAF AVHRR cloud detection and analysis using dynamic thresholds and radiative transfer modeling. Part I: Algorithm description. J. Appl. Meteor., 44, 39-54.

Dybbroe, A., K.-G. Karlsson, and A. Thoss, 2005b: NWCSAF AVHRR cloud detection and analysis using dynamic thresholds and radiative transfer modeling. Part II: Tuning and validation. J. Appl. Meteor., 44, 55-71.

Edwards, D. P., 1988: Atmospheric transmittance and radiance calculations using line-by-line computer models. In Modelling of the Atmosphere, vol. 928, 94-116, Proc. SPIE.

Embury, O., C. J. Merchant, and M. J. Filipiak, 2010: A reprocessing for climate of sea surface temperature from the Along-Track Scanning Radiometers: Basis in radiative transfer. Remote Sens. Environ., 116, 47-61.

Emde, C., and B. Mayer, 2007: Simulation of solar radiation during a total solar eclipse: A challenge for radiative transfer. Atmos. Chem. Phys., 7, 2259-2270.

Emde, C., R. Buras, and B. Mayer, 2011: ALIS: An efficient method to compute high spectral resolution polarized solar radiances using the Monte Carlo approach. J. Quant. Spectrosc. Radiat. Transfer, 112, 1622-1631.

Emde, C., R. Buras, B. Mayer, and M. Blumthaler, 2010: The impact of aerosols on polarized sky radiance: model development, validation, and applications. Atmos. Chem. Phys., 10, 383-396.

Emili, E., A. Lyapustin, Y. Wang, C. Popp, S. Korkin, M. Zebisch, S. Wunderle, and M. Petitta, 2011: High spatial resolution aerosol retrieval with MAIAC: Application to mountain regions. J. Geophys. Res., 116, D23211, doi:10.1029/2011JD016297.

Eplee, R. E., J.-Q. Sun, G. Meister, F. S. Patt, X. Xiong, and C. R. McClain, 2011: Cross calibration of SeaWiFS and MODIS using on-orbit observations of the Moon. Appl. Opt., 50, 120-133.

Eplee, R. E., G. Meister, F. S. Patt, R. A. Barnes, S. W. Bailey, B. A. Franz, and C. R. McClain, 2012: On-orbit calibration of SeaWiFS. Appl. Opt., 51, 8702-8730.

EUMETSAT, 2012: Post-EPS Mission Requirements Document, EUM/PEPS/REQ/06/0043.

EUMETSAT, 2015: EPS-SG End User Requirements Document, EUM/PEPS/REQ/09/0151.

Evans, K. F., and G. L. Stephens, 1991: A new polarized atmospheric radiative transfer model. J. Quant. Spectrosc. Radiat. Transfer, 46, 413–423.

Evans, K. F., and W. J. Wiscombe, 2004: An algorithm for generating stochastic cloud fields from radar profile statistics. Atmos. Res., 72, 263-289.

Ferwerda, J. G., S. D. Jones, and M. Reston, 2006: A free online reference library for hyperspectral reflectance signatures. SPIE, Newsroom, doi: 10.1117/2.1200612.0551.

Filipiak, M. 2008: Refractive indices (500-3500 cm^{-1}) and emissivity (600-3350 cm^{-1}) of pure water and seawater [Dataset].

Frey, R. A., S. A. Ackerman, Y. Liu, K. I. Strabala, H. Zhang, J. R. Key, and X. Wang, 2008: Cloud detection with MODIS, Part I: Improvements in the MODIS cloud mask for collection 5. J. Atmos. Oceanic Technol., 25, 1057-1072.

Gao, B. C., and Y. J. Kaufman, 2003: Water vapor retrievals using Moderate resolution Imaging Spectroradiometer (MODIS) near-infrared channels. J. Geophys. Res., 108(D13), doi: 10.1029/2002JD003023.

Gassó, S., 2008. The impact of weak volcanic activity on marine clouds. J. Geophys. Res., 113, doi:10.1029/2007JD009106.

Gentemann, C. L., P. J. Minnett, P. LeBorgne, and C. J. Merchant, 2008: Multi-satellite measurements of large diurnal warming events. Geophys. Res. Lett., 35, doi: 10.1029/2008GL035730.

Gentemann, C. L., P. J. Minnett, and B. Ward, 2009: Profiles of Ocean Surface Heating (POSH): A new model of upper ocean diurnal thermal variability. J. Geophys. Res., 114, doi: 10.1029/2008JC004825.

Giglio, L., J. Descloitres, C. O. Justice, and Y. J. Kaufman, 2003: An enhanced contextual fire detection algorithm for MODIS. Remote Sens. Environ., 87, 273–282.

Goerss, J. S., C. S. Velden, and J. D. Hawkins, 1998: The impact of mltispectral GOES-8 wind information on Atlantic tropical cyclone track forecasts in 1995. Part II: NOGAPS forecasts. Mon. Wea. Rev., 126, 1219-1227.

Goloub, P., M. Herman, H. Chepfer, J. Riedi, G. Brogniez, P. Couvert, and G. Séze, 2000: Cloud thermodynamical phase classification from the POLDER spaceborne instrument. J. Geophys. Res., 105 (D11), 14747–14759.

Good, S. A., G. K. Corlett, J. J. Remedios, E. J. Noyes, and D. T. Llewellyn-Jones, 2007: The global trend in sea surface temperature from 20 years of Advanced Very High Resolution Radiometer data. J. Climate, 20, 1255-1264.

Goody, R., J. Anderson, T. Karl, R. B. Miller, G. North, J. Simpson, G. Stephens, and W. Washington, 2002: Why monitor the climate? Bull. Amer. Meteor. Soc., 83, 873-878.

Govaerts, Y. M., A. Arriaga, and J. Schmetz, 2001: Operational vicarious calibration of the MSG/SEVIRI solar channels. Adv. Space. Res., 28, 21-30.

Grainger, R. G., J. Lucas, G. E. Thomas, and G. Ewan, 2004: The calculation of Mie derivatives. Appl. Opt., 43(28), 5386-5393.

Guanter, L., L. Gómez-Chova, and J. Moreno, 2008: Coupled retrieval of aerosol optical thickness, columnar water vapor and surface reflectance maps from ENVISAT/MERIS data over land. Remote Sens. Environ., 112, 2898-2913.

Halthore, R. N., D. Crisp, S. E. Schwartz, G. P. Anderson, A. Berk, B. Bonnel, O. Boucher, F.-L. Chang, M.-D. Chou, E. E. Clothiaux, P. Dubuisson, B. Fomin, Y. Fouquart, S. Freidenreich, C. Gautier, S. Kato, I. Laszlo, Z. Li, J. H. Mather, A. Plana-Fattori, V. Ramaswamy, P. Ricchiazzi, Y. Shiren, A. Trishenko, and W. Wiscombe, 2005: Intercomparison of shortwave radiative transfer codes and measurements. J. Geophys. Res., 110, D11206, doi:10.1029/2004JD005293.

Hanafin, J. A., and P. J. Minnett, 2005: Infrared-emissivity measurements of a wind-roughened sea surface. Appl. Opt., 44, 398-411.

Hansen, J., R. Ruedy, M. Sato, and K. Lo, 2010: Global surface temperature change. Rev. Geophys., 48, doi: 10.1029/2010RG000345.

Harder, J. W., G. Thuillier, E. C. Richard, S. W. Brown, K. R. Lykke, M. Snow, W. E. McClintock, J. M. Fontenla, T. N. Woods, and P. Pilewskie, 2010: The SORCE SIM solar spectrum: Comparison with recent observations. Solar Phys., 263, 3-24, DOI 10.1007/s11207-010-9555-y.

Hashino, T., and G. J. Tripoli, 2007: The Spectral Ice Habit Prediction System (SHIPS). Part I: Model description and simulation of the vapor deposition process. J. Atmos. Sci., 64, 2210–2237.

Hashino, T., and G. J. Tripoli, 2008: The Spectral Ice Habit Prediction System (SHIPS). Part II: Simulation of nucleation and depositional growth of polycrystals. J. Atmos. Sci., 65, 3071–3094.

Hashino, T., and G. J. Tripoli, 2011a: The Spectral Ice Habit Prediction System (SHIPS). Part III: Description of the ice particle model and the habit-dependent aggregation model. J. Atmos. Sci., 68, 1125–1141.

Hashino, T., and G. J. Tripoli, 2011b: The Spectral Ice Habit Prediction System (SHIPS). Part IV: Box model simulations of the habit-dependent aggregation process. J. Atmos. Sci., 68, 1142–1161.

Heidinger, A., and W. C. Straka, 2013: ABI Cloud Mask – Algorithm Theoretical Basis Document, V. 3.0. NOAA-NESDIS, Center for Satellite Applications and Research, 106 pp. [available at http://www.star.nesdis.noaa.gov/goesr/docs/ATBD/Cloud_Mask.pdf]

Henyey, L. G., and J. L. Greenstein, 1941: Diffuse radiation in the galaxy. Astrophys. J., 93, 70-83.

Herman, J. R., and E. A. Celarier, 1997: Earth surface reflectivity climatology at 340– 380 nm from TOMS data. J. Geophys. Res., 102, 28,003–28,011.

Hess, M., P. Koepke, and I. Schult, 1998: Optical properties of aerosols and clouds: The software package OPAC. Bull. Amer. Meteor. Soc., 79, 831–844.

Holben B. N., T. F. Eck, I. Slutsker, D. Tanré, J. P. Buis, A. Setzer, E. Vermote, J. A. Reagan, Y. J. Kaufman, T. Nakajima, F. Lavenu, I. Jankowiak, and A. Smirnov, 1998: AERONET - A federated instrument network and data archive for aerosol characterization. Remote Sens. Environ., 66, 1–16.

Holzer-Popp, T., M. Schroedter, and G. Gesell, 2002: Retrieving aerosol optical depth and type in the boundary layer over land and ocean from simultaneous GOME spectrometer and ATSR-2 radiometer measurements, 1, Method description. J. Geophys. Res., 107(D21), 4578,

doi:10.1029/2001JD002013

House, L. L., and L. W. Avery, 1969: The Monte Carlo technique applied to radiative transfer. J. Quant. Spectrosc. Radiat. Transfer, 9, 1579-1591.

Hsu, N. C., Tsay, S.-C., King, M. D., and J. R. Herman, 2004: Aerosol properties over bright-reflecting source regions, IEEE Transactions on Geoscience and Remote Sensing, vol. 42, no. 3, pp. 557-569.

doi: 10.1109/TGRS.2004.824067

Hungershoefer, K., K. Zeromskiene, Y. Iinuma, G. Helas, J. Trentmann, T. Trautmann, R. S. Parmar, A. Wiedensohler, M. O. Andreae, and O. Schmid, 2008: Modelling the optical properties of fresh biomass burning aerosol produced in a smoke chamber: results from the EFEU campaign.

Atmos. Chem. Phys., 8, 3427–3439.

Inoue, T., 1985: On the temperature and effective emissivity determination of semi-transparent cirrus clouds by bi-spectral measurements in the 10 micron window region. J. Meteor. Soc. Japan, 63, 88-98.

Inoue, T., 1987: A cloud type classification with NOAA 7 split-window measurements. J. Geophys. Res., 92D, 3991-4000.

Jacquinet-Husson, N., and 52 co-authors, 2008: The GEISA spectroscopic database: Current and future archive for Earth and planetary atmosphere studies. J. Quant. Spectrosc. Radiat. Transfer, 109, 1043-1059.

Jakosky, B. M., G. W. Finiol, and B. G. Henderson, 1990: Directional variations in thermal emission from geologic surfaces. Geophys. Res. Lett., 17, 985–988.

Joro, S., 2010: Comparison of satellite cloud masks with ceilometer sky conditions in Southern Finland. J. Appl. Meteor. Climatol., 49, 2508–2526.

Kahnert, M., and A. Devasthale, 2011: Black carbon fractal morphology and short-wave radiative impact: a modelling study. Atmos. Chem. Phys., 11, 11745-11759, doi:10.5194/acp-11-11745-2011.

Kahnert, M., T. Nousiainen, and B. Veihelmann, 2005: Spherical and spheroidal model particles as an error source in aerosol climate forcing and radiance computations: A case study for feldspar aerosols. J. Geophys. Res., 110, D18S13, doi:10.1029/2004JD005558.

Karlsson, K.-G., and E. Johansson, 2013: On the optimal method for evaluating cloud products from passive satellite imagery using CALIPSO-CALIOP data: example investigating the CM SAF CLARA-A1 dataset. Atmos. Meas. Tech., 6, 1271-1286, doi:10.5194/amt-6-1271-2013.

Kelder, H., B. Kerridge, I. Isaksen, B. Carli, N. Harris, and E. Hilsenrath, 2006: Position paper on Post-EPS atmospheric chemistry data user requirements in the Post-EPS time frame beyond 2020, Issue 0 Draft H, EUM/C/59/06/DOC/35 Annex III.

Kilpatrick, K. A., G. P. Podestá, and R. Evans, 2001: Overview of the NOAA/NASA Pathfinder algorithm for sea surface temperature and associated matchup database. J. Geophys. Res., 106, 9179-9198.

Kokhanovsky, A. A., 2004: The depth of sunlight penetration in cloud fields for remote sensing. IEEE Geosci. Remote Sens. Lett., 1(4), 242-245.

Kotchenova, S. Y., E. F. Vermote, R. Matarrese, and F. Klemm, 2006: Validation of a vector version of the 6S radiative transfer code for atmospheric correction of satellite data. Part I: Path radiance. Appl. Opt., 45, 6762–6774.

Kubar, T. L., D. E. Waliser, and J.-L. Li, 2011: Boundary layer and cloud structure controls on tropical low cloud cover using A-Train satellite data and ECMWF analyses. J. Climate, 24, 194–215.

Kurucz, R. L., 1993: ATLAS9 Stellar Atmosphere Programs and 2 km/s Grid. Harvard-Smithsonian Center for Astrophysics CD-ROM No. 13, 1993.

Kusmierczyk-Michulec, J., and G. de Leeuw, 2005: Aerosol optical thickness retrieval over land and water using Global Ozone Monitoring Experiment (GOME) data. J. Geophys. Res., 110, D10S05, doi:10.1029/2004JD004780

Lacis, A. A., and V. Oinas, 1991: A description of the correlated k distribution method for modeling nongray gaseous absorption, thermal emission and multiple scattering in vertically inhomogeneous atmospheres. J. Geophys. Res., 96, 9027-9063.

Latham, J., A. M. Blyth, H. J. Christian, W. Deierlingd, and A. M. Gadian, 2004: Determination of precipitation rates and yields from lightning measurements. J. Hydrol., 288, 13-19.

Le Borgne, P., H. Roquet, and C. J. Merchant, 2011: Estimation of sea surface temperature from the Spinning Enhanced Visible and Infrared Imager, improved using numerical weather prediction. Remote Sens. Environ., 115, 55-65.

Lensky, I. M., and D. Rosenfeld, 2008: Clouds-Aerosols-Precipitation Satellite Analysis Tool (CAPSAT). Atmos. Chem. Phys., 8, 6739–6753.

Leslie, L., J. LeMarshall, R. Morison, C. Spinoso, R. Purser, N. Pescod, and R. Seecamp, 1998: Improved hurricane track forecasting from the continuous assimilation of high quality satellite wind data. Mon. Wea. Rev., 126(5), 1248–1257.

Levoni, C., E. Cattani, M. Cervino, R. Guzzi, and W. Di Nicolantonio, 2001: Effectiveness of the MS-method for computation of the intensity field reflected by a multi-layer plane-parallel atmosphere. J. Quant. Spectrosc. Radiat. Transfer, 69, 635-650.

Lindstrot, R., R. Preusker, H. Diedrich, L. Doppler, R. Bennartz, and J. Fischer, 2012: 1D-Var retrieval of daytime total columnar water vapour from MERIS measurements. Atmos. Meas. Tech., 5, 631-646.

Liu, Q., X. Liang, Y. Han, P. van Delst, Y. Cen, A. Ignatov, and F. Weng, 2009: Effect of out–of–

band response in NOAA–16 AVHRR channel 3b on top–of–atmosphere radiances calculated with the community radiative transfer model. J. Atmos. Oceanic Technol., 26(9), 1968–1972.

Los, S., G. Collatz, P. Sellers, C. Malmström, N. Pollack, R. De Fries, L. Bounoua, M. Parris, C. Tucker, and D. Dazlich, 2000: A global 9-yr biophysical land surface dataset from NOAA AVHRR data. J. Hydrometeor., 1(4), 183–199.

Lyapustin, A. I., 2005: Radiative transfer code SHARM for atmospheric and terrestrial application. Appl. Opt., 44, 7764–7772.

Lyapustin, A., J. Martonchik, Y. J. Wang, I. Laszlo, and S. Korkin, 2011: Multiangle implementation of atmospheric correction (MAIAC): 1. Radiative transfer basis and look-up tables. J. Geophys. Res., 116, doi:10.1029/2010JD014986.

Lyapustin, A., Y. Wang, I. Laszlo, R. Kahn, S. Korkin, L. Remer, R. Levy, and J. S. Reid, 2011: Multiangle implementation of atmospheric correction (MAIAC): Aerosol algorithm. J. Geophys. Res., 116, doi: 10.1029/2010JD014985.

Macke, A., and M. Grossklaus, 1998: Light scattering by nonspherical raindrops: Implications for lidar remote sensing of rainrates. J. Quant. Spectrosc. Radiat. Transfer, 60, 355-363.

Macke, A., J. Mueller, and E. Raschke, 1996: Single scattering properties of atmospheric ice crystals. J. Atmos. Sci., 53(19), 2813-2825.

Macke, A., M. Mishchenko, K. Muinonen, and B. Carlson, 1995: Scattering of light by large nonspherical particles: ray-tracing approximation versus T-matrix method. Opt. Lett., 20, 1934-1936.

Mackie, S., C. J. Merchant, C. Old, O. Embury, and P. Francis, 2010: Generalised Bayesian cloud detection for satellite imagery. Part 1: Technique and validation for night-time imagery over land and sea. Int. J. Remote Sens., 31(10), 2573-2594.

Marseille, G. J., K. Houchi, J. de Kloe, and A. Stoffelen, 2011: The definition of an atmospheric database for Aeolus. Atmos. Meas. Tech., 4, 67–88.

Martucci, G., J. Ovadnevaite, D. Ceburnis, H. Berresheim, S. Varghese, D. Martin, R. Flanagan, and C. D. O'Dowd, 2012: Impact of volcanic ash plume aerosol on cloud microphysics. Atmos. Environ., 48, 205-218.

Mayer, B., 2009: Radiative transfer in the cloudy atmosphere. EPJ Web of Conf., 1, 75-99.

Mayer, B., S. W. Koch, and C. D. Whiteman, 2010: Validating the MYSTIC three-dimensional

radiative transfer model with observations from the complex topography of Arizona's Meteor Crater. Atmos. Chem. Phys., 10, 8685-8696.

Masuda, K., 2006: Infrared sea surface emissivity including multiple reflection effect for isotropic gaussian slope distribution model. Remote Sens. Environ., 103 (4), 488–496.

McMillin, L., 1975: Estimation of sea-surface temperatures from two infrared window measurements with different absorption. J. Geophys. Res., 80, 5113-5117.

Merchant, C. J., J. J. Simpson, and A. R. Harris, 2003: A cross-calibration of GMS-5 thermal channels against ATSR-2. Remote Sens. Environ., 84, 268-282.

Merchant, C. J., A. R. Harris, E. Maturi, and S. MacCallum, 2005: Probabilistic physically based cloud screening of satellite infrared imagery for operational sea surface temperature retrieval. Quart. J. Roy. Meteor. Soc., 131, 2735–2755.

Merchant, C. J., O. Embury, P. Le Borgne, and B. Bellec, 2006: Saharan dust in nighttime thermal imagery: Detection and reduction of related biases in retrieved sea surface temperature. Remote Sens. Environ., 104, 15-30.

Merchant, C. J., P. Le Borgne, A. Marsouin, and H. Roquet, 2008: Optimal estimation of sea surface temperature from split-window observations. Remote Sens. Environ., 112 (5), 2469-2484.

Merchant, C. J., P. LeBorgne, H. Roquet, and G. Legendre, 2013: Extended optimal estimation techniques for sea surface temperature from the Spinning Enhanced Visible and Infra-Red Imager (SEVIRI). Remote Sens. Environ., 131, 287-297.

Minnett, P. J., 1986: A numerical study of the effects of anomalous North Atlantic atmospheric conditions on the infrared measurement of sea-surface temperature from space. J. Geophys. Res., 91, 8509-8521.

Minnett, P. J., and I. J. Barton, 2010: Remote sensing of the earth’s surface temperature. In: Radiometric Temperature Measurements and Applications, Z. M. Zhang, B. K. Tsai, and G. Machin, Eds., Academic Press/Elsevier, 333-391.

Minnett, P. J., and G. K. Corlett, 2012: A pathway to generating climate data records of sea-surface temperature from satellite Measurements. Deep-Sea Research II, 77-80, 44-51.

Mie, G., 1908: Beiträge zur Optik trüber Medien, speziell kolloidaler Metallösungen. Ann. Phys., 330, 377–445.

Mishchenko, M. I., L. D. Travis, and D. W. Mackowski, 1996: T-matrix computations of light scattering by nonspherical particles: A review. J. Quant. Spectrosc. Radiat. Transfer, 55, 535-575.

Mitrescu, C., T. L'Ecuyer, J. Haynes, S. Miller, and F. J. Turk, 2010: CloudSat precipitation profiling algorithm—Model description. J. Appl. Meteor. Climatol., 49, 991-1003.

Nakajima, T., and M. D. King, 1990: Determination of the optical thickness and effective particle radius of clouds from reflected solar radiation measurements. Part I: Theory. J. Atmos. Sci., 47, 1878-1893.

Nalli, N., P. J. Minnett, and P. van Delst, 2008: Emissivity and reflection model for calculating unpolarized isotropic water surface-leaving radiance in the infrared. I: Theoretical development and calculations. Appl. Opt., 47, 3701-3721.

Neckel, H., and D. Labs, 1984: The solar spectrum between 3300 and 12500 Å. Solar Phys., 90, 205-258.

National Research Council, 2007: Earth science and applications from space: National imperatives for the next decade and beyond. The National Academies Press, Washington DC. (http://www.nap.edu/catalog.php?record_id=11820).

Noël, S., M. Buchwitz, H. Bovensmann, and J. P. Burrows, 2002: Retrieval of total water vapour column amounts from GOME/ERS-2 data. Adv. Space Res., 29(11), 1697-1702.

Nolin, A. W., and J. Dozier, 2000: A hyperspectral method for remotely sensing the grain size of snow. Remote Sens. Environ., 74, 207-216.

O'Dowd, C. D., D. Ceburnis, J. Ovadnevaite, G. Martucci, J. Bialek, C. Monahan, H. Berresheim, A. Vaishya, T. Grigas, S. G. Jennings, P. McVeigh, S. Varghese, R. Flanagan, D. Martin, E. Moran, K. Lambkin, T. Semmler, C. Perrino, and R. McGrath, 2012: The Eyjafjallajökull ash plume – Part I: Physical, chemical and optical characteristics. Atmos. Environ., 48, 129–142.

Ohring, G., S. Lord, J. Derber, K. Mitchell, and M. Ji, 2002: Applications of satellite remote sensing in numerical weather and climate prediction. Adv. Space Res., 30(11), 2433–2439.

Oreopoulos, L., E. Mlawer, J. Delamere, T. Shippert, J. Cole, B. Fomin, M. Iacono, Z. Jin, J. Li, J. Manners, P. Räisänen, F. Rose, Y. Zhang, M. J. Wilson, and W. B. Rossow, 2012: The continual intercomparison of radiation codes: Results from phase I. J. Geophys. Res., 117, D06118, doi:10.1029/2011JD016821.

Painter, T. H., K. Rittger, C. McKezie, P. Slaughter, and R. E. Davis, 2009: Retrieval of subpixel snow covered area, grain size, and albedo from MODIS. Remote Sens. Environ., 113, 868-879.

Parol, F., J. C. Buriez, C. Vanbauce, J. Riedi, L. C. Labonnote, M. Doutriaux-Boucher, M. Vesperini, G. Séze, P. Couvert, M. Viollier, and F. M. Bréon, 2004: Review of capabilities of multi-angle and polarization cloud measurements from POLDER. Adv. Space Res., 33, 1080-1088.

Phillips, P. L., and P. Schlüssel, 2005: Classification of IASI inhomogeneous scenes using co-located AVHRR data. Proc. SPIE, 5979, 597905, doi:10.1117/12.627605.

Pielke, R. A. Jr., 2008: Climate predictions and observations. Nature Geosci., 1, 206.

Pincus, R., R. Hofmann, J. Anderson, K. Raeder, N. Collins, and J. Whittaker, 2011: Can fully accounting for clouds in data assimilation improve short–term forecasts by global models? Mon. Wea. Rev., 139(3), 946–957.

Platnick, S., and J. M. Fontenla, 2008: Model calculations of solar spectral irradiance in the 3.7-µm band for earth remote sensing applications. J. Appl. Meteor. Climatol., 47, 124-134.

Platnick, S., M. D King, S. A Ackerman, W. P. Menzel, B. Baum, J. C. Riedi, and R. A. Frey, 2003: The MODIS cloud products: algorithms and examples from Terra. IEEEE Trans. Geosci. Remote Sens., 41, 459–473.

Polkinghorne, R., and T. Vukicevic, 2011: Data assimilation of cloud–affected radiances in a cloud–resolving model. Mon. Wea. Rev., 139(3), 755–773.

Pougatchev, N., T. August, X. Calbet, T. Hultberg, O. Oduleye, P. Schlüssel, B. Stiller, K. St. Germain, and G. Bingham, 2009: IASI temperature and water vapor retrievals – Error assessment and validation. Atmos. Chem. Phys., 9, 6453–6458.

Ptashnik, I. V., R. A. McPheat, K. P. Shine, K. M. Smith, and R. G. Williams, 2011: Water vapor self-continuum absorption in near-infrared windows derived from laboratory measurements. J. Geophys. Res., 116, D16305, doi:10.1029/2011JD015603.

Pullen, S., C. Jones, and G. Rooney, 2011: Using satellite–derived snow cover data to implement a snow analysis in the Met Office global NWP Model. J. Appl. Meteor. Climatol., 50(5), 958–973.

Rabier, F., 2005: Overview of global data assimilation developments in numerical weather-prediction centres. Quart. J. Roy. Meteor. Soc., 131, 3215–3233.

Randall, D., S. Krueger, C. Bretherton, J. Curry, P. Duynkerke, M. Moncrieff, B. Ryan, D. Starr, M. Miller, W. Rossow, G. Tselioudis, and B. Wielicki, 2003: Confronting models with data. The GEWEX Cloud Systems Study. Bull. Amer. Meteor. Soc., 84, 455-469.

Remedios, J. J., R. J. Leigh, A. M. Waterfall, D. P. Moore, H. Sembhi, I. Parkes, J. Greenhough, M. Chipperfield, and D. Hauglustaine, 2007: MIPAS reference atmospheres and comparisons to v4.61/v4.62 MIPAS level 2 geophysical data sets. Atmos. Chem. Phys. Discussions, 7 (4), 9973–10017. http://www.atmos-chem-phys-discuss.net/7/9973/2007/

Remer, L. A., D. Tanré, and Y. J. Kaufman, 2006: Algorithm for remote sensing of tropospheric aerosol from MODIS: Collection 5 Product ID: MOD04/MYD04, MODIS ATBD-MOD-02.

Remer, L. A., Y. J. Kaufman, D. Tanré, S. Mattoo, D. A. Chu, J. V. Martins, R.-R. Li, C. Ichoku, R. C. Levy, R. G. Kleidman, T. F. Eck, E. Vermote, and B. N. Holben, 2005: The MODIS aerosol algorithm, products, and validation. J. Atmos. Sci., 62, 947-973.

Reynolds, R. W., 1993: Impact of Mount Pinatubo aerosols on satellite-derived sea surface temperature. J. Climate, 6, 768-774.

Riedi, J., B. Marchant, S. Platnick, B. A. Baum, F. Thieuleux, C. Oudard, F. Parol, J.-M. Nicolas, and P. Dubuisson, 2010: Cloud thermodynamic phase inferred from merged POLDER and MODIS data. Atmos. Chem. Phys., 10, 11851–11865.

Rizzi, R., P. Bauer, S. Crewell, M. Leroy, C. Mätzler, W. P. Menzel, B. Ritter, J. E. Russell, and A. Thoss, 2006: Position paper - cloud, precipitation and large-scale land surface imaging (CPL) observational requirements for meteorology, hydrology and climate, Version 1.k, EUM//59/06/DOC/35 Annex VI.

Robinson, D., R. Barry, J. Campbell, R. Defries, W. J. Emery, M. Halem, J. Hurrell, A. Laing, R. B. Miller, R. Myeneni, R. Somerville, P. D. Try, and T. V. Haar, 2004: Climate data records from environmental satellites. National Academy of Sciences, 136 pp.

Roca, R., J.-C. Bergès, H. Brogniez, M. Capderou, P. Chambon, O. Chomette, S. Cloché, T. Fiolleau, I. Jobard, J. Lémond, M. Ly, L. Picon, P. Raberanto, A. Szantai, and M. Viollier, 2010: On the water and energy cycles in the Tropics. Compte Rendus Geosci., 342, 390-402.

Rohn, M., G. Kelly, and R. W. Saunders, 2001: Impact of a new cloud motion wind product from Meteosat on NWP analyses and forecasts. Mon. Wea. Rev., 129, 2392–2403.

Rosenfeld, D., and I. M. Lensky, 1998: Satellite–based insights into precipitation formation processes in continental and maritime convective clouds. Bull. Amer. Meteor. Soc., 79, 2457–2476.

Rosenfeld, D., E. Cattani, S. Melani, and V. Levizzani, 2004: Considerations on daylight operation of 1.6- versus 3.7-µm channel on NOAA and METOP satellites. Bull. Amer. Meteor. Soc., 85, 873–881.

Rother, T., 2009: Electromagnetic wave scattering on nonspherical particles – Basic methodology and simulations. Springer Series in Optical Sciences, 294 p, Springer, ISBN 978-3-642-00703-3.

Rothman, L., D. Jacquemart, A. Barbe, D. C. Benner, M. Birk, L. Brown, M. Carleer, C. Chackerian, K. Chance, L. Coudert, V. Dana, V. Devi, J.-M. Flaud, R. Gamache, A. Goldman, J.-M. Hartmann, K. Jucks, A. Maki, J.-Y. Mandin, S. Massie, J. Orphal, A. Perrin, C. Rinsland, M. Smith, J. Tennyson, R. Tolchenov, R. Toth, J. V. Auwera, P. Varanasi, and G. Wagner, 2005 : The HITRAN 2004 molecular spectroscopic database. J. Quant. Spectrosc. Radiat. Transfer, 96 (2), 139–204.

Rothman, L. S., and 52 co-authors, 2009: The HITRAN 2008 molecular spectroscopic database. J. Quant. Spectrosc. Radiat. Transfer, 110, 533–572.

Sassen, K. Z., and Z. Wang, 2008: Classifying clouds around the globe with the CloudSat radar: 1-year of results. Geophys. Res. Lett., 35, L04805, doi:10.1029/2007GL032591.

Satheesh, S. K., and K. Krishna Moorthy, 2005: Radiative effects of natural aerosols: A review. Atmos. Environ., 39, 2089-2110.

Saunders, R. W., and K. T. Kriebel, 1988: An improved method for detecting clear sky and cloudy radiances from AVHRR data. Int. J. Remote Sens., 9, 123-150. (Correction, 1988, Int. J. Remote Sens., 1989, 1393-1394).

Saunders, R., J. Hocking, P. Rayer, M. Matricardi, A. Geer, N. Bormann, P. Brunel, F. Karbou, and F. Aires, 2011: RTTOV-10 science and validation report, NWPSAF-MO-TV-023.

Schmidt, K., J. Wauer, T. Rother, and T. Trautmann, 2009: Scattering database for spheroidal particles. Appl. Opt., 48, 2154-2164.

Schmidt, S., V. Venema, F. Di Giuseppe, R. Scheirer, M. Wendisch and P. Pilewskie, 2007: Reproducing cloud microphysical and irradiance measurements using three 3D cloud generators. Quart. J. Roy. Meteor. Soc., 133, 765-780.

Seeman, S. W., E. E. Borbas, R. O. Knuteson, G. R. Stephenson, and H.-L. Huang, 2008: Development of a global infrared emissivity database for application to clear sky sounding retrievals from multi-spectral satellite radiances measurements. J. Appl. Meteor. Climatol., 47, 108-123.

Shanmugham, P., and Y. H. Ahn, 2007: Reference solar irradiance spectra and consequences of their disparities in remote sensing of the ocean colour. Annales Geophys., 25, 1235–1252.

Shettle, E. P., and R. W. Fenn, 1979: Models for the aerosols of the lower atmosphere and the

effects of humidity variations on their optical properties. Air Force Geophysics Laboratory Tech. Rep. AFG-TR-79-0214.

Siegel, D. A., M. Wang, S. Maritorena, and W. Robinson, 2000: Atmospheric correction of satellite ocean color imagery: The black pixel assumption. Appl. Opt., 39, 3582-3591.

Smirnov, A., B. N. Holben, I. Slutsker, D. M. Giles, C. R. McClain, T. F. Eck, S. M. Sakerin, A. Macke, P. Croot, G. Zibordi, P. K. Quinn, J. Sciare, S. Kinne, M. Harvey, T. J. Smyth, S. Piketh, T. Zielinski, A. Proshutinsky, J. I. Goes, N. B. Nelson, P. Larouche, V. F. Radionov, P. Goloub, K. Krishna Moorthy, R. Matarrese, E. J. Robertson, and F. Jourdin, 2009: Maritime Aerosol Network as a component of Aerosol Robotic Network. J. Geophys. Res., 114, D06204, doi:10.1029/2008JD011257.

Smolarkiewicz, P. K., and L. G. Margolin, 2007: On forward –in-time differencing for fluids: An eulerian/semi-lagrangian non-hydrostatic model for stratified flows. Atmos.-Ocean, 35, 127-152.

Soloviev, A., and R. Lukas, 1997: Observation of large diurnal warming events in the near-surface layer of the western equatorial Pacific warm pool. Deep Sea Research Part I: Oceanographic Research Papers, 44, 1055-1076.

Sorek-Hamer, M., Kloog, I., Koutrakis, P., Strawa, A. W., Chatfield, R., Cohen, A., Ridgway, W. L., Broday, D. M.,2015: Assessment of PM2.5 concentrations over bright surfaces using MODIS satellite observations. Remote Sensing of Environment, Volume 163, 15 June 2015, Pages 180-185, ISSN 0034-4257, http://dx.doi.org/10.1016/j.rse.2015.03.014.

Sorooshian, S., R. G. Lawford, P. Try, W. Rossow, J. Roads, J. Polcher, G. Sommeria, and R. Schiffer, 2005: Water and energy cycles: Investigating the links. WMO Bulletin, 7 pp.

Spurr, R. J., and D. Spurr, 2006: VLIDORT: A linearized pseudo-spherical vector discrete ordinate radiative transfer model for forward model and retrieval studies in multilayer multiple scattering media. J. Quant. Spectrosc. Radiat. Transfer, 102, 316–342.

Stammer, D., J. Johannessen, P.-Y. LeTraon, P. Minnett, H. Roquet, and M. Srokosz, 2006: Position paper – Requirements for ocean observations relevant to Post-EPS, Version 1.A, EUM//59/06/DOC/35 Annex VII.

Stamnes, K., and R. Swanson, 1981: A new look at the discrete ordinate method for radiative transfer calculations in anisotropically scattering atmospheres. J. Atmos. Sci., 38, 387-399.

Stephens, G. L., 2005: Cloud feedbacks in the climate system: A critical review. J. Climate, 18, 237-273.

Stoffelen, A., M. Bonavita, J. Eyre, M. Goldberg, H. Järvinen, C. Serio, J.-N. Thépaut, and V. Wulfmeyer, 2006: Position paper – Post-EPS developments on atmospheric sounding and wind profiling, Version 2.D, EUM//59/06/DOC/35 Annex IV.

Stone, T. C., 2008: Radiometric calibration stability and inter-calibration of solar-band instruments in orbit using the moon. Proc. SPIE, 7081, 1-9, doi:10.1117/12.795227.

Stone, T. C., 2011: Personal communication.

Strabala, K., 1998: MODIS cloud mask user guide, Univ. Wisconsin-Madison, Cooperative Institute for Meteorological Satellite Studies, 32 pp. [available online at http://cimss.ssec.wisc.edu/modis/CMUSERSGUIDE.PDF]

Stubenrauch, C. J., W. B. Rossow, and S. Kinne, 2012: Assessment of global cloud datasets from satellites: A project of the World Climate Research Programme Global Energy and Water Cycle Experiment (GEWEX) Radiation Panel. WCRP Rep. 23/2012, 176 pp. [Available online at www.wcrp-climate.org/documents/GEWEX_ Cloud_Assessment_2012.pdf]

Stubenrauch, C. J., W. B. Rossow, S. Kinnes, S. Ackerman, G. Cesana, H. Chepfer, L. DiGirolamo, B. Getzwich, A. Guignard, A. Heidinger, B. C. Maddux, W. P. Menzel, P. Minnis, C. Pearl, S. Platnick, C. Poulsen, J. Riedi, S. Sun-Mack, A. Walther, D. Winker, S. Zeng, and G. Zhao, 2013: Assessment of global cloud datasets from satellites. Bull. Amer. Meteor. Soc., 94, 1031-1049.

Susskind, J., C. D. Barnet, and J. M. Blaisdell, 2003: Retrieval of atmospheric and surface parameters from AIRS/AMSU/HSB data in the presence of clouds. IEEE Trans. Geosci. Remote Sens., 41, 390– 409.

Tett, S., J. Bates, R. Boers, A. Chédin, S. Dewitte, M. McCarthy, J. Schulz, and W. Thomas, 2006: Post-EPS: Generic requirements on climate monitoring, Version 1 Draft P, EUM//59/06/DOC/35 Annex V.

Thuillier, G., M. Hersé, D. Labs, T. Foujols, W. Peetermans, D. Gillotay, P. Simon, and H. Mandel, 2003: The solar spectral irradiance from 200 to 2400 nm as measured by the SOLSPEC spectrometer from the ATLAS and EURECA missions. Solar Phys., 214, 1–22.

Tomassini, M., G. Kelly, and R. Saunders, 1999: Use and impact of satellite atmospheric motion winds on ECMWF analyses and forecasts. Mon. Wea. Rev., 127, 971–986.

Toracinta, E. R., D. J. Cecil, E. J. Zipser, and S. W. Nesbitt, 2002: Radar, passive microwave, and lightning characteristics of precipitating systems in the Tropics. Mon. Wea. Rev., 130, 802-824.

Trenberth, K. E., T. R. Karl, and T. W. Spence, 2002: The need for a system approach to climate

observations. Bull. Amer. Meteor. Soc., 83, 1593-1602.

Trenberth, K. E., A. Dai, R. M. Rasmussen, and D. B. Parsons, 2003: The changing character of precipitation. Bull. Amer. Meteor. Soc., 84, 1205-1217.

Trenberth, K. E., B. Mooreb, T. R. Karl, and C. Nobred, 2006: Monitoring and prediction of the Earth's climate: A future perspective. J. Climate, 19, 5001-5008.

UNESCO, 2009: Water in a changing world. World Water Development Report 3, 349 pp.

Varnai, T., and R. Davies, 1999: Effects of cloud heterogeneities on shortwave radiation: comparison of cloud-top variability and internal heterogeneity. J. Atmos. Sci., 56, 4206-4224.

Varnai, T., and A. Marshak, 2001: Statistical analysis of the uncertainties in cloud optical depth retrievals caused by three-dimensional radiative effects. J. Atmos. Sci., 58, 1540-1548.

VIIRS Aerosol Optical Thickness and Particle Size Parameter Algorithm Theoretical Basis Document (ATBD), © Northrop Grumman Corporation and Raytheon Company, D43313 Rev F, 2010.

Vukicevic, T., M. Sengupta, A. Jones, and T. Vonder Haar, 2006: Cloud-resolving satellite data assimilation: Information content of IR window observations and uncertainties in estimation. J. Atmos. Sci., 63(3), 901–919.

Walton, C. C., W. G. Pichel, J. F. Sapper, and D. A. May, 1998: The development and operational application of nonlinear algorithms for the measurement of sea surface temperatures with the NOAA polar-orbiting environmental satellites. J. Geophys. Res., 103, 27999-28012.

Wang, M., K. D. Knobelspiesse, and C. R. McClain, 2005: Study of the Sea-Viewing Wide Field-of-View Sensor (SeaWiFS) aerosol optical property data over ocean in combination with the ocean color products. J. Geophys. Res., 110, D10S06, doi: 10.1029/2004JD004950.

Watts, P. D., R. Bennartz, and F. Fell, 2011: Retrieval of two-layer cloud properties from multispectral observations using optimal estimation. J. Geophys. Res., 116, D16203, doi:16210.11029/12011JD015883.

Watts, P. D., C. T. Mutlow, A. J. Baran, and A. M. Zavody, 1998: Study on cloud properties derived from Meteosat Second Generation observations, EUMETSAT ITT no. 97/181, 344 pp.

Wehrli, C., 1986: World Climate Research Programme (WCRP) Publication Series No. 7, WMO ITD-No. 149, pp 119-126, October 1986. WRC85 standard spectrum, see also ftp://ftp.pmodwrc.ch/pub/publications/pmod615.asc

Wielicki, B. A., R. D. Cess, M. D. King, D. A. Randall, and E. F. Harrison, 1995: Mission to planet Earth: Role of clouds and radiation in climate. Bull. Amer. Meteor. Soc., 76, 2125-2153.

Wiscombe, W. J., 1996: Mie scattering calculations: Advances in technique and fast, vector-speed computer codes. NCAR Tech. Note, NCAR/TN-140+STR, 64 pp.

Wiscombe, W. J., and J. W. Evans, 1977: Exponential-sum fitting of transmission functions. J. Comput. Phys., 24, 416-444.

Wooster, M. J., G. Roberts, G. L. W. Perry, and Y. J. Kaufman, 2005: Retrieval of biomass combustion rates and totals from fire radiative power observations. J. Geophys. Res., 110, D24311, doi:10.1029/2005JD006318.

Xie, Y., J. Qu, and X. Hao, 2005: Smoke plume detecting using MODIS measurements in eastern United States[C]. East FIRE Conference Proceedings, Fairfax, VA, May 11-13, 2005.

Xiong, X., W. Barnes, X. Xie, and V. Salomonson, 2005: On-orbit performance of Aqua MODIS onboard calibrators. Sensors, Systems, and Next-Generation Satellites IX, Brugge, Belgium, SPIE. 5978, 59780U-59789.

Xu, K.-M., R. T. Cederwall, L. J. Donner, W. W. Grabowski, F. Guichard, D. E. Johnson, M. Khairoutdinov, S. K. Krueger, J. C. Petch and D. A. Randall, 2002: An intercomparison of cloud-resolving models with the Atmospheric Radiation Measurement Summer 1997 Intensive Observation Period data. Quart. J. Roy. Meteor. Soc., 128, 593-624.

Yuan, T., L. A. Remer, and H. Yu, 2011: Microphysical, macrophysical and radiative signatures of volcanic aerosols in trade wind cumulus observed by the A-Train. Atmos. Chem. Phys., 11, 7119-7132.

Yurkin, M. A., and A. G. Hoekstra, 2007: The discrete dipole approximation: An overview and recent developments. J. Quant. Spectrosc. Radiat. Transfer, 112, 2234-2247.

Zapotocny, T. H., J. A. Jung, J. F. LeMarshall, and R. E. Treadon, 2008: Two-season impact study of four satellite data types and rawinsonde data in the NCEP global data assimilation system. Wea. Forecasting, 23, 80-100.

Závody, A. M., C. T. Mutlow, and D. T. Llewellyn-Jones, 1995: A radiative transfer model for sea-surface temperature retrieval for the Along Track Scanning Radiometer. J. Geophys. Res., 100, 937-952.

Zdunkowski, W. G., and G. Korb, 1974: An approximative method for the determination of short-wave radiative fluxes in scattering and absorbing media. Contrib. Atmos. Phys., 47, 129-144.

Zinner, T., and B. Mayer, 2006: Remote sensing of stratocumulus clouds: Uncertainty and biases due to inhomogeneity. J. Geophys. Res., 111(D14209), doi:10.1029/2005JD006955.